

Master's Thesis

Estimation of Finger Joint Center of Rotation
Using Finger Motion and Hand Anthropometry

LIM ZHI CHAN

Department of Industrial and Management Engineering
(Human Factors and Ergonomics Program)

Pohang University of Science and Technology

2018

손가락 동작 및 손 측정 자료를 이용한
손가락 관절 회전 중심 추정

Estimation of Finger Joint Center of Rotation
Using Finger Motion and Hand Anthropometry

Estimation of Finger Joint Center of Rotation Using Finger Motion and Hand Anthropometry

by

LIM ZHI CHAN

Department of Industrial and Management Engineering
(Human Factors and Ergonomics Program)

Pohang University of Science and Technology

A thesis submitted to the faculty of the Pohang University of Science
and Technology in partial fulfillment of the requirements for the degree
of Master of Science in the Department of Industrial and Management
Engineering (Human Factors and Ergonomics Program)

Pohang, Korea

06. 15. 2018

Approved by

Heecheon You (*Heecheon You*)

Academic Advisor

Estimation of Finger Joint Center of Rotation Using Finger Motion and Hand Anthropometry

LIM ZHI CHAN

The undersigned have examined this thesis and hereby certify that it is
worthy of acceptance for a master's degree from POSTECH

06/15/2018

Committee Chair Heecheon You
Heecheon You

Member Hyunbo Cho
Hyunbo Cho

Member Wonsup Lee
Wonsup Lee

MIME LIM ZHI CHAN
20162757 Estimation of Finger Joint Center of Rotation Using Finger Motion and Hand Anthropometry
손가락 동작 및 손 측정 자료를 이용한 손가락 관절 회전 중심 추정
Department of Industrial and Management Engineering (Human Factors and Ergonomics Program), 2018, 83P, Advisor: Dr. Heecheon You, Text in English.

ABSTRACT

A joint center of rotation (CoR) reflects the interface around which the relative motions between two adjacent bone segments occur. The CoR which is fixed during motion is defined as a fixed joint CoR, while the CoR around which the distal segment moves at a certain instant of time from a starting position to an ending position is denoted as an instantaneous joint CoR. Joint CoRs can be anatomically or biomechanically determined from medical scan data (skeleton-based estimation) and/or motion capture data (surface-based estimation). The skeleton-based estimation provides accurate estimated joint CoR. However, the duration of data collection can be lengthy and procedure of data processing such as reconstruction of a 3D skeleton model from CT/ MRI images can be complicated. Moreover, the medical scan such as CT scan is harmful to human body due to radiation. On the other hand, the surface-based estimation method is cost-effective, safe, and fast in motion data acquisition. However, the estimated CoR may not be as accurate as the skeleton-based method due to the effects of soft tissue deformation of the hand during motion capture.

The present study was aimed to (1) compare existing methods for joint CoR estimation based on CT measurement, (2) apply the Delonge-Kasa's circle-fitting method for finger joint CoR estimation using motion capture data and check its

validity in estimating finger joint CoR, and (3) form regression models to predict finger joint CoRs using hand anthropometric data. A motion data pre-processing algorithm was developed to transform the coordinate system of the motion capture data to that of the 3D reconstructed skeleton model from CT scan.

Firstly, the present study was to implement or modify 4 existing methods (Figueroa et al.'s, Reuleaux's, Delonge-Kasa's circle fitting, and bone curvature-based methods) for better finger joint CoR estimation using hand CT scan data and compare those methods in terms of variation of estimated joint CoRs, defined as mean distance among estimated CoRs at different postures for a joint. Hand CT scan data containing different hand postures were collected to obtain the relative motion of finger bone segments. Figueroa et al.'s and Reuleaux's methods were used to estimate instantaneous joint CoRs, while the Delonge-Kasa's and bone curvature-based methods were used to estimate fixed joint CoRs. As result, The Figueroa et al.'s method showed significantly lower mean distance among the estimated MCP joint CoRs for the index, middle, ring, and little fingers than the Reuleaux's method; while the Delonge-Kasa's method showed lower variations of the estimated fixed joint CoRs for 8 out of 12 joints of the index, middle, ring, and little fingers than the Figueroa et al.'s, the Reuleaux's, and the bone curvature-based methods.

Secondly, the present study was to validate the application of the Delonge-Kasa's circle fitting method to hand joints CoRs estimation based on cost-effective motion capture data. Natural finger motion with the largest active ROM at each joint was captured by a motion capture system. The motion-based joint CoRs were then compared with the CT-based CoRs for validation of the Delonge-Kasa's method in joint CoR estimation. As result, 78% of the MCP joint CoRs were found located near to the CT-based CoR with an average mean distance of 3.6 ± 2.2 mm, 95% of the PIP joint CoRs were found located near to the CT-based CoR with an average mean distance of 2.6 ± 1.5 mm, and 78% of the DIP joint CoRs were found located close to the CT-based CoRs with an average mean distance of 2.7 ± 1.1 mm. Large errors (mean distance > 7.0 mm; bolded values in Table 4.5) of joint CoRs were found due

to the insufficient ROM (< 45°, 56°, and 59° for the MCP, PIP, and DIP joints respectively) of distal segments.

Lastly, the present study was to establish novel regression models for joint CoR estimation using hand anthropometric data. Fixed joint CoRs estimated using CT scans were used as dependent variable in the regression analysis, while the hand anthropometric data were used as independent variables. The regression models were evaluated using an adjusted R^2 value and a standard error. The x coordinate of the joint CoR was calculated using a deterministic solution based on the sine rule for the right-angled triangle. The segment length from the landmark on the CMC to that on the MCP joint for digit i ($i = \text{digit } 2\sim 5$) and the angle between the segment of CMC-MCP joint of digit 3 and that of digit i were used as the independent variables x coordinate of joint CoR. A regression analysis was applied to analyse the relationship between a selected hand anthropometric measures and the y and z coordinates of the joint CoR respectively. The perpendicular length from the landmark on the CMC joint to that on the corresponding joint j ($j = \text{MCP, PIP, DIP}$ joints) was selected as the independent variable for the y coordinate of joint CoR. While the finger joint depth of joint j for digit i was selected as the independent variable for the z coordinate of joint CoR. As result, the adjusted R^2 value of the regression equation ($n = 4 \text{ fingers} \times 3 \text{ joints per finger} \times 9 \text{ participants} = 108$) for predicting the y and z coordinates of the joint CoR were 0.996 and 0.814 with a standard error of 2.0 mm and 1.1 mm respectively.

Keywords: Finger joint center of rotation, finger motion, hand anthropometry

TABLE OF CONTENTS

ABSTRACT	i
TABLE OF CONTENTS	iv
LIST OF FIGURES	vii
LIST OF TABLES	xiii
ABBREVIATIONS	xiv
Chapter 1 INTRODUCTION	1
1.1 Problem Statement	1
1.2 Objectives of the Study	5
1.3 Organization of the Thesis	7
Chapter 2 LITERATURE REVIEW	8
2.1 Anatomy of the Hand.....	8
2.2.1 Bone Structure of Hand Joint.....	8
2.1.2 Trajectory of Natural Finger Motion.....	9
2.1.3 Estimation of Joint CoRs	11
2.2 Techniques for Joint CoR Estimation Using Medical Scan Data.....	12
2.2.1 Type of Medical Scan Data	13
2.2.2 Estimation of Fixed Joint CoR.....	15
2.2.3 Estimation of Instantaneous Joint CoR	16
2.3 Techniques for Joint CoR Estimation Using Motion Capture Data	21

Chapter 3 MATERIALS AND METHODS.....	28
3.1 CT-Based Joint CoR Estimation Methods	28
3.1.1 Experiment.....	28
3.1.2 CT Data Pre-Processing	32
3.1.3 Modification of Joint CoR Estimation Methods	38
3.2 Motion-Based Joint CoR Estimation Method.....	43
3.2.1 Experiment.....	43
3.2.2 Pre-Processing of Motion Data.....	45
3.2.3 Joint CoR Estimation Method.....	48
3.3 Hand Anthropometry-Based Joint CoR Estimation Method.....	49
3.3.1 Dependent Variable	50
3.3.2 Independent Variables	50
3.3.3 Joint CoR Estimation Using Hand Anthropometry.....	52
Chapter 4 RESULTS.....	55
4.1 Estimated Joint CoRs Based on CT Scans	55
4.2 Estimated Joint CoR Based on Surface Motion Capture	65
4.3 Hand Anthropometry-Based Joint CoR Estimation Formulas	67
Chapter 5 DISCUSSION	73
5.1 CT-Based Joint CoR Estimation	73
5.2 Motion-Based Joint CoR Estimation	76

5.3	Hand Anthropometry-Based Joint CoR Estimation	77
5.4	Applications	79
5.5	Future Studies	80
Chapter 6 CONCLUSION	82
REFERENCES		84
APPENDICES		87
Appendix A: Institutional Review Board Certification and Documents	87	
Appendix B: Informed Consent for Participants	90	
Appendix C: MATLAB Codes for Joint CoR Estimation by CT Scan.....	92	
Appendix D: Mean distances of instantaneous joint CoRs.....	100	
Appendix E: Instantaneous joint CoRs	101	
Appendix F: Fixed estimated joint CoRs.....	110	
Appendix G: Scatter Plot of Dependent Variables to Independent Variables .	124	
ACKNOWLEDGEMENTS	120	
CURRICULUM VITAE	121	

LIST OF FIGURES

Figure 1.1. Joint centers of rotation (CoRs): (a) fixed proximal interphalangeal (PIP) and distal interphalangeal (DIP) joint CoRs and (b) instantaneous joint CoRs	2
Figure 1.2. Research framework of the present study for finger joint CoRs estimation	6
Figure 2.1. Hand bone structure (Figueroa et al., 2016)	9
Figure 2.2. Types of joint centers of rotation (CoRs): (a) fixed interphalangeal (IP), proximal interphalangeal (PIP), and distal interphalangeal (DIP) CoRs of each finger joint and (b) instantaneous joint CoRs of femoral condyles (Houglum et al., 2012)	12
Figure 2.3. Bone curvature-based method for joint center of rotation estimation (Fowler et al., 2001).....	15
Figure 2.4. Estimation of a joint center of rotation (CoR) using Figueroa et al.'s method: (a) a template (yellow) and target (blue) bones at different postures, (b) an initial alignment of the template bone to the target bone, (c) an alignment of the template bone to the target bone, (d) rotation of the aligned template back to its original posture, and (e) estimation of the joint CoR by the intersection of the centerlines of the distal bone segments at different postures.....	17
Figure 2.5. Identification of centerline (local Y-axis) of a radius bone (Figueroa et al., 2016)	19
Figure 2.6. Reueaux's method: (a) defined landmarks, (b) trajectory of landmark A and B, and (c) estimation of instantaneous joint center of rotation by Reueaux's method (Silva et al., 2005).....	21
Figure 2.7. Placement of landmarks A and B to find IC (instantaneous joint center of rotation) of the knee joint (Claessens, 2017)	21
Figure 2.8. Markers attached to the dorsum of the hand with 21 bony landmarks (http://www.3dvcf.com/DATA/PUBLISH/1760/1760.php)	22

Figure 2.9. Estimation of joint center of rotation by fitting a circle to motion data (Al-Sharadqah et al., 2009).....	23
Figure 2.10. Circles (solid) fitted to the points randomly generated at different locations of a circle (dotted) (a) accurate fitting when the points were generated around the entire circle, (b) almost accurate fitting when the points were generated around half of the circle, (c) biased fitting when the points were generated around quarter of the circle, and (d) very biased fitting when the points were generated around 1/8 of the circle (Al-Sharadqah et al., 2009).....	26
Figure 2.11. Geometric relationship between surface links of metacarpophalangeal (MCP), proximal interphalangeal (PIP), and distal interphalangeal (DIP) joints and their internal links used for estimation of joint center of rotation (Zhang et al., 2003)	27
Figure 3.1. Apparatus used in the CT scanning experiment: (a) CT scanning system, (b) radiation shielding apron, (c) stainless steel ball bearing, and (d) hand fixing device	30
Figure 3.2. Hand postures for CT scan in the present study	32
Figure 3.3. Flow chart of a CT scan data pre-processing method.....	33
Figure 3.4. Procedure of masking technique and threshold-based segmentation method (by Dr. Liver and MITK): (a) collected CT scan data, (b) masking technique, (c) masked skeleton region, (d) threshold selection, and (e) reconstructed 3D skeleton model	34
Figure 3.5. Separation of bone segments from the template posture: (a) the template posture and an example of separated bone segments of the index finger, and (b) separation of a metacarpophalangeal (MCP) segment and a proximal interphalangeal (PIP) segment using a subtraction tool in MITK	35
Figure 3.6. Registration of a template bone segment to a target bone segment: (a) selection of 3 points on each surface of the template and target bone segments at similar locations, (b) a rough registration of the two segments by aligning the 3 selected points on each segment, and (c) a fine registration of the two segments ...	36

Figure 3.7. Template posture (Posture 1) and the remaining 9 postures (Postures 2 to 10) registered from the template posture	36
Figure 3.8. Alignment of proximal bone segments of a joint between two postures.....	37
Figure 3.9. Aligned proximal bone segments from Postures 1 to 10 for the metacarpophalangeal (MCP), proximal interphalangeal (PIP), and distal interphalangeal (DIP) joints with the relative motions of their distal bone segments	38
Figure 3.10. Procedure of determining the centerline of a bone segment: (a) selected bone shaft, (b) determined centroid from a plane perpendicular to the bone shaft, and (c) centerline of the bone segment generated by fitting a linear line to the centroids	39
Figure 3.11. Placement of landmarks for a proximal interphalangeal (PIP) joint center of rotation (CoR) estimation using Reuleaux's Method: (a) landmarks A and B placed at the distal interphalangeal (DIP) segment and (b) the two landmarks selected on each bone surface at different postures	40
Figure 3.12. Proximal interphalangeal (PIP) joint center of rotation (CoR) estimation using Delonge-Kasa's method by fitting a circle to the motion of landmarks selected at the bone heads of distal interphalanges (DIP) segments	41
Figure 3.13. Contour identification from a bone head where a joint motion occurs	42
Figure 3.14. Selection of landmarks from the generated contour line of a bone head: (a) smoothed data points, (b) sampled data points having equal intervals, and (c) selected equally spaced landmarks and landmark A (having largest curvature)	42
Figure 3.15. Estimation of joint center of rotation by the bone curvature-based method as the centroid of the intersection points of the normal lines of the tangent lines going through the equally spaced landmarks and landmark A.....	42
Figure 3.16. Apparatus used in the motion capture experiment: (a) motion analysis system, (b) motion cameras, (c) motion camera setup, and (d) marker attachment.	44
Figure 3.17. Finger flexion/extension (F/E) motions at different joints: (a) fingertip motion for distal interphalangeal (DIP) joint center of rotation (CoR) estimation, (b)	

DIP segment motion for proximal interphalangeal (PIP) joint CoR estimation, and (c) PIP segment motion for metacarpophalangeal (MCP) joint CoR estimation	45
Figure 3.18. Transformation of bone surface data and motion capture data to have the same designated origin and axes at the markers placed at the surface of the proximal interphalangeal (PIP) joint	47
Figure 3.19. Transformation of the distal interphalangeal (DIP) surface marker location at each frame from the motion capture data by aligning the surface marker locations at the initial frame (full extension posture) from the motion capture data and CT-reconstructed data, respectively	47
Figure 3.20. Estimated proximal interphalangeal (PIP) joint centers of rotation by Delonge-Kasa's method using surface marker motion at the proximal interphalangeal (PIP; green) and distal interphalangeal (DIP; blue) joints	49
Figure 3.21. Estimated proximal interphalangeal (PIP) joint centers of rotation (CoRs) by Delonge-Kasa's method using motion data and CT scan data (DIP: distal interphalangeal).....	49
Figure 3.22. Hand anthropometric dimensions: (a) segment length from the landmark on the carpometacarpal (CMC) joint to the corresponding metacarpophalangeal (MCP) joint ($SL_{CMC-MCPi}$; i = digit 2~5), (b) angle between the segment of CMC-MCP joint of the middle finger and that of another finger (αi), (c) perpendicular length from the landmark on the CMC joint to that on the corresponding joint ($PL_{CMC_Markerji}$; j = MCP, proximal interphalangeal (PIP), distal interphalangeal (DIP) joints), and (d) finger joint depth (JDi)	51
Figure 3.23. Landmarks placement on the surface of the bone model for measuring (a) the finger joint depth (JDi ; i = digit 2~5; j = metacarpophalangeal (MCP), proximal interphalangeal (PIP), distal interphalangeal (DIP) joints), the perpendicular length from the landmark on the carpometacarpal (CMC) joint to that on the corresponding joint ($PL_{CMC_Markerji}$), (b) the segment length from landmark on the CMC joint to that on the (MCP) joint ($SL_{CMC-MCPi}$), and the angle between the segment of CMC-MCP joint of the middle finger and that of another finger (αi).....	51

Figure 3.24. Estimation of x coordinate of metacarpophalangeal (MCP) joint center of rotation of digit 2 ($X_{CoR}MCP2$) using the sine rule for right-angled triangle (CMC: carpometacarpal; PIP: proximal interphalangeal; DIP: distal interphalangeal joints; TP: fingertip).....	53
Figure 3.25. Estimation of y coordinate ($Y_{CoR}MCPi$) of metacarpophalangeal (MCP) joint center of rotation (CoR) for digit i using the perpendicular length from the joint to the horizontal line going through the carpometacarpal (CMC) joint ($PL_{CMC_Marker}MCPi$) (PIP: proximal interphalangeal; DIP: distal interphalangeal; TP: fingertip)	54
Figure 3.26. Estimation of z coordinate ($Z_{CoR}PIP_i$) of proximal interphalangeal (PIP) joint center of rotation (CoR) using the PIP joint depth for digit i ($JDPIP_i$) (CMC: carpometacarpal; MCP: metacarpophalangeal; DIP: distal interphalangeal; TP: fingertip)	54
Figure 4.1. Estimated instantaneous joint centers of rotation (CoRs) of metacarpophalangeal (MCP), proximal interphalangeal (PIP), and distal interphalangeal (DIP) for the middle finger.....	57
Figure 4.2. Comparison of mean distances of the estimated instantaneous metacarpophalangeal (MCP) joint centers of rotation by Figueroa et al.'s and Reuleaux's methods for participant 1 (* $p < 0.001$)	58
Figure 4.3. Comparison of mean distances of the estimated instantaneous proximal interphalangeal (PIP) joint centers of rotation by Figueroa et al.'s and Reuleaux's methods for participant 1 (* $p < 0.001$)	59
Figure 4.4. Comparison of the mean distances of the estimated instantaneous distal interphalangeal (DIP) joint centers of rotation by Figueroa et al.'s and Reuleaux's methods for participant 1 (* $p < 0.001$)	60
Figure 4.5. Identification of a centroid (black dot) from four estimated fixed CoRs of a joint by Figueroa et al's (cyan), Reuleaux's (blue), Delonge-Kasa's (red), and bone curvature-based (green) methods	64

Figure 4.6. Two cases of an accurate (left) and inaccurate (right) estimation of motion-based CoRs (black dots) with corresponding rotation angles, blue dots: CT-based CoRs.....	67
Figure 4.7. Calculation of x coordinate of a joint center of rotation (X_{CoRji} ; $i = \text{digit } 2\sim 5$; $j = \text{metacarpophalangeal (MCP), proximal interphalangeal (PIP), distal interphalangeal (DIP) joints}$) using the sine rule for angle right-triangle (CMC: carpometacarpal; TP: fingertip)	68
Figure 4.8. Scatter plot of y coordinate of the joint centers of rotation to the perpendicular length from the (a) metacarpophalangeal ($PL_{CMC_MarkerMCP3}$), (b) proximal interphalangeal ($PL_{CMC_MarkerPIP3}$), (c) distal interphalangeal ($PL_{CMC_MarkerDIP3}$) joints to the horizontal line going through the Carpometacarpal (CMC) joint, and (d) combination of all the joints	70
Figure 4.9. Scatter plot of z coordinate of the joint centers of rotation to (a) metacarpophalangeal ($JDMCP3$), (b) proximal interphalangeal ($JDPPIP3$), (c) distal interphalangeal ($JDDIP3$) joints depth, and (d) combination of all the joint depth data	72
Figure 5.1. Instantaneous finger joint centers of rotation incorrectly estimated by Reuleaux's method (left) and correctly estimated by Figueroa et al.'s method (right) for a motion of the distal bone segment around a joint with a rotation angle of 5° (illustrated for the distal interphalangeal joint of the little finger of Participant 1) .	74
Figure 5.2. Instantaneous finger joint centers of rotation incorrectly estimated by Figueroa et al.'s method (left), Reuleaux's method (middle), and bone curvature-based method (right) for a motion of the distal bone segment around a joint with a rotation angle of 2° (illustrated for the proximal interphalangeal joint of the ring finger of Participant 1).....	76
Figure 5.3. Relationship between dependent variable and independent variable for joint center of rotation (CoR) estimation at different joints including the distal interphalangeal (DIP), proximal interphalangeal (PIP), and metacarpophalangeal (MCP) joints: (a) y coordinate of a joint CoR with the perpendicular length from the	

joint to the horizontal line going through the carpometacarpal (CMC) joint and (b) z coordinate of a joint CoR with the joint depth.....	79
--	----

LIST OF TABLES

Table 1.1. Joint center of rotation (CoR) estimation methods: Figueroa et al.'s, Reuleaux's, bone curvature-based, and Delonge-Kasa's circle fitting methods.....	3
Table 2.1. Static constraint of each joint movement (Cobos et al., 2008).....	11
Table 2.2. Comparison of medical scanning technique (Kasban et al., 2015)	14
Table 2.3. Geometric fitting and algebraic fitting methods for estimation of joint center of rotation (CoR)	24
Table 3.1. Demographic information of participants in the present study	29
Table 4.1. Summary of paired <i>t</i> -test results: Differences in the mean distance between Figueroa et al.'s and Reuleaux's methods (degree of freedom = 989 for all the participants except participant 8 and 967 for participant 8).....	61
Table 4.2. Mean distance \pm SE among four fixed CoRs estimated by Figueroa et al.'s, Reuleaux's, Delonge-Kasa's, and bone curvature-based methods at each joint of 9 participants.....	63
Table 4.3. Distances of four fixed center of rotations (CoRs) estimated by Figueroa et al.'s, Reuleaux's, Delonge-Kasa's, and bone curvature-based methods to the centroid of the four CoRs at a joint having a mean distance larger than 2.0 mm among each other	64
Table 4.4. Distance between motion-based and CT-based joint center of rotation at each joint of all participants	66
Table 4.5. Rotation angle in motion capture at each joint of all participants	66

ABBREVIATIONS

Symbol	Definition
DHM	Digital hand modelling
CoR	Center of rotation
2D	2-dimensional
3D	3-dimensional
ROM	Range of motion
DoF	Degree of freedom
IP	Interphalangeal
TP	Finger tip
DIP	Distal interphalangeal
PIP	Proximal interphalangeal
MCP	Metacarpophalangeal
CMC	Carpometacarpal
MRI	Magnetic resonance imaging
CT	Computed tomography
FE	Flexion-extension
AA	Abduction-adduction
PCA	Principal component analysis
ICP	Iterative closest point

Chapter 1 INTRODUCTION

1.1 Problem Statement

A joint center of rotation (CoR) reflects the interface around which the relative motions between two adjacent bone segments occur (Kinzel et al., 1983). The CoR which is fixed during motion is defined as a fixed joint CoR (Zatsiorsky, 1998; Figure 1.1.a), while the CoR around which the distal segment moves at a certain instant of time from a starting position to an ending position is denoted as an instantaneous joint CoR (Challis, 2002; Figure 1.1.b). Joint CoRs have been widely used in clinical applications and biomechanical analyses for ergonomic product design. In clinical applications, fixed joint CoRs are used for joint replacement surgery (Lim et al., 2009; Marin et al., 2003) and clinical diagnostic of arthritis injury (Abouhossein et al., 2012; Ahmadi et al., 2009; Muggleton et al., 1998; Petit et al., 2003; Staub et al., 2014), while in biomechanical analyses for ergonomic product design, instantaneous joint CoRs are usually required for accurate digital human modelling (DHM) (Kurihara et al., 2004; Veber et al., 2006). In DHM, joint CoRs have played a significant role in constructing a link model for a digital hand model by connecting two adjacent CoRs for animation and motion analyses. Instantaneous joint CoRs can help practitioners to track changes of hand posture and determine most appropriate postures for certain tasks with a product. The predicted appropriate hand postures can then be used for hand-held product design (Chaffin., 2008; Frederick et al., 1995; Seo et al., 2007),

biomedical (Gamage et al., 2002), prosthetic, and robotic applications (Liu et al., 1989).



Figure 1.1. Joint centers of rotation (CoRs): (a) fixed proximal interphalangeal (PIP) and distal interphalangeal (DIP) joint CoRs and (b) instantaneous joint CoRs

Joint CoRs can be anatomically or biomechanically determined from medical scan data (skeleton-based estimation) and/or motion capture data (surface-based estimation) (Zatsiorsky, 1998). An anatomical joint CoR can be determined based on the contour of the head of a proximal bone segment (known as the bone curvature-based method; Fowler et al., 2001), while a biomechanical joint CoR can be estimated from the motion of a distal bone segment using various methods such as Figueroa et al.'s method (Figueroa et al., 2016), Reuleaux's method (Reuleaux, 1875), and Delonge-Kasa's circle-fitting method (Kasa, 1976) as shown in Table 1.1. The bone curvature-based method and the circle-fitting method are used to estimate fixed joint CoRs, while Reuleaux's and Figueroa et al.'s methods are used to

determine instantaneous joint CoRs. The estimated joint CoRs from the four methods can be

Table 1.1. Joint center of rotation (CoR) estimation methods: Figueroa et al.'s, Reuleaux's, bone curvature-based, and Delonge-Kasa's circle fitting methods

Instantaneous Joint CoR Estimation			
Figueroa et al's	Reuleaux's	Bone curvature	Delonge-Kasa
 (Figueroa et al., 2016)	 (Reuleaux, 1875)	 (Fowler et al., 2001)	 (KASA, 1976)

evaluated by the skeleton-based estimation using the 3D reconstructed skeleton model segmented from medical scan data of magnetic resonance imaging (MRI) or computed tomography (CT). However, the duration of data collection can be lengthy and procedure of data processing such as the reconstruction of a 3D skeleton model from CT/ MRI images can be complicated. Moreover, to examine the motion of a skeleton model for instantaneous joint CoR estimation, several scan data of the hand in different postures are needed. For instance, Figueroa et al. (2016) and Kurihara et al. (2004) collected five sets of CT scan data with different static postures to estimate instantaneous joint CoRs from one posture to another; Stillfried et al. (2010) applied the similar approach using six sets of MRI scan data; Miyata et al. (2010) spent 48 minutes to collect MRI scan data of four static postures of the hand. Furthermore,

medical scan such as CT scan is harmful to the human body due to radiation. A surface motion-based method allows the estimation of a joint CoR using the dynamic motion of a joint that is tracked by a marker attached on the hand skin surface. The motion-based joint CoR estimation method is cost-effective, safe, and fast in motion data acquisition (Lin et al., 2000). However, the estimated CoR may not be as accurate as the skeleton-based method due to the effects of soft tissue deformation of the hand during motion capture (Celveri et al., 2005).

The circle fitting method is commonly used for fixed joint CoR estimation using motion capture data (Gamage et al., 2002; Halvorsen et al., 1999; Knight et al., 2009). In the circle fitting method, a joint CoR is estimated as the center of a circle fitted to the trajectory of the surface marker motion. However, the circle fitting method requires at least 45° of range of motion (ROM) (Ehrig et al., 2005) and has not been applied to the estimation of a finger joint CoR. For example, Delonge-Kasa's method (Kasa, 1976) was originally applied to a big joint with a large ROM for joint CoR estimation by Knight et al. (2009). The geometric circle fitting method proposed by Piazza et al. (2004) used an iterative computation method to estimate finger joint CoRs, which is computationally intensive. Moreover, Piazza et al.'s method needs an initial guess of the joint CoR to optimally and iteratively solve a cost function (Piazza et al., 2004). Many researchers have proposed new methods which improve the existing methods to compensate critical bias (Halvorsen et al., 1999) or reduce computational efforts (Pratt, 1987). However, the comparison of estimated joint CoRs with skeleton-based joint CoRs has not been conducted. The performance of the joint

CoR estimation methods has been usually inspected by performing a statistical analysis such as root mean square error (RMS) test (Ehrig et al., 2005).

To improve the existing methods, an in-depth study needs to be conducted to compare various joint CoR estimation methods and improve the existing methods for better estimation accuracy. Furthermore, finger joint CoR estimation models using hand anthropometric data can be established for practical joint CoR estimation.

1.2 Objectives of the Study

As displayed in Figure 1.2, the present study was aimed to (1) compare existing methods for joint CoR estimation based on CT measurement, (2) apply the Delonge-Kasa's circle-fitting method for finger joint CoR estimation using motion capture data and check its validity in estimating finger joint CoR, and (3) form regression models to predict finger joint CoRs using hand anthropometric data.

Firstly, the present study was to implement or modify four existing methods (Figueroa et al.'s, Reuleaux's, Delonge-Kasa's circle fitting, and bone curvature-based methods) for better finger joint CoR estimation using hand CT scan data and compare those methods in terms of variation of estimated joint CoRs, defined as mean distance among estimated CoRs at different postures for a joint. Hand CT scan data containing different hand postures were collected to obtain the relative motion of finger bone segments. Skeleton models of all postures were reconstructed from CT scan data. Figueroa et al.'s and Reuleaux's methods were used to estimate

instantaneous joint CoRs, while Delonge-Kasa's and the bone curvature-based methods were used to estimate fixed joint CoRs.

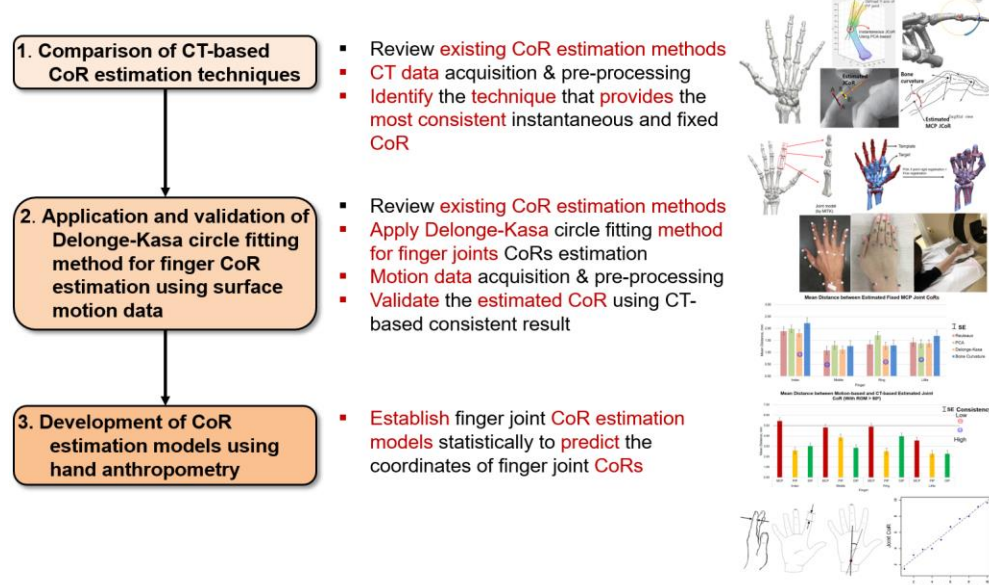


Figure 1.2. Research framework of the present study for finger joint CoRs

estimation

Secondly, the present study was to validate the application of Delonge-Kasa's circle fitting method to hand joints CoRs estimation based on cost-effective motion capture data. Natural finger motion with the largest active ROM at each joint was captured by a motion capture system. An experimental protocol was developed to easily collect finger motion data without false positive or negative errors during capture. A motion data pre-processing algorithm was developed to transform the coordinate system of the motion capture data to that of the 3D reconstructed skeleton

model from CT scan. Then joint CoR was estimated using Delonge-Kasa's circle fitting method based on the transformed motion data. The motion-based joint CoRs were then compared with the CT-based CoRs for validation of Delonge-Kasa's method in joint CoR estimation.

Lastly, the present study was to establish novel regression models for joint CoR estimation using hand anthropometric data. Fixed joint CoRs estimated using CT scans were used as dependent variable in the regression analysis. The regression models were evaluated using adjusted R^2 value and standard error.

1.3 Organization of the Thesis

The thesis was organized into 6 chapters. Chapter 1 introduced research background, problems, and objectives of the study. Chapter 2 reviewed existing studies including human hand anatomy and existing joint CoR estimation methods. Chapter 3 explained experiments for data collection, modification of existing joint CoR estimation methods, and regression analysis for joint CoR estimation. Chapter 4 showed the results including the comparison of CT-based methods, validation of the motion-based method, and hand anthropometry-based joint CoR estimation formulas. Chapter 5 discussed the significance, findings, limitations, and recommendations of the study. Lastly, Chapter 6 presented the conclusion of the study.

Chapter 2 LITERATURE REVIEW

In this study, the literature review examines (1) the anatomy of hand joint, (2) existing methods of joint CoR estimation based on medical scan data, and (3) the existing methods of joint CoR estimation based on motion capture data.

2.1 Anatomy of the Hand

Human hands are capable of a wide range of functions that composed of fine (perform delicate tasks like precisely hold small object or power grasping task) and gross (take up big or heavy object) motor movement where such high-level multitude of functions are facilitated by 19 articulations, 31 muscles, and 27 degrees of freedom (DoF) (Liu et al. 1989).

2.2.1 Bone Structure of Hand Joint

The bone structure of hand joint consists of 29 bones that constitute the basic skeleton of the wrist and hand (Figure 2.1). The 29 bones included radius, ulna, 8 carpal bones (consisting of hamate, pisiform, triquetral, lunate, scaphoid, capitate, trapezium, and trapezoid), 5 metacarpals, 5 proximal phalanges, 4 middle phalanges, and 5 distal phalanges. The bones of the hand are naturally assembled into the carpus through a

unique bone arrangement with the joints listed as: (1) metacarpophalangeal (MCP) joints of fingers and carpometacarpal (CMC) joint at the palm, (2) interphalangeal (IP) joint, MCP joint and CMC joint at the thumb, and (3) distal interphalangeal (DIP) joints, proximal interphalangeal (PIP) joints and MCP joints at the four fingers.

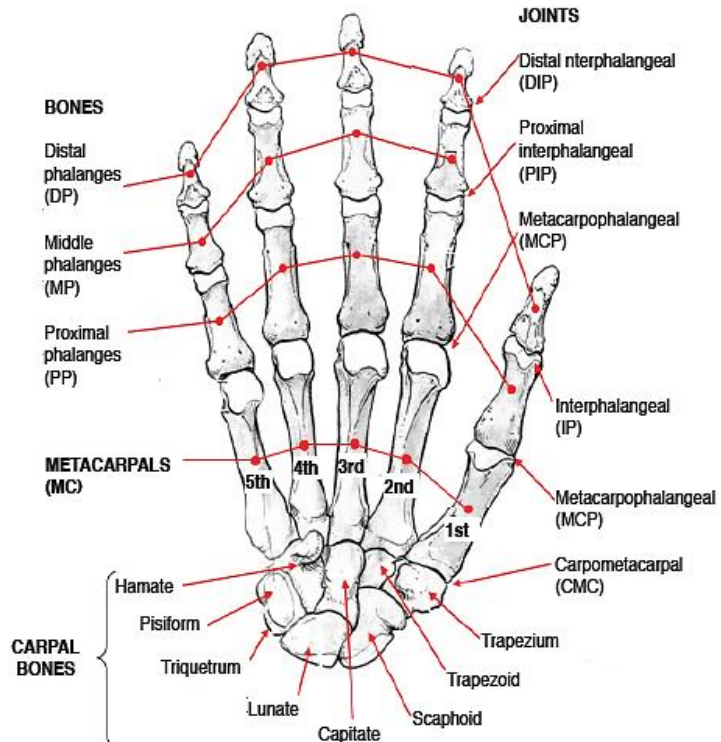


Figure 2.1. Hand bone structure (Figueroa et al., 2016)

2.1.2 Trajectory of Natural Finger Motion

The human hand consists of 27 allowable degrees of freedom (DoF) comprising the movement of flexion/extension (F/E), abduction/adduction (Ab/Ad), rotation, and translation where each finger joint moves according to the allowable ROM, as shown in Table 2.1.

The MCP joints of hand are the condyloid joints allowing 2 DoFs with the movements of F/E and Ab/Ad. For the movement of F/E, the MCP joints takes place through less than 40° and 60° of motion, respectively (Cobos et al., 2008). For the movement of Ab/Ad, the allowable range of angle is approximately 45° to 60° for all MCP joints. As shown in Table 2.1, the index and little fingers reach 15° and 5° higher than the middle and ring fingers, respectively (Cobos et al., 2008). Hamill et al., (2015) reported that the movement of Ab/Ad was extremely restricted during flexion due to the tightness of collateral ligaments during flexing movement. The PIP and DIP joints are the hinge joints allowing 1 DoF with F/E movement. Both joints connect three types of bones: proximal phalanges, middle phalanges, and distal phalanges and rotate like a hinge joint. The ranges of flexion at PIP and DIP joints are approximately 110° and 90°, respectively. For extension, the allowable ranges for both PIP and DIP joints are < 10°. Hamill et al., (2015) clarified that maximum flexion movement of fingers can be obtained when the wrist is slightly in an extension posture since the extrinsic muscle tendons are not long enough to reach the maximum range of motion at the wrist and fingers.

Table 2.1. Static constraint of each joint movement (Cobos et al., 2008)

Finger	Joint	Flexion	Extension	Abduction/ adduction
Thumb	CMC	50° - 90°	15°	45° - 60°
	MCP	75° - 80°	0°	5°
	IP	75° - 80°	5° - 10°	5°
Index	CMC	5°	0°	0°
	MCP	90°	30° - 40°	60°
	PIP	110°	0°	0°
	DIP	80° - 90°	5°	0°
Middle	CMC	5°	0°	0°
	MCP	90°	30° - 40°	45°
	PIP	110°	0°	0°
	DIP	80° - 90°	5°	0°
Ring	CMC	10°	0°	0°
	MCP	90°	30° - 40°	45°
	PIP	120°	0°	0°
	DIP	80° - 90°	5°	0°
Little	CMC	15°	0°	0°
	MCP	90°	30° - 40°	50°
	PIP	135°	0°	0°
	DIP	90°	5°	0°

CMC: carpometacarpal, MCP: metacarpophalangeal, IP: interphalangeal, PIP: proximal interphalangeal,

DIP: distal interphalangeal

2.1.3 Estimation of Joint CoRs

In general, the local center of contour in the sagittal view of the bone head has denoted the fixed joint CoR (Figure 2.2.a; Taylor et al., 1955). However, due to the multiple motions (for MCP joint) and the incongruity of joint surface, human hand joint axes are complex and are not stationary like the mechanism of a door hinge, the joint CoR may shift instantaneously during rotation, as shown in Figure 2.2.b. However, in most of the applications, the determination of instantaneous joint CoR does not apply to

finger joints due to subtle changes in the displacement of CoRs. Therefore, most of applications have considered fixed joint CoRs for all the finger joints (Zatsiorsky, 1998). An in-depth study on the instantaneous CoR at the finger joints can be conducted to evaluate the variation of the instantaneous CoRs at finger joints during motion.

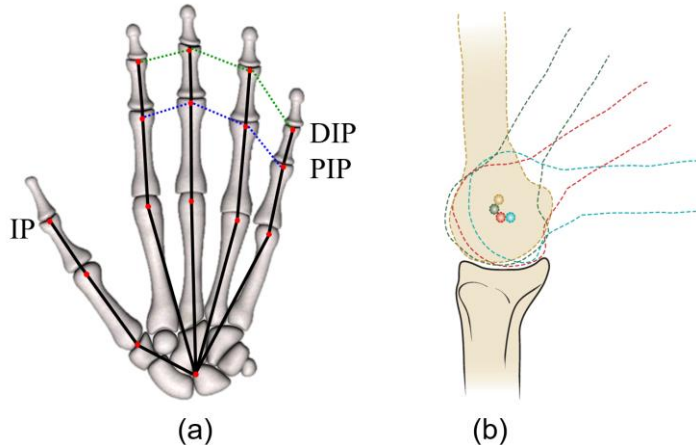


Figure 2.2. Types of joint centers of rotation (CoRs): (a) fixed interphalangeal (IP), proximal interphalangeal (PIP), and distal interphalangeal (DIP) CoRs of each finger joint and (b) instantaneous joint CoRs of femoral condyles (Houglum et al., 2012)

2.2 Techniques for Joint CoR Estimation Using Medical Scan Data

2.2.1 Type of Medical Scan Data

The technologies of medical scanning (Table 2.2) are a non-invasive and painless methods to acquire a sight inside the body without opening the body surgically (Kasban et al, 2015). The X-ray radiography is commonly used for a medical diagnostic purpose such as chiropractic in a 2-dimensional view. CT is an extended technology of X-ray which provides a clearer visualization and detailed examination of the human body in a 3D view. The MRI technique provides a similar application with CT, but more focusing on examining the abnormalities of the brain, spinal cord, and abdominal organs or observing unhealthy tissues in the body. The ultrasonography technique is commonly used for diagnosing the development of fetus during pregnancy and scanning the solid organs of the abdomen such as pancreas, liver, gallbladder and kidneys (Kasban et al., 2015). Many studies on the joint CoR estimation have been conducted using MRI (Stillfried et al, 2010) and CT (Kurihara et al., 2004; Figueroa et al., 2016) data. However, compared to CT, the bone surface definition using MRI images is less appropriate to kinematic modelling as it does not provide sufficient delineation between bone and the soft tissue, especially within the joint capsule (Hollerbach et al., 1996). The CT measurement allows speedy scan and offers the highest resolution scanning in a 3D view among all techniques and therefore serves as the best method for measurement in the present study.

Table 2.2. Comparison of medical scanning technique (Kasban et al., 2015)

Technique	Description
X-Ray	<u>Advantages</u> <ul style="list-style-type: none"> - Quick and support medical and surgical treatment planning <u>Disadvantages</u> <ul style="list-style-type: none"> - Exposure to ionizing radiation - Not applicable for digital hand modelling (estimated joint CoR was displayed only in a 2D view)
CT	<u>Advantages</u> <ul style="list-style-type: none"> - Quick and provides global view of veins - Higher bone resolution as the soft tissue contrast is low <u>Disadvantages</u> <ul style="list-style-type: none"> - Exposure to ionizing radiation - Unable to collect dynamic data - Relatively expensive
MRI	<u>Advantages</u> <ul style="list-style-type: none"> - No ionizing radiation - Good soft tissue contrast <u>Disadvantages</u> <ul style="list-style-type: none"> - Relatively low sensitivity - Long scan duration (12 minutes per scan (Miyata et al., 2010)) - Unable to collect dynamic data - Relatively expensive
Ultrasonography	<u>Advantages</u> <ul style="list-style-type: none"> - No ionizing radiation - Provides real time information <u>Disadvantages</u> <ul style="list-style-type: none"> - No standardized guidelines - Blinding procedures are challenging - Affected by hydration status

2.2.2 Estimation of Fixed Joint CoR

An et al. (1983) and Fowler et al. (2001) used a bone curvature-based method to geometrically estimate the fixed CoR of a joint by identifying the center of the joint's proximal bone head in the sagittal view (Figure 2.3). A reconstructed skeleton model was extracted from MRI data of the hand. The contour line of the bone head is defined from the contact region between the convex surface of proximal bone and concave surface of distal bone (Figure 2.3). The starting and ending points of the contour line is defined from the first and last contact points between the head of a proximal phalange bone and the base of the adjacent bone. The fixed joint CoR is determined based on the center of arc of the contour line.

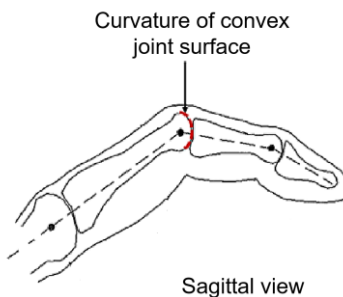


Figure 2.3. Bone curvature-based method for joint center of rotation estimation
(Fowler et al., 2001)

2.2.3 Estimation of Instantaneous Joint CoR

Figueroa et al. (2016) recommended a statistical based instantaneous joint CoR estimation procedure (named as Figueroa et al.'s method) by biomechanically identifying the intersection point between the centerlines of the distal bone segments at two different postures in F/E movement (Figure 2.4). To determine the relative motion of finger joints, five different hand poses (flat hand down, resting hand, lateral pinch, power grip, pinch grip) are separately collected by CT and reconstructed into 3D skeleton models (Figueroa et al., 2016). The skeleton model at flat hand down posture is set as a template (yellow in Figure 2.4.a) and the rest are targets (blue in Figure 2.4a). The targets are pre-aligned to the template by aligning the carpal bones using the iterative closest point (ICP) algorithm (Besl and McKay, 1992) (Figure 2.4.b). To define the local coordinate of the bone model, the ICP algorithm is performed by aligning each individual bone from the template to the targets and the axis line is assigned to the target bone (Figure 2.4.c). To examine the relative motion of the distal bone, the target proximal bones are aligned to the template proximal bone.

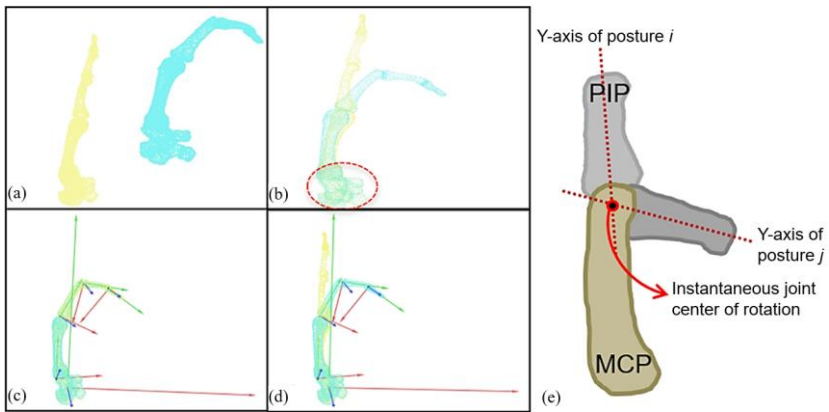


Figure 2.4. Estimation of a joint center of rotation (CoR) using Figueroa et al.’s method: (a) a template (yellow) and target (blue) bones at different postures, (b) an initial alignment of the template bone to the target bone, (c) an alignment of the template bone to the target bone, (d) rotation of the aligned template back to its original posture, and (e) estimation of the joint CoR by the intersection of the centerlines of the distal bone segments at different postures

To determine the centerline of distal bone, the principal component analysis (PCA) method is performed. The PCA method reduces the dimensionality of each bone’s local coordinate into 3 directions and allows redefining the axis direction (Figueroa et al., 2016). The PCA method composed of:

- (a) Determine the mean distances for each dimension (axis) and subtract the mean (\bar{x}) for individual dimensions to determine the variance of the bone surfaces data (x), where n is the total number of bone surface data and x_i is the i^{th} bone surface data

$$\text{var}(x) = \sum_{i=1}^n (x_i - \bar{x})^2 \quad \text{Eq. 2.1}$$

(b) Compute the covariance matrix (COV)

$$cov(x, y) = \frac{\sum_{i=1}^n (x_i - \bar{x})(y_i - \bar{y})}{n-1} \quad \text{Eq. 2.2}$$

$$COV(x, y) = \begin{bmatrix} var(x) & cov(x, y) \\ cov(y, x) & var(y) \end{bmatrix} \quad \text{Eq. 2.3}$$

(c) Calculate the eigen values (λ) and eigenvectors (V) of the COV and categorize the vertices into 3 dimensions

$$\det(COV(x, y) - \lambda I) = 0 \quad \text{Eq. 2.4}$$

$$\det(COV(x, y) - \lambda I) \times [V] = 0 \quad \text{Eq. 2.5}$$

where I = identity matrix

(d) Sort the eigen vectors (V) in a descending order according to the determined eigen value where the first principal component of the transformed bone surface data (denoted as a temporary Y-axis) contains the most significant eigenvector and the

transformed bone is the newly determined local position of the bone segment (Wu et al., 2005).

$$\text{Transformed bone} = [\text{original bone}] \cdot [\text{Sorted } V] \quad \text{Eq. 2.6}$$

The bone shaft region is selected to determine the centroids of the planes that are perpendicular to the bone shaft. Centroids are identified for the planes perpendicular to the selected bone shaft and the centerline (denoted as the local Y -axis line; Figure 2.5) of the bone shaft is drawn by linearly fitting a line to the identified centroids using the 1st order polynomial linear fitting function in Matlab (MathWorks, Inc., Natick, MA, USA). The intersection point between the determined centerlines of the distal segments at two postures is considered as an instantaneous joint CoR (Figure 2.4.e).

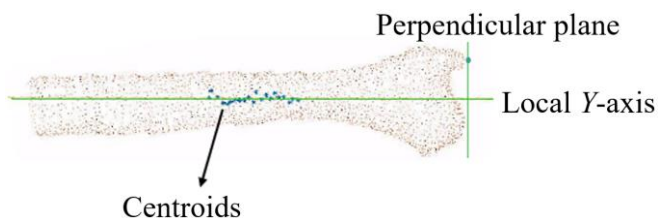


Figure 2.5. Identification of centerline (local Y -axis) of a radius bone (Figueroa et al., 2016)

Reuleaux (1875) proposed a geometric based procedure to estimate the instantaneous joint CoR from a planar motion using the displacement vector of two landmarks. Silva et al. (2005) has applied the Reuleaux's method to estimating a finger joint CoR (Figure 2.6). Two landmarks (denoted as the landmark A and B) were selected from the distal bones surface and their displacement vectors were identified at different postures (denoted as the landmark A' and B'). The instantaneous joint CoR is located at the intersection of the perpendicular bisectors of A to A' and B to B'. Reuleaux's method has also been widely utilized by many researchers (Halvorsen et al., 1999; Silva et al., 2005) due to the facile measurement and quick procedure.

Errors in the instantaneous joint CoR can be significant if the landmarks A and B are not appropriately positioned or if the intersection angle is too small. Challis (2001) suggested that the position of a pair of landmarks should be located closer to the estimated CoR, i.e., the closer the centroid of a pair of landmarks to the CoR, the more accurate the CoR position. Claessens (2017) defined the landmark at different sides at the knee (Figure 2.7) which shows a larger angle between two mid-perpendicular bisector lines.

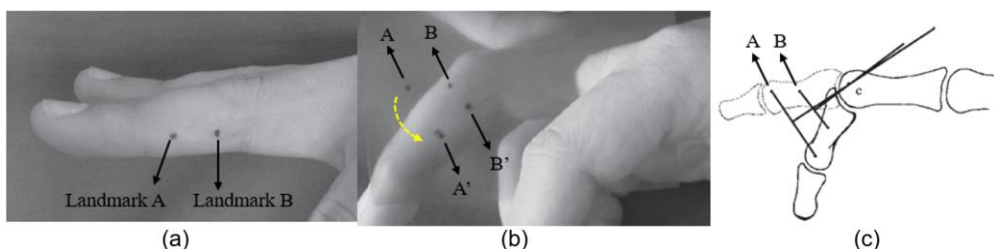


Figure 2.6. Reueaux's method: (a) defined landmarks, (b) trajectory of landmark A and B, and (c) estimation of instantaneous joint center of rotation by Reuleaux's method (Silva et al., 2005)

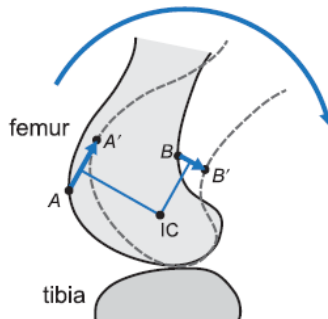


Figure 2.7. Placement of landmarks A and B to find IC (instantaneous joint center of rotation) of the knee joint (Claessens, 2017)

2.3 Techniques for Joint CoR Estimation Using Motion Capture Data

In previous studies, motion analysis was commonly performed to form a hand link model from surface markers attached to the dorsum of the hand (known as surface technique) (Figure 2.8). However, the surface technique cannot precisely determine the human hand skeleton as the position of joint CoR cannot simply be substituted by the position of the surface marker. A link model that interconnects joint CoRs needs to be generated for accurate analysis, modelling and simulation of natural motion (Halvorsen et al., 1999; Knight et al., 2010; Piazza et al., 2004; Zhang et al., 2003).

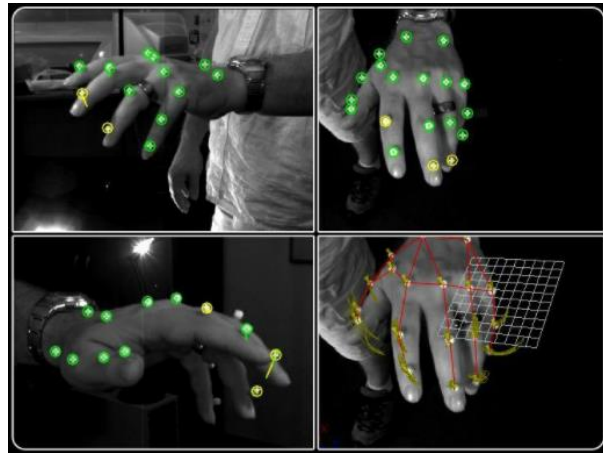


Figure 2.8. Markers attached to the dorsum of the hand with 21 bony landmarks

[\(<http://www.3dvcf.com/DATA/PUBLISH/1760/1760.php>\)](http://www.3dvcf.com/DATA/PUBLISH/1760/1760.php)

The circle fitting method is known as one of the most efficient and simple approach to biomechanically estimate the fixed joint CoR using motion capture data. By assuming the proximal segment remains stationary, while the distal segment is rotating within an allowable ROM, a circle is fitted to the trajectory of the distal segment where the center of the fitted circle is denoted as a fixed joint CoR. The relative rotation movement of a surface marker lies in a 2D space, while the arc shaped trajectory of the surface marker during movement is expressed by a set of n points $P_i(x_i, y_i)$, where $i = 1, \dots, n$ ($n \geq 3$). The fixed joint CoR $C_i(x_c, y_c)$ and the radius r can be determined from a circle that fitted to motion data $P_i(x_i, y_i)$ (Figure 2.9). This optimization of the fitting task is conducted by minimizing the sum of the squared Euclidean distances between the circle and the marker position (Ehrig et al., 2005), as shown in Eq. 2.7.

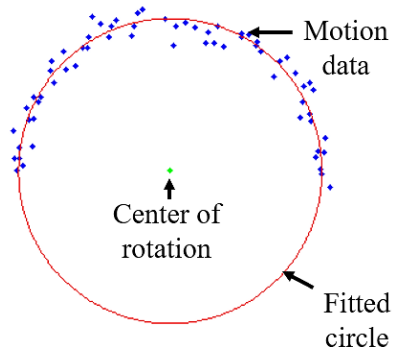


Figure 2.9. Estimation of joint center of rotation by fitting a circle to motion data

(Al-Sharadqah et al., 2009)

$$(x_i - x_c)^2 + (y_i - y_c)^2 = r^2 \quad \text{Eq. 2.7}$$

The circle fitting algorithm can be solved in two ways: geometric circle fitting method (Gamage et al., 2002; Piazza et al., 2004) and algebraic circle fitting method (Kasa, 1976; Pratt, 1987), as summarized in Table 2.3. The geometric fitting method solves a cost function iteratively, while the algebraic fitting method provides a closed-form solution without any iteration.

Table 2.3. Geometric fitting and algebraic fitting methods for estimation of joint center of rotation (CoR)

Fitting type	Geometric fitting	Algebraic fitting
Description	Minimize the sum of the squares of the distances to given points using Eq. 2.8	Determine the parameters of an algebraic equation in the least squares using Eq. 2.9
Iteration	Yes	No
Initial guess of CoR	Yes	No

Piazza et al., (2004) proposed a geometric fitting method by minimizing a non-linear equation (Eq. 2.8). In the geometric fitting method, an initial guess of joint CoR is required. Then an iterative procedure is needed to find a joint CoR (Al-Sharadqah et al., 2009). Moreover, the number of iterations can be increased if the initial guess of CoR is not properly defined.

$$v = \min \sum_{i=1}^N [(x_i - x_c)^2 + (y_i - y_c)^2 - R]^2 \quad \text{Eq. 2.8}$$

Knight et al. (2010) determined the fixed CoR at big joints (e.g., knee, elbow, shoulder, wrist, and pelvis.) of the human body from a set of motion data using Delonge-Kasa's circle fitting method (Kasa, 1976). The Delonge-Kasa approach algebraically fits a circle by the least square method, in which a fixed joint CoR $C_i(x_c, y_c)$ is determined by minimizing the following least square equation (Eq. 2.9).

$$v = \min \sum_{i=1}^N [(x_i - x_c)^2 + (y_i - y_c)^2 - R^2]^2 \quad \text{Eq. 2.9}$$

where the radius R can be determined directly as

$$R = \frac{1}{n} \sum_{i=1}^n (x_i - x_c) + (y_i - y_c) \quad \text{Eq. 2.10}$$

To examine the corresponding joint motion, Knight picked the marker coordinate that attached at the segment of adjacent bone as landmark to estimate its joint CoR. Al-Sharadqah et al. (2009) reported that Delonge-Kasa method was suffering from providing an accurate CoR when one observes incomplete circular arcs. The Delonge-Kasa method has known to be heavily biased toward small circles (Al-Sharadqah et al., 2009), as shown in Figure 2.10. Surface markers should be appropriately positioned to obtain a trajectory with a large amount of data points and coverage of an arc. Moreover, Kasa (1976) reported that the accuracy can be improved by increasing the number of data points.

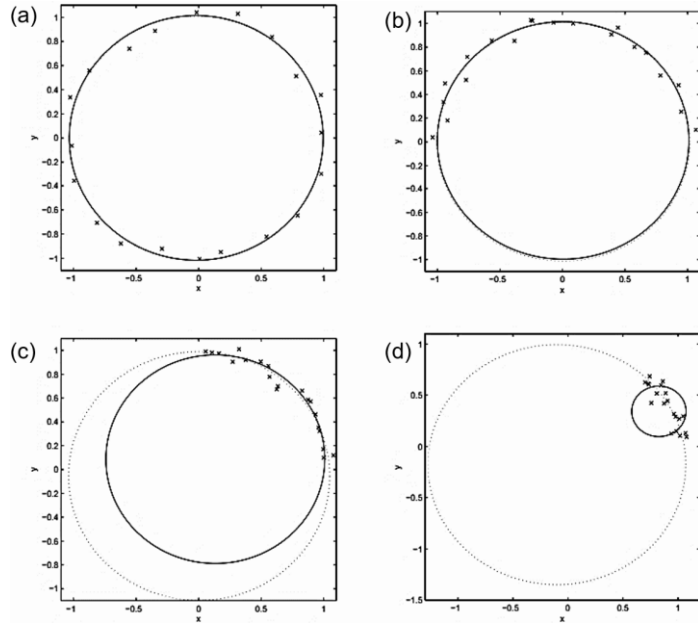


Figure 2.10. Circles (solid) fitted to the points randomly generated at different locations of a circle (dotted) (a) accurate fitting when the points were generated around the entire circle, (b) almost accurate fitting when the points were generated around half of the circle, (c) biased fitting when the points were generated around quarter of the circle, and (d) very biased fitting when the points were generated around 1/8 of the circle (Al-Sharadqah et al., 2009)

Zhang et al. (2003) proposed a different method to estimate joint CoR by minimizing the variation of internal link lengths over F/E movement using the following objective function (Eq. 2.11), where the internal link vector (L_k^i) and the surface link length ($l_k^i(t)$) are described in Figure 2.11. The finger segmental joint

$$J^i = \sum_{k=1}^3 \left\{ \sum_{t=1}^T (|L_k^i| - |l_k^i(t) + d_{k-1}^i(t) - d_k^i(t)|)^2 \right\} \quad \text{Eq. 2.9}$$

CoR can be determined by identifying the constant length (d_k^i) from the surface marker to the corresponding joint CoR, where i represents a finger ($i = 2, \dots, 5$) and k represents the corresponding DIP, PIP, and MCP joints ($k = 1, 2, 3$), respectively. However, Zhang et al.'s method requires a complex computation procedure. A fast, practical, and simple procedure for the estimation of a joint CoR using motion capture data is needed.

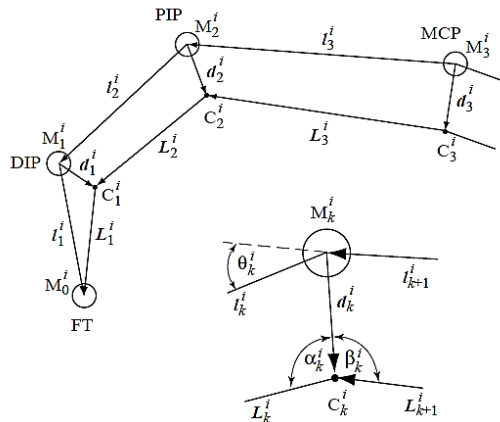


Figure 2.11. Geometric relationship between surface links of metacarpophalangeal (MCP), proximal interphalangeal (PIP), and distal interphalangeal (DIP) joints and their internal links used for estimation of joint center of rotation (Zhang et al., 2003)

Chapter 3 MATERIALS AND METHODS

This chapter introduces the implementation, modification, and development of three groups of joint CoR estimation methods including CT-based, motion-based, and hand anthropometry-based estimation methods.

3.1 CT-Based Joint CoR Estimation Methods

Various methods including Figueroa et al.'s (Figueroa et al., 2016), Reuleaux's (Reuleaux, 1875), Delonge-Kasa's circle-fitting (Kasa, 1976), and bone curvature-based (Fowler et al., 2001) methods were modified and compared for joint CoR estimation using CT scans.

3.1.1 Experiment

Participants

Nine adults (6 males and 3 females) in their 20s to 30s (Table 3.1) having no neurological or musculoskeletal disorders in their dominant hands participated in the CT scan experiment. Participants were grouped into 3 categories according to their hand lengths (small, medium, and large) by referring to the hand length distribution

of Korean population (Size Korea, 2010). The present study was approved by the Institutional Review Board (IRB) of S-Pohang Stroke and Spine Hospital.

Table 3.1. Demographic information of participants in the present study

Hand length distribution	Gender	Age	Hand length (mm)
Large 67 th %ile ~ 95 th %ile: >188.5 mm	Male	29	202.2
	Male	23	191.7
	Male	23	190.2
Medium 34 th %ile ~ 66 th %ile: 178.3~188.4 mm	Male	32	182.9
	Male	26	182.0
	Male	24	179.7
Small 1 st %ile ~ 33 rd %ile: <178.2 mm	Female	24	177.2
	Female	25	175.7
	Female	22	161.9

Apparatus

A CT scanning system ICT256 & Briliance64 (Philips, Netherland) (Figure 3.1.a) was used to scan the hand of a participant at different postures in the CT scan experiment. A posture consisted of 576 to 670 CT slices depending on the hand length of the participant with a resolution of 512×512 pixels and a thickness of 0.44 mm for each slice. A lead-free radiation shielding apron FC001 (Longkou Sanyi Medical Device Co., Ltd., China; Figure 3.1.b) was used to cover the body parts of a

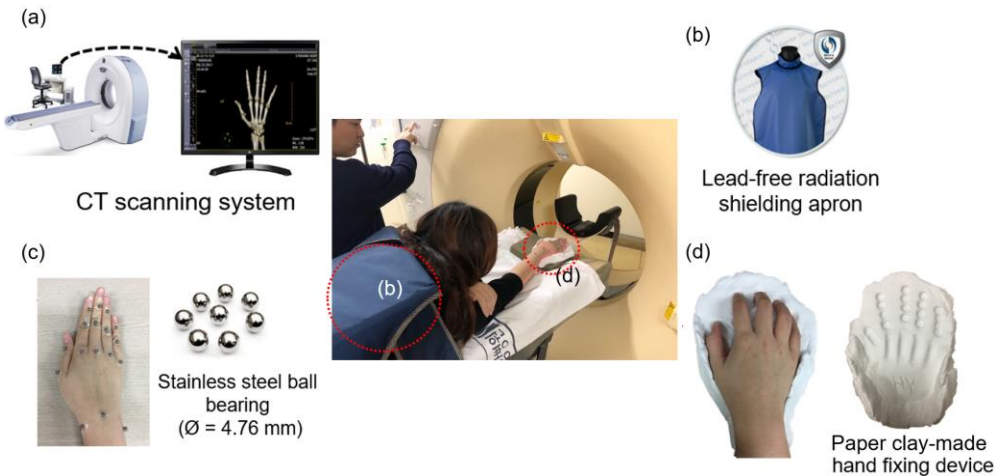


Figure 3.1. Apparatus used in the CT scanning experiment: (a) CT scanning system, (b) radiation shielding apron, (c) stainless steel ball bearing, and (d) hand fixing device

participant to reduce radiation exposure. Seventeen stainless steel ball bearings markers with a diameter of 4.76 mm were attached to the palpable bony landmarks on the dorsum of the participant's hand (Figure 3.1.c) for the alignment of estimated joint CoRs with motion data. A hand posture fixing device was fabricated using paper clay (Figure 3.1.d) for all participants according to their hand lengths and widths to fix their hands during the CT scan.

Experimental Procedure

The CT scan experiment consisted of 3 main stages: (1) preparation of the experiment, (2) the main experiment, and (3) debriefing. The duration of the

experiment was 30 minutes per participant. In the preparation stage, the purposes, procedures, and risk factors of the experiment were explained. Then, the hand fixing device was fabricated using paper clay. After that, participants were allowed to practice to be familiar with the experiment. Lastly, signed informed consents were obtained from the participants.

In the main experiment stage, CT images of a participant's hand were collected by a radiologist at S-Pohang Stroke and Spine Hospital. Before lying on the scanning table of the CT scanner, the palpable bony landmarks on the dorsum of the participant's hand were marked using an oil-based marker pen. Nineteen stainless steel ball bearings were attached to the landmarks using double-sided tape. During the experiment, the participant lied down with the right arm stretched above the head and the hand palm facing down. The hand fixing device was placed on the scanning table to fix the position of the wrist and the hand during the scan. The hand position of the participant was adjusted by the radiologist before the scan. The participant was allowed to practice ten postures (starting from a full extension posture and ending with the fist posture; Figure 3.2) by placing the hand on the fixing device. The radiation shielding apron was put on the participant to cover the body parts after the participant lied down. The participant was told to sustain a hand position during CT scan. After the scan of Posture 1, the stainless steel ball bearings were removed. Then the scan was repeated until all the postures were scanned.



Figure 3.2. Hand postures for CT scan in the present study

3.1.2 CT Data Pre-Processing

As shown in Figure 3.3, a 4-step method was proposed to pre-process the scanned CT data: (1) 3D hand skeleton reconstruction from the CT data for each hand posture, (2) hand skeleton template preparation, (3) registration of the template to other hand skeletons, and (4) alignment of the proximal bone segment at different postures for each hand joint to assess the relative motion of the distal bone segment. Different from the Figueroa et al.'s method, we proposed to use the same bone surface through registration of the template posture to other postures for better estimation of hand joint CoR. Furthermore, Reuleaux's and Delonge-Kasa's methods also require the use of the same bone surface for selection of landmarks at the same location on the bone surface at different postures.

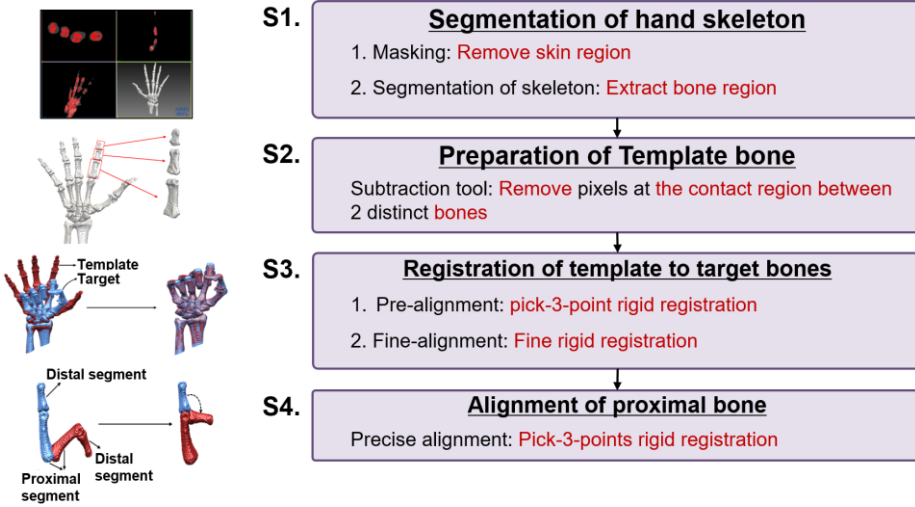


Figure 3.3. Flow chart of a CT scan data pre-processing method

Segmentation and Reconstruction of CT Raw Images

The current step reconstructed a set of 3D skeleton models at different postures from the collected CT scan data. First, the bone area was masked using a 3D sphere at different CT slices by the masking technique in Dr. Liver (Humanopia Co. Ltd, Pohang, Korea; Figure 3.4.b). Then the bone was reconstructed from the masked CT images using a threshold-based segmentation method in Medical Scanning Interaction Toolkit (MITK; Nolden et al., 2013; Figure 3.4.d). All the reconstructed skeleton models (Figure 3.4.e) were exported as the polygon file format (PLY) files.

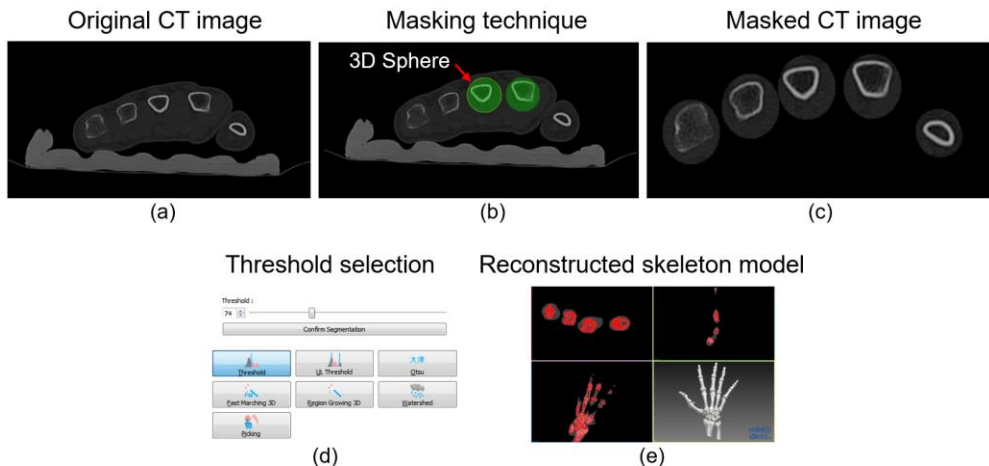


Figure 3.4. Procedure of masking technique and threshold-based segmentation method (by Dr. Liver and MITK): (a) collected CT scan data, (b) masking technique, (c) masked skeleton region, (d) threshold selection, and (e) reconstructed 3D skeleton model

Separation of Bone Segments from the Template Posture

Twenty-nine bone segments from the template posture (Posture 1) were separated (Figure 3.5.a) by removing the connected voxels at the contact region between two neighbouring bone segments using a subtraction tool in MITK (Figure 3.5.b). The separated bone segments from the template posture were then exported as individual PLY files by RapidForm 2006 (Inus Technology, Inc., Korea).

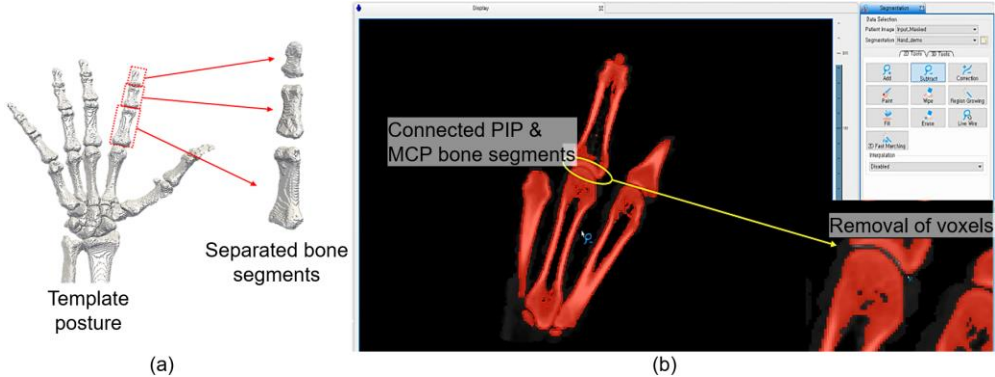


Figure 3.5. Separation of bone segments from the template posture: (a) the template posture and an example of separated bone segments of the index finger, and (b) separation of a metacarpophalangeal (MCP) segment and a proximal interphalangeal (PIP) segment using a subtraction tool in MITK

Rigid Registration of Template Bone Segments to Target Bone Segments

The 29 bone segments of the template posture were registered to those of the remaining 9 postures (Postures 2 to 10) using the rigid registration method in RapidForm 2006. First, three points were selected on each surface of the template and target bone segments at similar locations (Figure 3.6.a). Then, the two bone segments were roughly registered by aligning the three selected points on each of the two segments (Figure 3.6.b). Lastly, a fine registration was performed using the automatic registration method in RapidForm 2006 (Figure 3.6.c). The registered hand skeletons overlaid with the original skeletons of the 9 postures were shown in Figure 3.7.

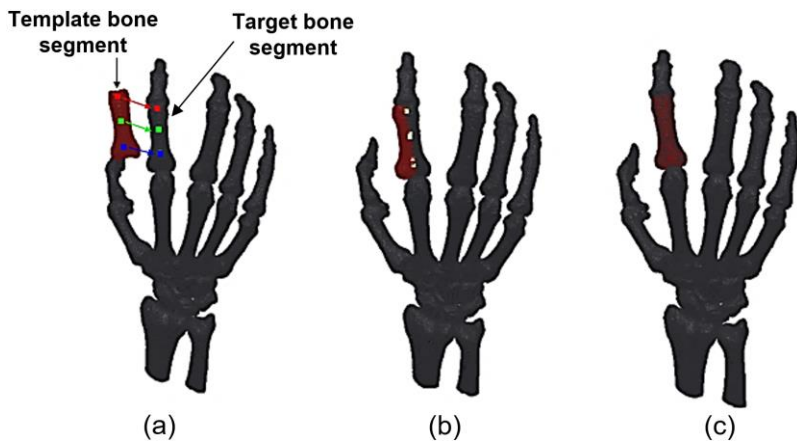


Figure 3.6. Registration of a template bone segment to a target bone segment: (a) selection of 3 points on each surface of the template and target bone segments at similar locations, (b) a rough registration of the two segments by aligning the 3 selected points on each segment, and (c) a fine registration of the two segments

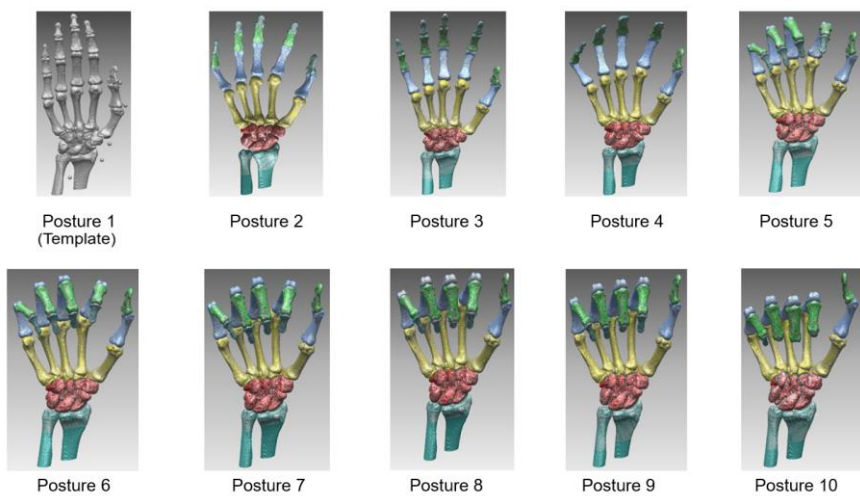


Figure 3.7. Template posture (Posture 1) and the remaining 9 postures (Postures 2 to 10) registered from the template posture

Alignment of Proximal Bone Segments

Proximal bone segments of a joint from Postures 1 to 10 were aligned to assess the relative motion of the distal bone segment of the joint. The proximal bone segments at different postures were aligned (Figure 3.8) using the 3-point registration method described above. The aligned proximal bone segments from Postures 1 to 10 for the MCP, PIP, and DIP joints with the relative motions of their distal bone segments were shown in Figure 3.9.

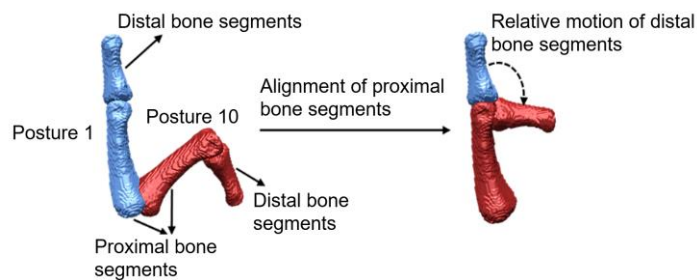


Figure 3.8. Alignment of proximal bone segments of a joint between two postures

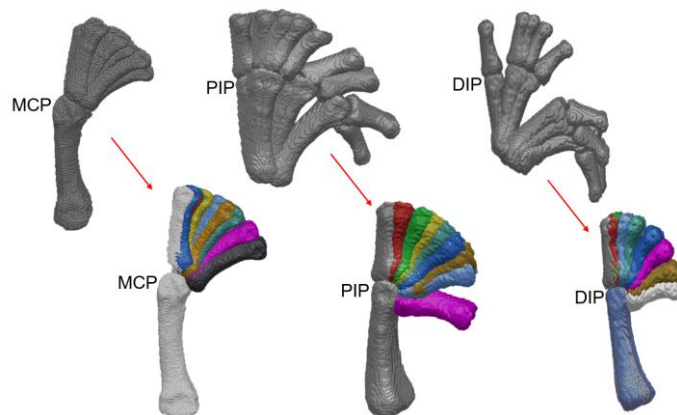


Figure 3.9. Aligned proximal bone segments from Postures 1 to 10 for the metacarpophalangeal (MCP), proximal interphalangeal (PIP), and distal interphalangeal (DIP) joints with the relative motions of their distal bone segments

3.1.3 Modification of Joint CoR Estimation Methods

The four methods including Figueroa et al.'s, Reuleaux's, Delonge-Kasa's, and bone curvature-based methods introduced in Section 2 were modified for CT-based joint CoR estimation. The four modified methods were computerized using Matlab 2018a (MathWorks, Inc., Natick, MA, USA).

Figueroa et al.'s Method

Figueroa et al.'s method was modified into the following steps: (1) bone shaft selection (Figure 3.10.a), (2) centroid determination of each intersection plane along the selected bone shaft (Figure 3.10.b), and (3) bone centerline identification (Figure 3.10.c). First, a bone shaft was selected by removing the head and base portions of a bone segment. Second, a centroid from each plane perpendicular to the bone shaft was determined using the K-mean clustering technique (Kanungo et al., 2002). The K-mean technique minimizes the squared error function (Eq. 3.1). Lastly, a 1st order polynomial function in Matlab (MathWorks, Inc., Natick, MA, USA) was used to linearly fit a line to the identified centroids as the centerline of the bone segment.

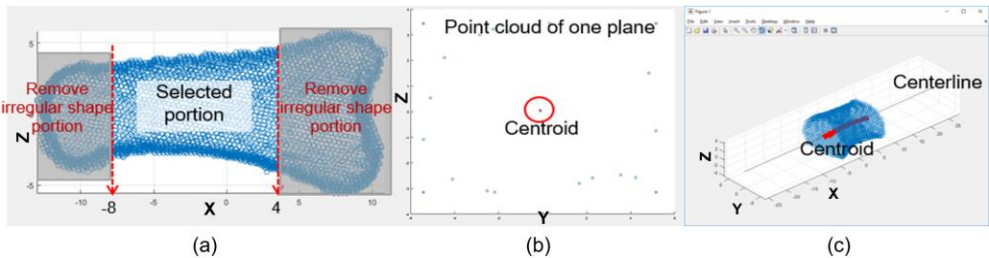


Figure 3.10. Procedure of determining the centerline of a bone segment: (a) selected bone shaft, (b) determined centroid from a plane perpendicular to the bone shaft, and (c) centerline of the bone segment generated by fitting a linear line to the centroids

$$\min \sum_{i=1}^K \sum_{j=1}^{K_i} (\|X_j - V_i\|)^2 \quad \text{Eq. 3.1}$$

Where: K_i = number of data points in the i^{th} cluster

K = number of cluster centers

V_i = centroid of the i^{th} cluster

X_j = data point in the i^{th} cluster

Reuleaux's Method

Reuleaux's method was modified for the selection of landmarks (Figure 3.11.a). Two landmarks (A and B; Figure 3.11.a) were selected at the same locations on each bone surface at different postures, as displayed in Figure 3.11.b. The selection of landmarks were performed in RapidForm 2006.

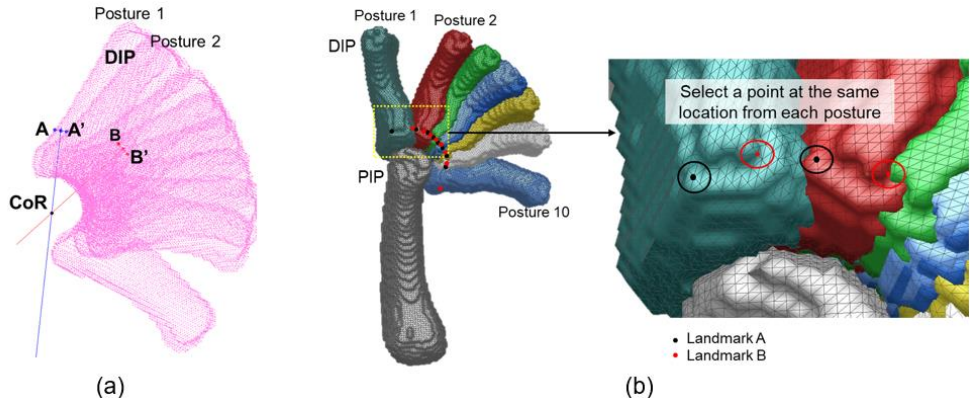


Figure 3.11. Placement of landmarks for a proximal interphalangeal (PIP) joint center of rotation (CoR) estimation using Reuleaux's Method: (a) landmarks A and B placed at the distal interphalangeal (DIP) segment and (b) the two landmarks selected on each bone surface at different postures

Delonge-Kasa's Method

Delonge-Kasa's method was modified for landmark selection. As shown in Figure 3.12, a landmark was selected from the same extremity point of the distal bone head at different postures.

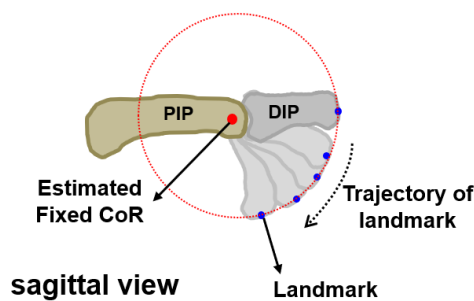


Figure 3.12. Proximal interphalangeal (PIP) joint center of rotation (CoR) estimation using Delonge-Kasa's method by fitting a circle to the motion of landmarks selected at the bone heads of distal interphalanges (DIP) segments

Bone Curvature-Based Method

The bone curvature-based method was modified into the following steps: (1) contour line determination (Figure 3.13), (2) landmarks selection from the contour line (Figure 3.14), and (3) joint CoR identification using the landmarks from the contour line by a tangent method (Figure 3.15; Soudan et al., 1979). First, the contour line of a bone head where joint motion occurs was identified with the starting and the ending points determined by the starting and ending contact points at the posture of full extension and flexion, respectively, in the sagittal view. The contour line was then smoothed using Gaussian-weighted moving average smoothing filter in Matlab (with a smoothing window of approximately 20~30). Second, data points along the smoothed contour line (Figure 3.14.a) were sampled with an equal interval (Figure 3.14.b). The data point having the largest curvature among the sampled data points was defined as landmark A and other landmarks with an equal interval were picked (Figure 3.14.c). Lastly, a tangent line and its normal were drawn at each landmark. The intersection points between the normal lines passing through landmark A and other landmarks were generated (Figure 3.15). Lastly, the K-mean clustering technique ($K = 1$) was then applied to find a centroid among the intersection points as the fixed joint CoR.

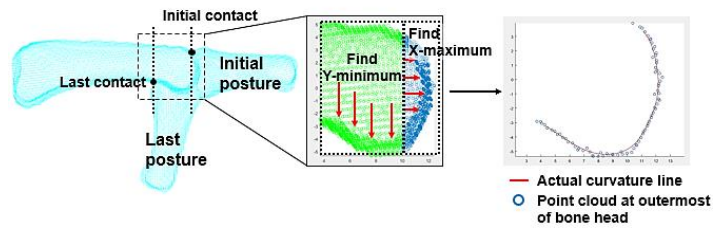


Figure 3.13. Contour identification from a bone head where a joint motion occurs

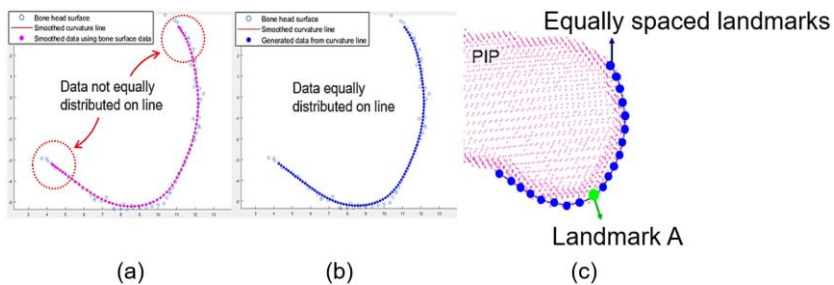


Figure 3.14. Selection of landmarks from the generated contour line of a bone head:
 (a) smoothed data points, (b) sampled data points having equal intervals, and (c)
 selected equally spaced landmarks and landmark A (having largest curvature)

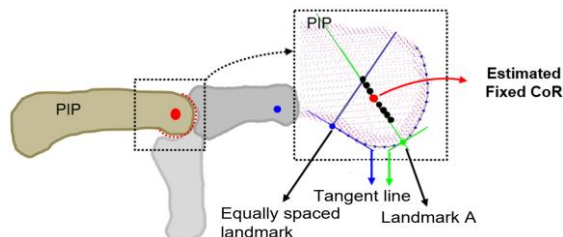


Figure 3.15. Estimation of joint center of rotation by the bone curvature-based
 method as the centroid of the intersection points of the normal lines of the tangent
 lines going through the equally spaced landmarks and landmark A

3.2 Motion-Based Joint CoR Estimation Method

3.2.1 Experiment

Participants

The same participants in the CT scan experiment participated in the motion capture experiment.

Apparatus

A motion analysis system (Figure 3.16.a) consisting of eight Osprey cameras (Motion Analysis Inc, USA; Figure 3.16.b) was used to capture surface motion of the hand at a frequency of 60 Hz. A table and a chair were placed and surrounded by the motion cameras (Figure 3.16.c) for motion capture. A custom-made stick (length = 15 mm) with a retro-reflective marker ($\varnothing = 5$ mm) attached was made and attached to the fingertip to generate a larger motion trajectory of the fingertip (Figure 3.16.d).



Figure 3.16. Apparatus used in the motion capture experiment: (a) motion analysis system, (b) motion cameras, (c) motion camera setup, and (d) marker attachment

Experimental Procedure

The motion capture experiment consisted of 3 main stages: (1) preparation of experiment, (2) main experiment, and (3) debriefing. The duration of the experiment was 40 minutes for each participant. In the preparation stage, a participant was asked to sit comfortably and place his or her hand and forearm on the table. Before the main experiment, the participant was allowed to practice finger motions. To avoid problems such as data missing during the capture or the appearance of ghost markers, the motion of each distal segment was separately captured (Figure 3.18). In the main experiment stage, the participant was asked to fix the proximal segment using the other hand and perform the F/E movement at the distal segment. The participant was asked to repeat each finger motion for 3 times while fixing the wrist and forearm on the table.

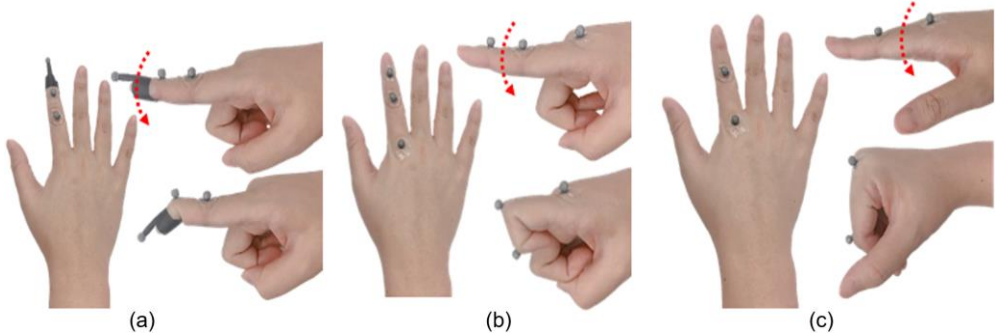


Figure 3.17. Finger flexion/extension (F/E) motions at different joints: (a) fingertip motion for distal interphalangeal (DIP) joint center of rotation (CoR) estimation, (b) DIP segment motion for proximal interphalangeal (PIP) joint CoR estimation, and (c) PIP segment motion for metacarpophalangeal (MCP) joint CoR estimation

3.2.2 Pre-Processing of Motion Data

Alignment of Motion Capture Data with 3D reconstructed Bone Model

A 3-step motion data pre-processing method was proposed to align the motion data with the reconstructed bone models for comparison of the motion-based CoRs with the CT-based CoRs. First, the origin was the marker placed at a joint and the three axes were defined, as shown in Figure 3.18. The X -axis was directed perpendicular to the bone shaft. The Y -axis was parallel to the bone shaft pointing distally, while the Z -axis was perpendicular to the XY -plane pointing dorsally. Second, the motion data and the bone model were transformed to the designated origin and axes, respectively. For the transformation of motion data (Eq. 3.2), the rotation angles (φ , ω , κ) was

obtained using the transformation matrix (M_G ; Eq. 3.4) by satisfying the following constraints: (1) the origin was the marker placed at the proximal joint and (2) the YZ -plane (Figure 3.19) coincides with the plane formed by the origin, the starting and ending points of the trajectory of the surface marker motion. Lastly, the distal surface marker location at each frame of the motion data was transformed by aligning the surface marker locations at the initial frame (full extension posture) from the motion capture data and CT-reconstructed data, respectively, as demonstrated in Figure 3.19.

$$\begin{bmatrix} X' \\ Y' \\ Z' \end{bmatrix} = M_G \begin{bmatrix} X \\ Y \\ Z \end{bmatrix} \quad \text{Eq. 3.2}$$

Where $\begin{bmatrix} X' \\ Y' \\ Z' \end{bmatrix}$ = transformed coordinates of the motion data

$\begin{bmatrix} X \\ Y \\ Z \end{bmatrix}$ = coordinates of the motion data

$$M_G = \begin{bmatrix} \cos \varphi \cos \kappa & \cos \omega \sin \kappa + \sin \omega \sin \varphi \cos \kappa & \sin \omega \sin \kappa - \cos \omega \sin \varphi \cos \kappa \\ -\cos \varphi \sin \kappa & \cos \omega \cos \kappa - \sin \omega \sin \varphi \sin \kappa & \sin \omega \cos \kappa + \cos \omega \sin \varphi \sin \kappa \\ \sin \varphi & -\sin \omega \cos \varphi & \cos \omega \cos \varphi \end{bmatrix} \quad \text{Eq. 3.3}$$

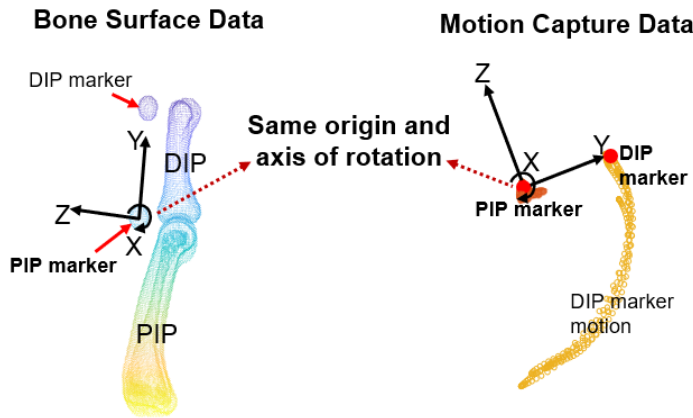


Figure 3.18. Transformation of bone surface data and motion capture data to have the same designated origin and axes at the markers placed at the surface of the proximal interphalangeal (PIP) joint

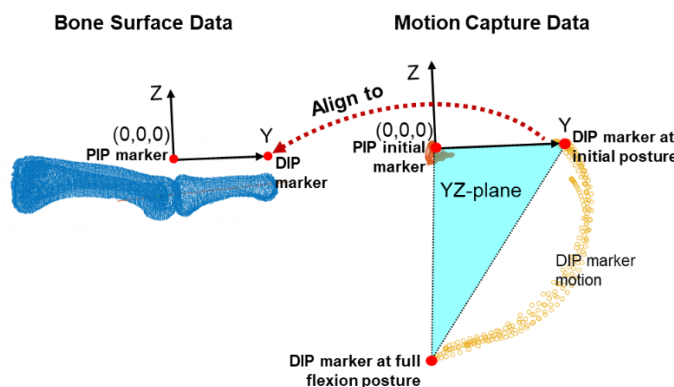


Figure 3.19. Transformation of the distal interphalangeal (DIP) surface marker location at each frame from the motion capture data by aligning the surface marker locations at the initial frame (full extension posture) from the motion capture data and CT-reconstructed data, respectively

3.2.3 Joint CoR Estimation Method

The present study applied Delonge-Kasa's method to estimate a finger joint CoR using an adjacent surface marker motion to the hand joint (Figure 3.20) and validated the estimated joint CoRs by comparison with the CT-based joint CoRs (Figure 3.21). As displayed in Figure 3.20, the marker of PIP joint showed least and linear motion compared to that of the DIP joint. The estimated joint CoR using the PIP marker motion was located near to the skin surface (marked in green in Figure 3.20), which was obviously incorrect, while the use of the DIP marker motion provided accurate estimation of joint CoR (marked in blue in Figure 3.20). To validate the estimated joint CoR, the location of the motion-based joint CoR was compared to that of the CT-based joint CoR, as shown in Figure 3.21.

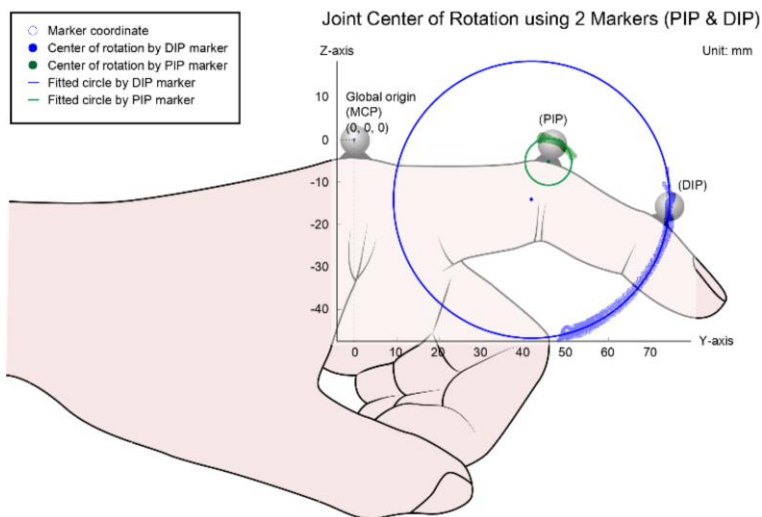


Figure 3.20. Estimated proximal interphalangeal (PIP) joint centers of rotation by Delonge-Kasa's method using surface marker motion at the proximal interphalangeal (PIP; green) and distal interphalangeal (DIP; blue) joints

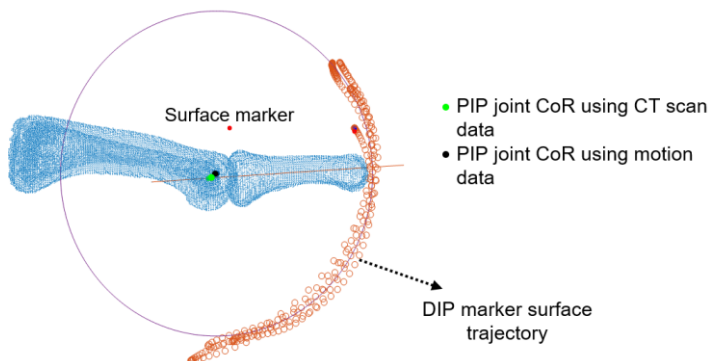


Figure 3.21. Estimated proximal interphalangeal (PIP) joint centers of rotation (CoRs) by Delonge-Kasa's method using motion data and CT scan data (DIP: distal interphalangeal)

3.3 Hand Anthropometry-Based Joint CoR Estimation Method

In the present study, geometric analysis and regression analysis were performed to establish formulas for estimation of fixed joint CoR using hand anthropometric data were proposed.

3.3.1 Dependent Variable

The fixed joint CoRs estimated from CT scans by Delonge-Kasa's method were selected as the dependent variable.

3.3.2 Independent Variables

Hand anthropometric data including segment length from the landmark on the CMC joint to that on the MCP joint ($SL_{CMC-MCP}^i; i = \text{digit } 2 \sim 5$), the finger joint depth ($JD_j^i; j = \text{MCP, PIP, or DIP joints}$), angle between the segment of CMC-MCP joint of the middle finger and that of the another finger (α^i), and the perpendicular length from the landmark on the CMC joint to that on the corresponding joint ($PL_{CMC_Marker_j}^i$) (Figure 3.22) were selected as independent variables. The hand anthropometric data were measured from thirty landmarks on the palpable bony landmarks of the reconstructed hand model at Posture 1 using RapidForm 2006 (Figure 3.23).

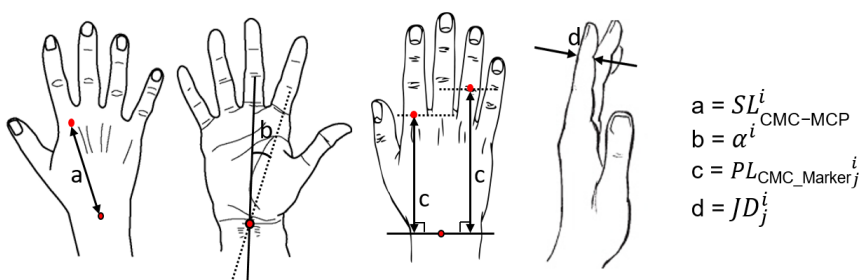


Figure 3.22. Hand anthropometric dimensions: (a) segment length from the landmark on the carpometacarpal (CMC) joint to the corresponding metacarpophalangeal (MCP) joint ($SL_{CMC-MCP}^i$; $i = \text{digit } 2\sim 5$), (b) angle between the segment of CMC-MCP joint of the middle finger and that of another finger (α^i), (c) perpendicular length from the landmark on the CMC joint to that on the corresponding joint ($PL_{CMC_Marker}^i$; $j = \text{MCP, proximal interphalangeal (PIP), distal interphalangeal (DIP) joints}$), and (d) finger joint depth (JD_j^i)

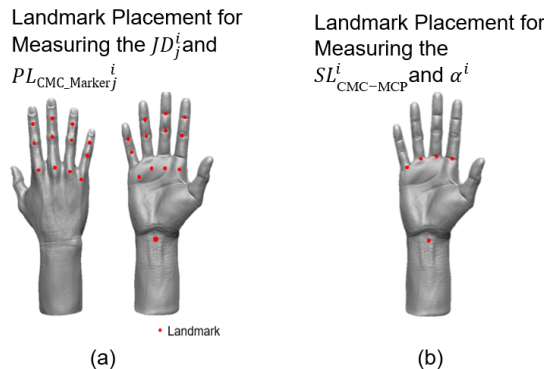


Figure 3.23. Landmarks placement on the surface of the bone model for measuring (a) the finger joint depth (JD_j^i ; $i = \text{digit } 2\sim 5$; $j = \text{metacarpophalangeal (MCP), proximal interphalangeal (PIP), distal interphalangeal (DIP) joints}$), the perpendicular length from the landmark on the carpometacarpal (CMC) joint to that on the corresponding joint ($PL_{CMC_Marker}^i$), (b) the segment length from landmark on the CMC joint to that on the (MCP) joint ($SL_{CMC-MCP}^i$), and the angle between the segment of CMC-MCP joint of the middle finger and that of another finger (α^i)

3.3.3 Joint CoR Estimation Using Hand Anthropometry

The x coordinate of a Joint CoR

The x coordinate of the joint CoR was calculated using a deterministic solution based on the sine rule for the right-angled triangle as shown in Figure 3.24. For example, the x coordinate of the MCP joint CoR of the index finger can be calculated by using the following equation:

$$X_{\text{CoR}_{\text{MCP}}}^2 = SL_{\text{CMC-MCP}}^2 \sin \alpha^2 \quad \text{Eq. 3.4}$$

Where $SL_{\text{CMC-MCP}}^2$ = the segment length from the CMC to MCP joint for digit 2

α^2 = the angle between Segment $^3_{\text{CMC-MCP}}$ and Segment $^i_{\text{CMC-MCP}}$ for digit 2

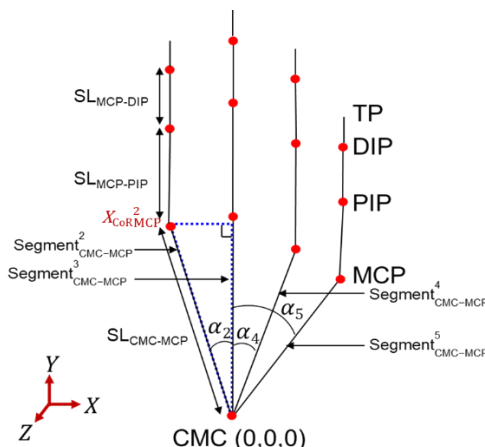


Figure 3.24. Estimation of x coordinate of metacarpophalangeal (MCP) joint center of rotation of digit 2 ($X_{\text{CoR}_{\text{MCP}}^2}$) using the sine rule for right-angled triangle (CMC: carpometacarpal; PIP: proximal interphalangeal; DIP: distal interphalangeal joints; TP: fingertip)

The y and z coordinates of a Joint CoR

Regression analysis was applied to analyse the relationship between a selected hand anthropometric measures and the y and z coordinates of the joint CoR using Minitab 14 (Minitab Inc., USA). The perpendicular length from the joint to the horizontal line going through the CMC joint ($PL_{\text{CMC}_j}^i$) was selected as an independent variable for the y coordinate of joint CoR ($Y_{\text{CoR}_j^i}$) (Figure 3.25). While the finger joint depth (JD_j^i) was selected as an independent variable for the z coordinate of joint CoR ($Z_{\text{CoR}_j^i}$) (Figure 3.26).

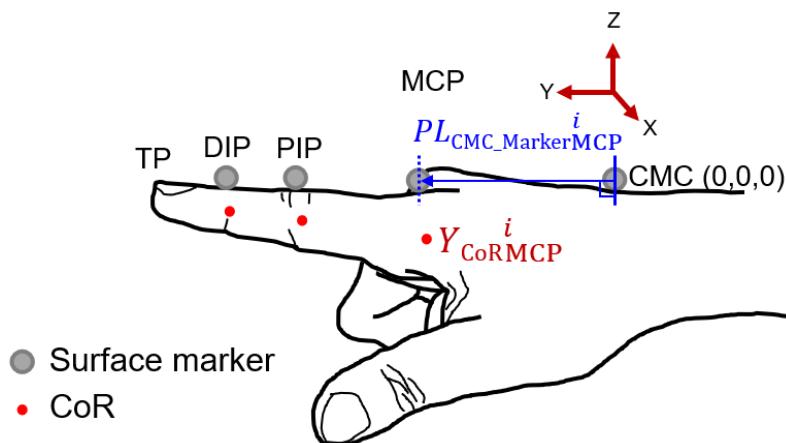


Figure 3.25. Estimation of y coordinate ($Y_{\text{CoR}_{\text{MCP}}^i}$) of metacarpophalangeal (MCP) joint center of rotation (CoR) for digit i using the perpendicular length from the joint to the horizontal line going through the carpometacarpal (CMC) joint ($PL_{\text{CMC}_\text{Marker} \text{MCP}}^i$) (PIP: proximal interphalangeal; DIP: distal interphalangeal; TP: fingertip)

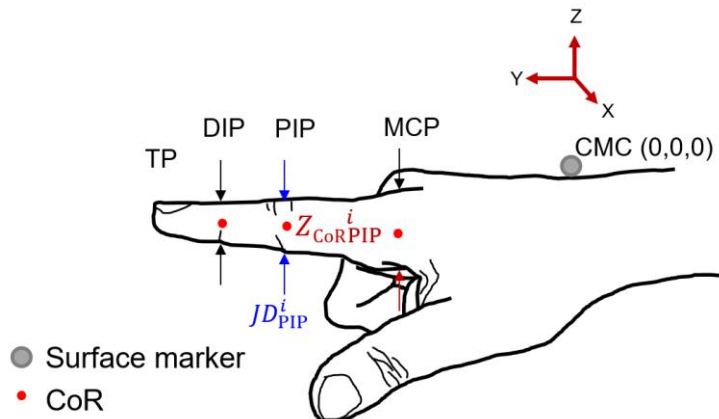


Figure 3.26. Estimation of z coordinate ($Z_{\text{CoR}_{\text{PIP}}^i}$) of proximal interphalangeal (PIP) joint center of rotation (CoR) using the PIP joint depth for digit i (JD_{PIP}^i) (CMC: carpometacarpal; MCP: metacarpophalangeal; DIP: distal interphalangeal; TP: fingertip)

Chapter 4 RESULTS

4.1 Estimated Joint CoRs Based on CT Scans

Evaluation of Instantaneous Joint CoR Estimation Methods

The instantaneous hand joints CoRs of nine participants were estimated using the Figueroa et al.'s and Reuleaux's methods. Forty-five instantaneous CoR results were identified at each joint (Figure 4.1) and represented in a 3D coordinate system (see Appendix E for the full results). For participant 8 (P8), CT data of Posture 8 were excluded due to data missing caused by hand movement during CT scan. Thus, for P8, only 36 instantaneous CoRs were estimated at each joint. The mean distance (variation) among all instantaneous joint CoRs and its standard error (SE) calculated by Eqs. 4.1 and 4.2, respectively, were used to investigate the accuracy of the estimated joint CoRs. The smaller the variation of the estimated joint CoRs, the more accurate the estimated joint CoRs are. Paired *t*-test was conducted ($\alpha = 0.001$) to compare the differences of the variation of the estimated instantaneous joint CoRs between Figueroa et al.'s and Reuleaux's methods.

$$\text{Mean distance of estimated joint CoR} = \frac{\sum_{i=1}^N \sum_{i \neq j} |X_i - X_j|^2}{C_N^2} \quad \text{Eq. 4.1}$$

where: N = the number of postures used for joint CoR estimation

X_i = the estimated joint CoR for posture i

C_N^2 = the number of all possible combinations of two estimated joint CoRs

chosen from N

$$\text{Standard error} = \sqrt{\frac{\sum_{i=1}^N (X_i - \bar{X})^2}{N-1}} \quad \text{Eq. 4.2}$$

where: N = the number of calculated distances between two estimated joint CoRs

X_i = the i^{th} distance

\bar{X} = the mean distance among the estimated joint CoRs

Estimated Instantaneous Joint CoRs

The instantaneous joint CoRs of the MCP, PIP, and DIP joints of the four fingers (2 to 5) at different postures were estimated by the Figueroa et al.'s and Reuleaux's methods for all the participants. For example, as shown in Figure 4.1, estimated instantaneous CoRs of the MCP, PIP, and DIP joints of the middle finger for participant 1 (P1) were illustrated. At each joint, mean distance \pm SE of the estimated instantaneous joint CoRs were measured.

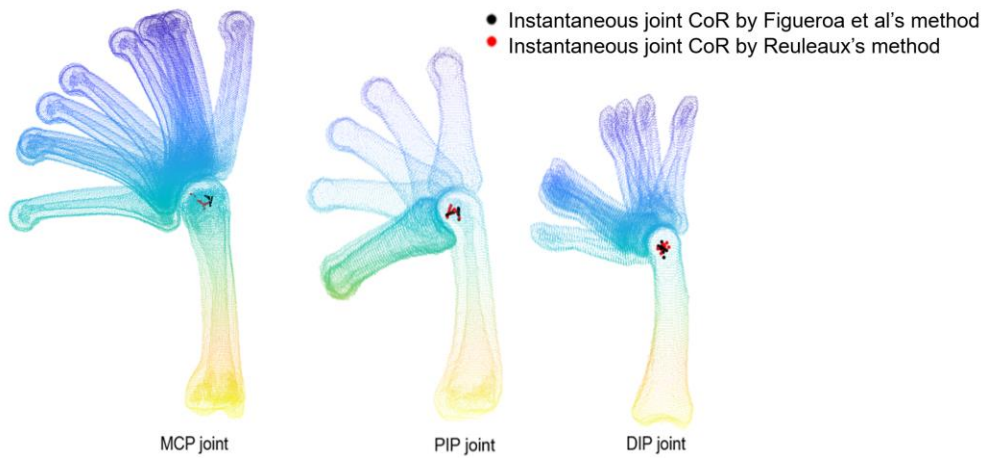


Figure 4.1. Estimated instantaneous joint centers of rotation (CoRs) of metacarpophalangeal (MCP), proximal interphalangeal (PIP), and distal interphalangeal (DIP) for the middle finger

Figueroa et al.'s method showed a significantly lower mean distance of the estimated MCP joint CoRs for the index, middle, ring, and little fingers than Reuleaux's method as shown in Figure 4.2. At the MCP joint of the index finger, the mean distance \pm SE (1.6 ± 1.2 mm) of Figueroa et al.'s method was 80% lower than that (7.8 ± 15.4 mm) of Reuleaux's method ($t(989) = -12.9, p < 0.001$). At the MCP joint of the middle finger, the mean distance \pm SE (1.1 ± 1.9 mm) of Figueroa et al.'s method was 31% lower than that (1.6 ± 1.4 mm) of Reuleaux's method ($t(989) = -9.5, p < 0.001$). At the MCP joint of the ring finger, the mean distance \pm SE (1.1 ± 0.8 mm) of the Figueroa et al.'s method was 16% lower than that (1.3 ± 1.0 mm) of Reuleaux's method ($t(989) = -8.0, p < 0.001$). At the MCP joint of the little finger,

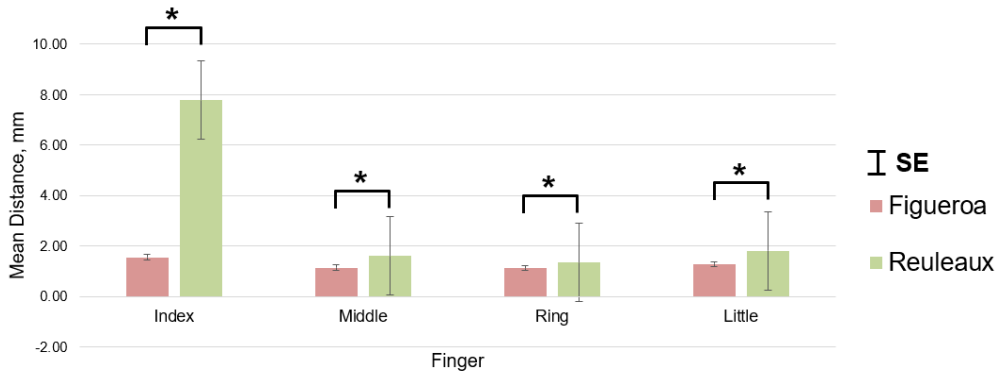


Figure 4.2. Comparison of mean distances of the estimated instantaneous metacarpophalangeal (MCP) joint centers of rotation by Figueroa et al.'s and Reuleaux's methods for participant 1 ($*p < 0.001$)

the mean distance \pm SE (1.3 ± 1.2 mm) of Figueroa et al.'s method was 28% lower than that (1.8 ± 1.4 mm) of Reuleaux's method ($t(989) = -17.2, p < 0.001$).

Figueroa et al.'s method showed significantly lower mean distance of the estimated PIP joint CoRs for the middle, ring, and little fingers than Reuleaux's method as shown in Figure 4.3. At the PIP joint of the index finger, the mean distance \pm SE (6.4 ± 8.3 mm) of Figueroa et al.'s method was similar to that (6.4 ± 8.9 mm) of Reuleaux's method ($t(989) = 0, p = 0.998$). At the PIP joint of the middle finger, the mean distance \pm SE (5.8 ± 13.3 mm) of Figueroa et al.'s method was 46% lower than that (10.7 ± 25.6 mm) of Reuleaux's method ($t(989) = -10.1, p < 0.001$). At the PIP joint of the ring finger, the mean distance \pm SE (4.0 ± 5.4 mm) of Figueroa et al.'s method was 8% lower than that (4.3 ± 6.6 mm) of Reuleaux's method ($t(989) = -9.5,$

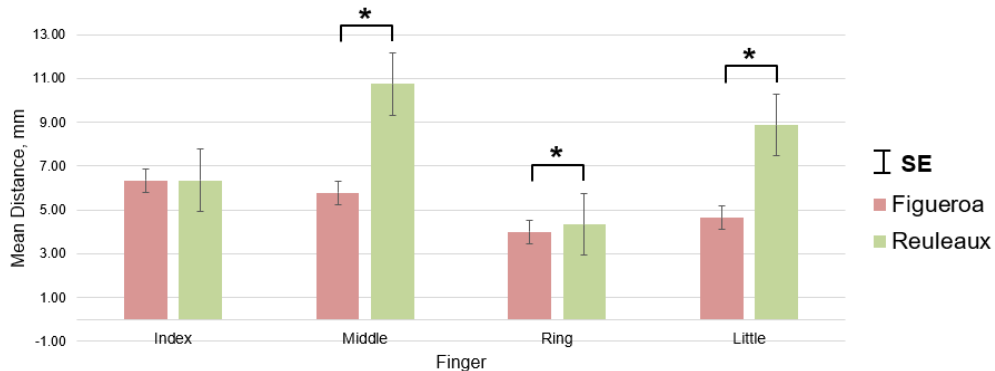


Figure 4.3. Comparison of mean distances of the estimated instantaneous proximal interphalangeal (PIP) joint centers of rotation by Figueroa et al.’s and Reuleaux’s methods for participant 1 (* $p < 0.001$)

$p < 0.001$). At the PIP joint of the little finger, the mean distance \pm SE (4.6 ± 10.5 mm) of Figueroa et al.’s method was 48% lower than that (8.9 ± 32.4 mm) of Reuleaux’s method ($t(989) = -5.8, p < 0.001$).

Figueroa et al.’s method showed significantly lower mean distance of the estimated DIP joint CoRs for the index, middle, ring, and little fingers than Reuleaux’s method as shown in Figure 4.4. At the DIP joint of the index finger, the mean distance \pm SE (0.7 ± 0.8 mm) of Figueroa et al.’s method was 36% lower than that (1.1 ± 1.1 mm) of Reuleaux’s method ($t(989) = -18.9, p < 0.001$). At the DIP joint of the middle finger, the mean distance \pm SE (0.3 ± 0.4 mm) of Figueroa et al.’s method was 25% lower than that (0.4 ± 0.4 mm) of Reuleaux’s method ($t(989) = -2.9, p = 0.004$). At the DIP joint of the ring finger, the mean distance \pm SE (0.4 ± 0.4

mm) of Figueroa et al.'s method was 33% lower than that (0.6 ± 0.6 mm) of Reuleaux's method ($t(989) = -14.8, p < 0.001$). At the DIP joint of the little finger, the mean distance \pm SE (1.8 ± 3.2 mm) of Figueroa et al.'s method was 10% lower than (2.0 ± 3.9 mm) of Reuleaux's method ($t(989) = 2.84, p = 0.005$). In summary, Figueroa et al.'s method showed a significantly lower mean distances among the estimated joint CoRs at 102 out of 108 hand joints than Reuleaux's method, as displayed in Table 4.1.

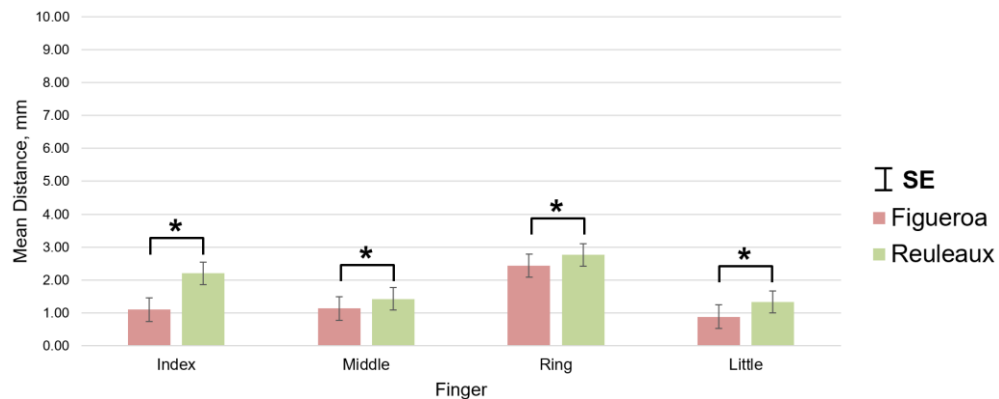


Figure 4.4. Comparison of the mean distances of the estimated instantaneous distal interphalangeal (DIP) joint centers of rotation by Figueroa et al.'s and Reuleaux's methods for participant 1 (* $p < 0.001$)

Table 4.1. Summary of paired *t*-test results: Differences in the mean distance between Figueroa et al.'s and Reuleaux's methods
 (degree of freedom = 989 for all the participants except participant 8 and 967 for participant 8)

Participant (Hand category)	MCP Joint				PIP Joint				DIP Joint			
	Index finger	Middle finger	Ring finger	Little finger	Index finger	Middle finger	Ring finger	Little finger	Index finger	Middle finger	Ring finger	Little finger
P1 (Large)	$t = -12.91$ $p < 0.05$	$t = -9.49$ $p < 0.05$	$t = -8.02$ $p < 0.05$	$t = -17.24$ $p < 0.05$	$t = 0.00$ $p = 0.998$	$t = -10.13$ $p < 0.05$	$t = 9.51$ $p < 0.05$	$t = 5.77$ $p < 0.05$	$t = -18.86$ $p < 0.05$	$t = -2.89$ $p = 0.004$	$t = -14.81$ $p < 0.05$	$t = 2.84$ $p = 0.005$
P2 (Large)	$t = -29.82$ $p < 0.05$	$t = -15.10$ $p < 0.05$	$t = -5.09$ $p < 0.05$	$t = -31.82$ $p < 0.05$	$t = -7.57$ $p < 0.05$	$t = 1.40$ $p = 0.162$	$t = 2.19$ $p = 0.029$	$t = -8.32$ $p < 0.05$	$t = -7.74$ $p < 0.05$	$t = -8.17$ $p < 0.05$	$t = -18.11$ $p < 0.05$	$t = -24.55$ $p < 0.05$
P3 (Large)	$t = -8.37$ $p < 0.05$	$t = -18.42$ $p < 0.05$	$t = -9.66$ $p < 0.05$	$t = -8.60$ $p < 0.05$	$t = -3.02$ $p = 0.003$	$t = -13.22$ $p < 0.05$	$t = 14.34$ $p < 0.05$	$t = -13.39$ $p < 0.05$	$t = 1.89$ $p = 0.059$	$t = -7.39$ $p < 0.05$	$t = -8.66$ $p < 0.05$	$t = -17.24$ $p < 0.05$
P4 (Medium)	$t = -7.21$ $p < 0.05$	$t = -19.16$ $p < 0.05$	$t = -13.73$ $p < 0.05$	$t = -9.52$ $p < 0.05$	$t = 8.47$ $p < 0.05$	$t = -10.75$ $p < 0.05$	$t = 6.74$ $p < 0.05$	$t = -6.82$ $p < 0.05$	$t = -13.10$ $p < 0.05$	$t = -0.01$ $p = 0.995$	$t = -6.54$ $p < 0.05$	$t = -11.90$ $p < 0.05$
P5 (Medium)	$t = -15.86$ $p < 0.05$	$t = -15.42$ $p < 0.05$	$t = -2.66$ $p = 0.008$	$t = -8.93$ $p < 0.05$	$t = -14.79$ $p < 0.05$	$t = -5.30$ $p < 0.05$	$t = -8.42$ $p < 0.05$	$t = -16.32$ $p < 0.05$	$t = 7.05$ $p < 0.05$	$t = 6.44$ $p < 0.05$	$t = 6.33$ $p < 0.05$	$t = -15.86$ $p < 0.05$
P6 (Medium)	$t = -6.80$ $p < 0.05$	$t = -4.81$ $p < 0.05$	$t = -21.18$ $p < 0.05$	$t = -11.80$ $p < 0.05$	$t = 8.54$ $p < 0.05$	$t = 2.60$ $p = 0.009$	$t = 12.61$ $p < 0.05$	$t = -6.98$ $p < 0.05$	$t = -16.19$ $p < 0.05$	$t = -9.27$ $p < 0.05$	$t = -10.38$ $p < 0.05$	$t = -14.12$ $p < 0.05$
P7 (Small)	$t = -14.93$ $p < 0.05$	$t = -5.13$ $p < 0.05$	$t = -7.50$ $p < 0.05$	$t = 8.58$ $p < 0.05$	$t = 33.48$ $p < 0.05$	$t = 8.35$ $p < 0.05$	$t = 14.79$ $p < 0.05$	$t = -9.12$ $p < 0.05$	$t = -21.83$ $p < 0.05$	$t = -8.09$ $p < 0.05$	$t = -2.85$ $p = 0.002$	$t = -3.03$ $p < 0.05$
P8 (Small)	$t = -18.70$ $p < 0.05$	$t = -21.12$ $p < 0.05$	$t = -38.80$ $p < 0.05$	$t = -4.80$ $p < 0.05$	$t = -25.00$ $p < 0.05$	$t = 0.84$ $p = 0.404$	$t = -9.00$ $p < 0.05$	$t = -9.26$ $p < 0.05$	$t = -8.96$ $p < 0.05$	$t = -8.21$ $p < 0.05$	$t = -6.49$ $p < 0.05$	$t = -11.89$ $p < 0.05$
P9 (Small)	$t = -17.26$ $p < 0.05$	$t = -3.00$ $p = 0.003$	$t = -13.40$ $p < 0.05$	$t = -16.49$ $p < 0.05$	$t = -14.10$ $p < 0.05$	$t = -16.13$ $p < 0.05$	$t = -5.58$ $p < 0.05$	$t = -6.64$ $p < 0.05$	$t = -13.27$ $p < 0.05$	$t = -11.30$ $p < 0.05$	$t = -10.98$ $p < 0.05$	$t = -1.38$ $p = 0.169$

Shaded area : $p < 0.05$

Evaluation of Fixed Joint CoR Estimation Methods

The performance of the four methods including Figueroa et al.'s, Reuleaux's, Delonge-Kasa's, and bone curvature-based methods in estimation of fixed joint CoRs was evaluated in terms of mean distance \pm SE among the four estimated fixed joint CoRs from the four methods for each joint. The centroid of all the instantaneous CoRs of a joint (estimated by Reuleaux's and Delonge-Kasa's methods respectively) was identified by the K-mean clustering method to obtain a fixed CoR for the joint. As shown in Table 4.2, mean distance among the estimated fixed joint CoRs by the four methods was smaller than 2.0 mm at the majority of the joints. To determine which method achieved the best performance, the centroid of the four estimated fixed CoRs by the four methods at a joint with a mean distance larger than 2.0 mm was identified, as shown in Figure 4.5. Then the distances of the four estimated fixed CoRs to the identified centroid at that joint were calculated respectively, as shown in Table 4.3. Among all the joints having a mean distance larger than 2.0 mm, the method that achieved the smallest mean distance between its estimated fixed CoR to the centroid was considered the most accurate method for estimation of fixed joint CoRs. Table 4.3 showed that Delonge-Kasa's method achieved the smallest mean distance (1.38 ± 1.08 mm) and therefore the most accurate method for fixed joint CoR estimation.

Table 4.2. Mean distance \pm SE among four fixed CoRs estimated by Figueroa et al.'s, Reuleaux's, Delonge-Kasa's, and bone curvature-based methods at each joint of 9 participants

Participant (Hand category)	MCP Joint				PIP Joint				DIP Joint			
	Index finger	Middle finger	Ring finger	Little finger	Index finger	Middle finger	Ring finger	Little finger	Index finger	Middle finger	Ring finger	Little finger
P1 (Large)	0.75 \pm 0.34	1.59 \pm 0.64	1.70 \pm 0.77	1.95 \pm 0.95	0.49 \pm 0.28	0.58 \pm 0.25	1.03 \pm 0.47	0.51 \pm 0.36	0.71 \pm 0.30	0.77 \pm 0.47	0.37 \pm 0.21	0.34 \pm 0.21
P2 (Large)	2.01 \pm 0.72	1.11 \pm 0.55	1.56 \pm 0.72	1.39 \pm 0.41	0.71 \pm 0.37	0.28 \pm 0.13	0.54 \pm 0.29	0.30 \pm 0.15	0.41 \pm 0.12	0.71 \pm 0.21	0.73 \pm 0.18	0.53 \pm 0.15
P3 (Large)	0.75 \pm 0.34	1.40 \pm 0.62	1.00 \pm 0.81	1.62 \pm 0.45	0.41 \pm 0.12	0.41 \pm 0.20	0.33 \pm 0.08	1.24 \pm 0.67	0.46 \pm 0.16	0.43 \pm 0.13	0.25 \pm 0.09	0.79 \pm 0.38
P4 (Medium)	3.38 \pm 1.20	1.21 \pm 0.48	1.68 \pm 0.68	1.16 \pm 0.39	0.25 \pm 0.12	0.46 \pm 0.16	0.39 \pm 0.12	0.54 \pm 0.26	0.84 \pm 0.27	0.62 \pm 0.21	0.49 \pm 0.23	0.28 \pm 0.17
P5 (Medium)	3.06 \pm 1.08	0.88 \pm 0.43	1.12 \pm 0.32	1.93 \pm 1.03	0.75 \pm 0.37	0.33 \pm 0.13	0.49 \pm 0.19	0.83 \pm 0.47	0.78 \pm 0.22	1.09 \pm 0.37	1.15 \pm 0.52	0.49 \pm 0.17
P6 (Medium)	1.52 \pm 0.49	1.22 \pm 0.66	1.62 \pm 0.89	1.55 \pm 0.71	0.42 \pm 0.19	0.35 \pm 0.15	0.08 \pm 0.04	0.29 \pm 0.08	0.39 \pm 0.23	0.67 \pm 0.22	0.25 \pm 0.12	0.29 \pm 0.09
P7 (Small)	2.02 \pm 0.56	1.57 \pm 0.35	2.28 \pm 0.73	1.35 \pm 0.72	0.49 \pm 0.24	0.70 \pm 0.43	0.67 \pm 0.28	0.49 \pm 0.17	0.60 \pm 0.25	0.60 \pm 0.33	0.34 \pm 0.16	0.25 \pm 0.10
P8 (Small)	1.97 \pm 0.88	0.87 \pm 0.39	0.70 \pm 0.31	1.21 \pm 0.54	1.00 \pm 0.45	0.85 \pm 0.38	0.73 \pm 0.33	0.31 \pm 0.14	0.63 \pm 0.44	0.50 \pm 0.21	0.47 \pm 0.24	0.45 \pm 0.16
P9 (Small)	2.31 \pm 0.83	0.86 \pm 0.45	0.97 \pm 0.35	1.03 \pm 0.27	0.16 \pm 0.10	0.36 \pm 0.18	0.45 \pm 0.20	0.66 \pm 0.59	0.77 \pm 0.42	0.74 \pm 0.31	0.85 \pm 0.34	0.29 \pm 0.14

MCP: metacarpophalangeal, PIP: proximal interphalangeal, DIP: distal interphalangeal

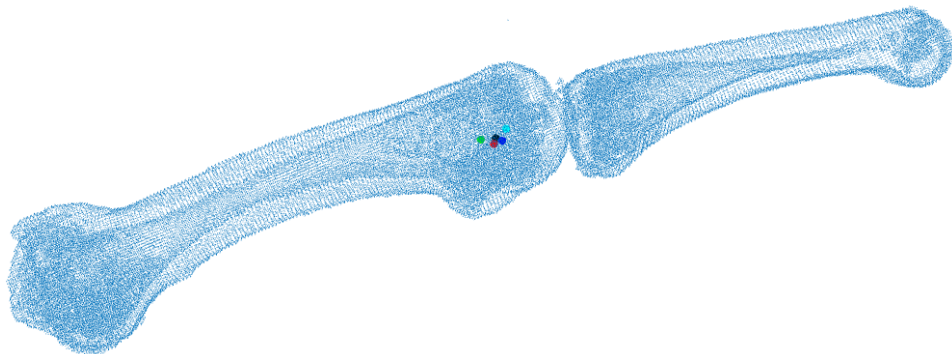


Figure 4.5. Identification of a centroid (black dot) from four estimated fixed CoRs of a joint by Figueroa et al's (cyan), Reuleaux's (blue), Delonge-Kasa's (red), and bone curvature-based (green) methods

Table 4.3. Distances of four fixed center of rotations (CoRs) estimated by Figueroa et al.'s, Reuleaux's, Delonge-Kasa's, and bone curvature-based methods to the centroid of the four CoRs at a joint having a mean distance larger than 2.0 mm among each other

Participant: Joint (Digit)	Distances of CoRs by various methods to the centroid			
	Delonge- Kasa's	Figueroa et al's	Reuleaux's	Bone curvature- based
P2: MCP (2)	0.69	1.64	0.79	1.75
P4: MCP (2)	3.70	1.71	3.34	4.48
P5: MCP (2)	1.25	1.40	2.00	1.41
P7: MCP (2)	0.78	0.85	1.58	1.66
P7: MCP (4)	0.54	1.66	1.38	1.91
P9: MCP (2)	1.30	1.49	1.01	2.03
Mean	1.38	1.46	1.68	2.21
SD	1.08	0.29	0.84	1.04

Bolded values: Smallest distance between estimated joint CoR and centroid, MCP: metacarpophalangeal

4.2 Estimated Joint CoR Based on Surface Motion Capture

Method

Distance between the fixed CoR estimated by Delonge-Kasa's method based on motion capture and that estimated by Delonge-Kasa's method based on CT scan at each joint of all participants was calculated to evaluate the performance of the motion-based method for fixed joint CoR estimation. The rotation angle from the starting posture to the ending posture in motion capture for each joint was also measured to access the effect of rotation angle on the performance of fixed CoR estimation.

Results

As shown in Table 4.7, for the MCP joints of the four fingers, 78% of the motion-based CoRs were found close to the CT-based CoRs with a distance smaller than 4.0 mm. For the PIP joints, 95% of the motion-based CoRs were found close to the CT-based CoRs with a distance smaller than 3.0 mm. For the DIP joints, 78% of the motion-based CoRs were found close to the CT-based CoRs with a distance smaller than 3.0 mm. Large errors (distance > 7.0 mm; bolded values in Table 4.4) of motion-based joint CoRs were found due to the insufficient rotation angles ($< 60^\circ$) in motion capture (bolded values in Table 4.5). Figure 4.6 showed two cases of an accurate and inaccurate estimation of motion-based CoRs with corresponding rotation angles in motion capture.

Table 4.4. Distance between motion-based and CT-based joint center of rotation at each joint of all participants

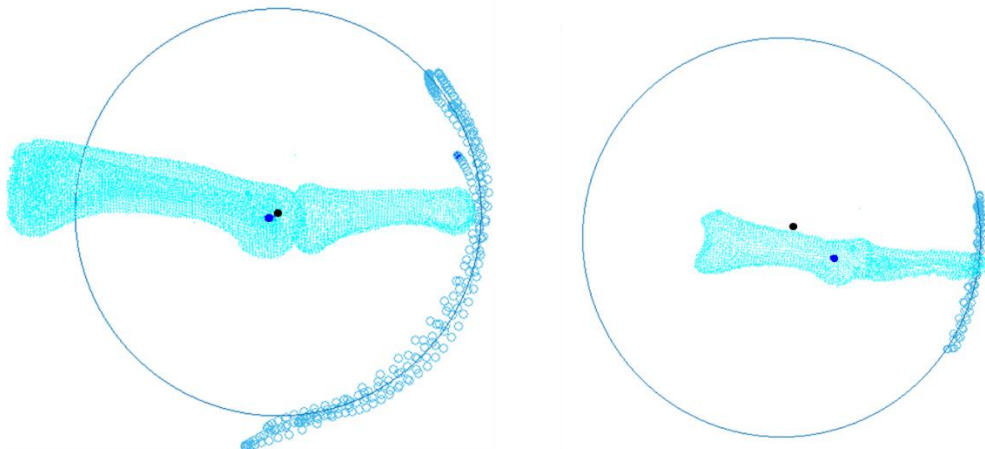
Participant	Index			Middle			Ring			Little		
	MCP	PIP	DIP	MCP	PIP	DIP	MCP	PIP	DIP	MCP	PIP	DIP
P1	5.0	1.4	4.5	3.2	2.7	3.5	0.8	3.6	14.1	4.5	3.1	5.4
P2	1.8	2.8	7.0	5.7	2.7	1.9	3.8	1.0	0.8	1.5	1.7	2.6
P3	4.8	3.5	2.3	1.1	2.3	1.4	3.0	5.4	3.3	3.3	5.3	6.6
P4	2.7	1.1	9.5	4.1	1.6	2.5	7.0	2.9	2.1	14.2	13.0	5.5
P5	3.2	6.0	3.4	6.5	10.5	3.5	3.8	1.9	3.5	6.3	1.8	4.3
P6	4.4	1.5	4.5	4.9	3.7	4.8	32.3	2.3	6.5	5.5	2.1	1.9
P7	4.9	2.9	1.4	8.3	5.2	3.1	7.9	1.6	2.1	3.2	1.5	0.7
P8	1.2	0.6	7.0	0.5	0.5	2.4	0.4	0.4	3.0	0.7	0.2	1.9
P9	4.9	3.6	1.9	9.1	5.4	2.5	12.4	3.5	2.5	3.4	2.5	6.5
Average	3.7	2.6	4.6	4.8	3.9	2.8	7.9	2.5	4.2	4.7	3.5	3.9
SD	1.4	1.6	2.6	2.8	2.8	0.9	9.3	1.4	3.8	3.7	3.6	2.1
Min	1.2	0.6	1.4	0.5	0.5	1.4	0.4	0.4	0.8	0.7	0.2	0.7
Max	5.0	6.0	9.5	9.1	10.5	4.8	32.3	5.4	14.1	14.2	13.0	6.6

Bolded values: Large errors in the mean distance between the estimated joint CoR using the surface motion capture and the CT-based joint CoR, MCP: metacarpophalangeal, PIP: proximal interphalangeal, DIP: distal interphalangeal

Table 4.5. Rotation angle in motion capture at each joint of all participants

Participant	Index			Middle			Ring			Little		
	MCP	PIP	DIP	MCP	PIP	DIP	MCP	PIP	DIP	MCP	PIP	DIP
P1	94	138	77	98	128	92	103	119	53	94	123	43
P2	72	113	43	81	118	81	79	108	79	81	113	73
P3	72	106	72	117	106	92	102	124	60	98	114	59
P4	90	115	57	86	105	33	70	118	88	45	55	57
P5	78	134	68	63	58	93	94	85	56	82	85	72
P6	107	134	76	91	142	65	41	121	55	100	110	67
P7	107	127	99	130	126	70	105	140	110	92	133	91
P8	94	110	52	94	105	73	109	109	75	93	115	97
P9	93	129	81	91	137	61	63	144	60	115	128	41
Average	90	123	69	95	114	73	85	119	71	89	108	67
SD	13	11	16	18	24	18	22	17	18	18	23	18
Min	72	106	43	63	58	33	41	85	53	45	55	41
Max	107	138	99	130	142	93	109	144	110	115	133	97

Bolded values: Small rotation angle, MCP: metacarpophalangeal, PIP: proximal interphalangeal, DIP: distal interphalangeal



Accurate joint CoR

(MCP joint of ring finger of participant 1)
Rotation angle: 103°

Inaccurate joint CoR

(DIP joint of little finger of participant 1)
Rotation angle: 59°

Figure 4.6. Two cases of an accurate (left) and inaccurate (right) estimation of motion-based CoRs (black dots) with corresponding rotation angles, blue dots: CT-based CoRs

4.3 Hand Anthropometry-Based Joint CoR Estimation Formulas

The x coordinate of a Joint CoR

The x coordinate of the joint CoR was calculated using the sine rule (Eq.4.3) for the right-angled triangle, as shown in Figure 4.7:

$$X_{\text{CoR}_j^i} = SL_{\text{CMC-MCP}}^i \sin \alpha^i \quad \text{Eq. 4.3}$$

Where: $X_{\text{CoR}_j^i}$ = x coordinate of CoR of joint j for digit i

$SL_{CMC-MCP}^i$ = segment length from the CMC to MCP joint for digit i

α^i = angle between Segment $_{CMC-MCP}^3$ and Segment $_{CMC-MCP}^i$ for digit i

j = MCP, PIP, DIP joints

i = digits 2~5

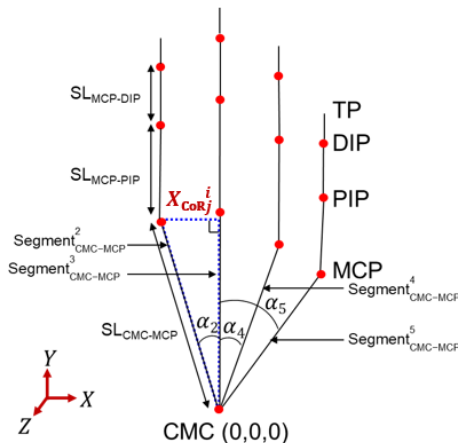


Figure 4.7. Calculation of x coordinate of a joint center of rotation ($X_{CoR_j^i}$; i = digit

2~5; j = metacarpophalangeal (MCP), proximal interphalangeal (PIP), distal

interphalangeal (DIP) joints) using the sine rule for angle right-triangle (CMC:

carpometacarpal; TP: fingertip)

The y coordinate of a Joint CoR

The y coordinate of a joint CoR was predicted from the linear regression equation

(Eq. 4.4) established using the perpendicular length from the joint to the horizontal

line going through the CMC joint ($PL_{CMC_Marker_j^i}$; i = digits 2, 3, 4, 5; j = MCP, PIP, or

DIP joints). The relationship of the $PL_{CMC_Marker_j}^i$ of each joint j on the y coordinate of the corresponding joint CoR for each finger ($n = 9$) was analysed, as demonstrated in Figures 4.8.a, 4.8.b, and 4.8.c for the middle finger respectively (Refer Appendix G for all the fingers). Based on Figure 4.8, $PL_{CMC_Marker_j}^i$ was linearly correlated to the y coordinate of the joint CoR ($Y_{CoR_j}^i$) (correlation = 0.998). As displayed in Figure 4.8.d, the relationship of $PL_{CMC_Marker_j}^i$ on the $Y_{CoR_j}^i$ for the combined data of all the joint at all fingers ($n = 4$ fingers \times 3 joints per finger \times 9 participants = 108) was similar trend with the analysed results of each joint. The adjusted R^2 value and standard error of regression analysis were used as the measures to evaluate the performance of the estimated regression model. The adjusted R^2 value of the regression equation ($n = 108$) for predicting the y coordinate of the joint CoR was 0.996 with a standard error of 2.0 mm.

$$Y_{CoR_j}^i = 1.05PL_{CMC_Marker_j}^i - 6.59 \quad \text{Eq. 4.4}$$

Where: $Y_{CoR_j}^i$ = y coordinate of CoR of joint j for digit i

$PL_{CMC_Marker_j}^i$ = perpendicular length from the joint j to the horizontal line going through the CMC joint for digit i

j = MCP, PIP, DIP joints

i = digits 2~5

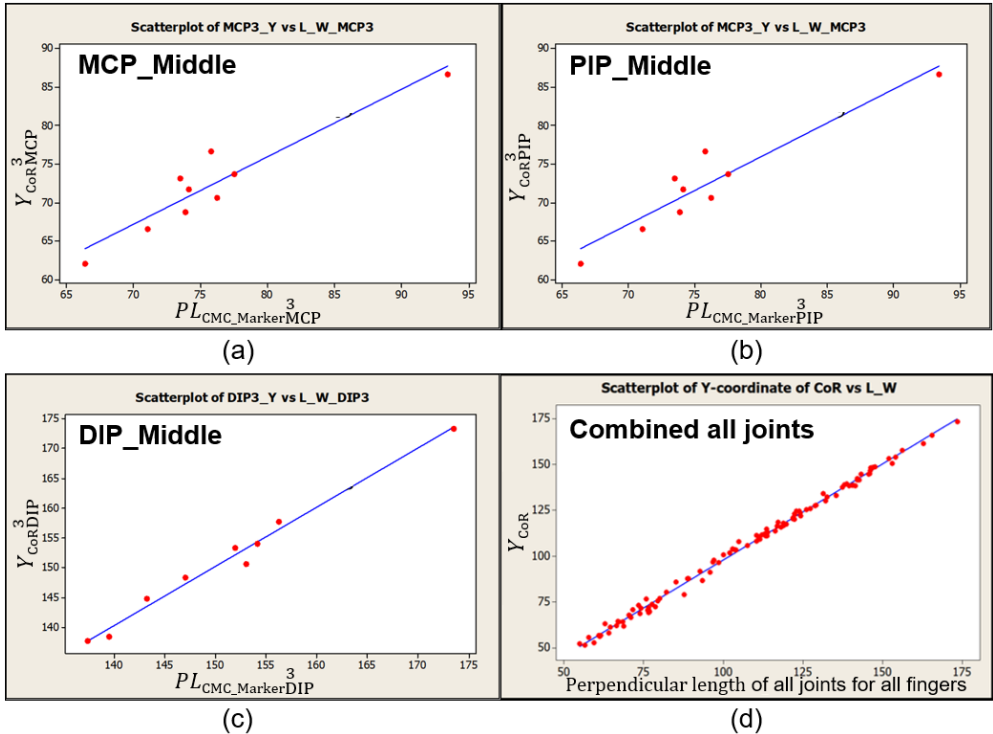


Figure 4.8. Scatter plot of y coordinate of the joint centers of rotation to the perpendicular length from the (a) metacarpophalangeal ($PL_{CMC_Marker}^{3}_{MCP}$), (b) proximal interphalangeal ($PL_{CMC_Marker}^{3}_{PIP}$), (c) distal interphalangeal ($PL_{CMC_Marker}^{3}_{DIP}$) joints to the horizontal line going through the Carpometacarpal (CMC) joint, and (d) combination of all the joints

The z coordinate of a Joint CoR

The z coordinate of a joint CoR was predicted established using the corresponding finger joint depth (JD_j^i) by the following linear regression equation (Eq. 4.5). The relationship of the JD_j^i of each joint j on the z coordinate of the corresponding joint

CoR for each finger ($n = 9$) was analysed, as demonstrated in Figure 4.9.a, 4.9.b, and 4.9.c for the middle finger respectively (Refer Appendix G for all the fingers). The JD_j^i were observed linearly correlated to the z coordinate of the joints CoRs ($Z_{\text{CoR}_j^i}$) (correlation = -0.903). The JD_j^i was inversely proportional to the $Z_{\text{CoR}_j^i}$ for all joints. According to the Figure 4.9.d, the relationship of JD_j^i on the $Z_{\text{CoR}_j^i}$ for the combined data of all the joint at all fingers ($n = 108$) was similar trend with the analysed results of each joint. The adjusted R^2 value of the regression equation ($n = 108$) for predicting the z coordinate of the joint CoR was 0.814 with a standard error of 1.1 mm.

$$Z_{\text{CoR}_j^i} = -0.37JD_j^i - 2.89 \quad \text{Eq. 4.5}$$

Where: $Z_{\text{CoR}_j^i}$ = z coordinate of CoR of joint j for digit i

JD_j^i = corresponding joint depth for digit i

j = MCP, PIP, DIP joints

i = digits 2~5

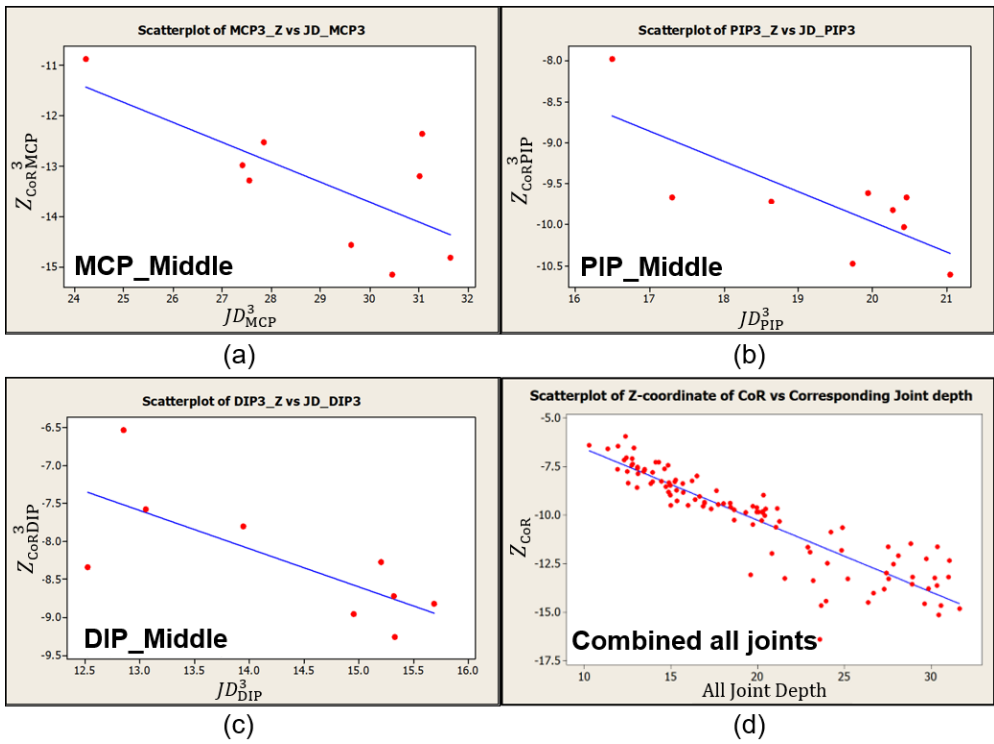


Figure 4.9. Scatter plot of z coordinate of the joint centers of rotation to (a) metacarpophalangeal (JD_{MCP}^3), (b) proximal interphalangeal (JD_{PIP}^3), (c) distal interphalangeal (JD_{DIP}^3) joints depth, and (d) combination of all the joint depth data

Chapter 5 DISCUSSION

5.1 CT-Based Joint CoR Estimation

The present study compared Figueroa et al.'s and Reuleaux's methods for estimation of instantaneous finger joint CoRs using CT scans in terms of the variation of estimated instantaneous CoRs at the finger joints. Then, Figueroa et al.'s, Reuleaux's, Delonge-Kasa's, and the bone curvature-based methods were compared for the estimation of fixed finger joint CoRs using CT scans. The method that provided closest estimation of CoR to the centroid of the CoRs estimated by the four methods was considered as the best performed method in fixed CoR estimation. The fixed CoRs estimated by the best performed method were then used for (1) validation of Delonge-Kasa's method for finding fixed finger joint CoRs using surface motion data and (2) establishment of fixed finger joint CoR estimation formulas using hand anthropometric data.

Instantaneous Joint CoR Estimation

Figueroa et al.'s method was found superior to Reuleaux's method for instantaneous finger joint CoR estimation. Compared to Reuleaux's method, the variation of the estimated instantaneous CoRs using Figueroa et al.'s method was reduced by 69% for MCP joint, 31% for PIP joint, and 26% for DIP joint. The reason why Reuleaux's method showed larger variation is that Reuleaux's method performed poorly in CoR

estimation if the rotation angle of the distal bone segment between two postures was small ($< 10^\circ$) (Challis, 2001), while Figueroa et al.'s method performed well even though the rotation angle of the distal bone segment between two postures was relatively small (5° to 10°) since Figueroa et al.'s method uses the centerline of the distal bone segment to find instantaneous CoR. As shown in Figure 5.1, for a rotation angle of the distal bone segment of 5° , Reuleaux's method provided an obvious wrong estimation of CoR that is outside of the bone, while Figueroa et al.'s method provided a reasonable estimation of CoR.

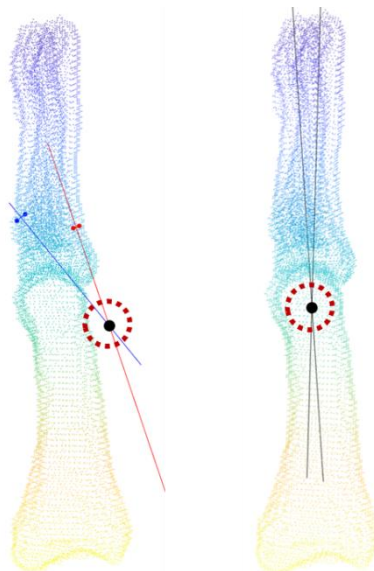


Figure 5.1. Instantaneous finger joint centers of rotation incorrectly estimated by Reuleaux's method (left) and correctly estimated by Figueroa et al.'s method (right) for a motion of the distal bone segment around a joint with a rotation angle of 5° (illustrated for the distal interphalangeal joint of the little finger of Participant 1)

Fixed Joint CoR Estimation

Delonge-Kasa's method achieved the best performance in fixed finger joint CoR estimation among the four methods. The mean (SD) distance of the estimated CoR to the centroid of the estimated CoRs of the four methods was 1.38 (1.08) mm for Delonge-Kasa's method, 1.46 (0.29) mm for Figueroa et al.'s method, 1.68 (0.84) mm for Reuleaux's method, and 2.21 (1.04) mm for the bone curvature-based method. Except Delonge-Kasa's method, a fixed joint CoR was identified as the centroid point of the instantaneous joint CoRs estimated by the other three methods. However, the three methods suffered from incorrect estimation of instantaneous CoRs if the rotation angle of the distal bone segment between two postures was smaller than 5°, as shown in Figure 5.2. Therefore, the identified centroid (fixed CoR) could be biased due to the incorrectly estimated instantaneous CoRs. The Delonge-Kasa's method estimated the fixed CoR by fitting a circle to the entire trajectory points of the head of the distal bone from the starting to the ending postures, and therefore could provide more accurate estimation of the fixed CoR.

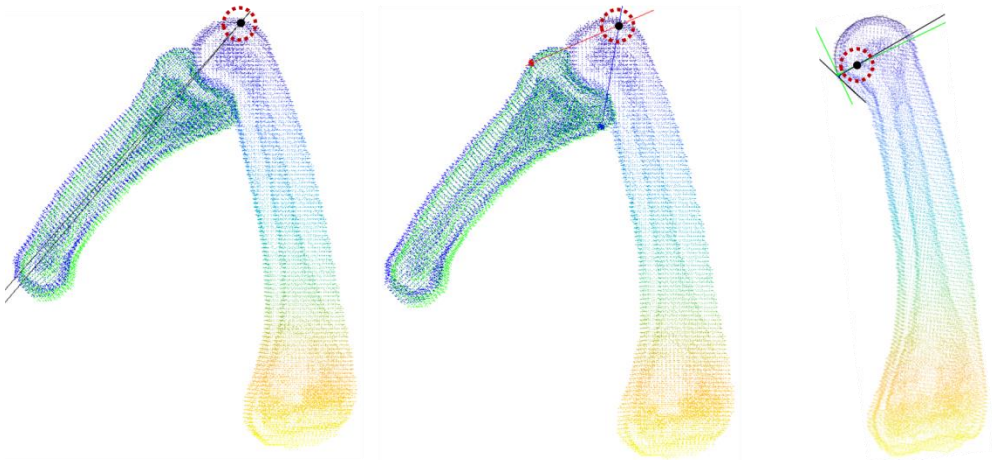


Figure 5.2. Instantaneous finger joint centers of rotation incorrectly estimated by Figueroa et al.'s method (left), Reuleaux's method (middle), and bone curvature-based method (right) for a motion of the distal bone segment around a joint with a rotation angle of 2° (illustrated for the proximal interphalangeal joint of the ring finger of Participant 1)

5.2 Motion-Based Joint CoR Estimation

This study implemented Delonge-Kasa's method that was conventionally used for estimation of fixed CoRs of large joints such as knee and elbow to estimate fixed finger joint CoRs using surface motion data and evaluated its performance by comparison with the fixed CoRs estimated by Delonge-Kasa's method using CT scans.

Delonge-Kasa's method based on surface motion data provided closest fixed CoR estimation to CT-based estimation for PIP joint (mean distance = 3.1 ± 2.6 mm), followed by DIP joint (mean distance = 3.9 ± 2.6 mm), and lastly MCP joint (mean distance = 5.3 ± 5.5 mm). As shown in Figure 2.10 in Chapter 2, Delonge-Kasa method can provide biased CoR estimation as the rotation angle (ROM) between the starting and ending postures decreases (Al-Sharadqah et al., 2009). The mean rotation angle (ROM) was $90^\circ \pm 18^\circ$ for an MCP joint, $116^\circ \pm 20^\circ$ for a PIP joint, and $70^\circ \pm 18^\circ$ for a DIP joint. That is why Delonge-Kasa's method best performed at a PIP joint. We noticed that though an MCP joint had larger mean rotation angle than a DIP joint, Delonge-Kasa's method showed lower performance at an MCP joint than that at a DIP joint. That could be explained by the larger skin deformation at MCP and PIP joints than a DIP joint and fingertip. For estimation of an MCP joint CoR, surface marker motions of MCP and PIP joints were used, while for estimation of a DIP joint CoR, surface marker motions of DIP joint and fingertip were used. A large skin deformation could result in a biased trajectory of marker motion around CoR, and therefore reduce the accuracy in CoR estimation. A further study needs to be conducted to analyse the effect of skin deformation on CoR estimation accuracy.

5.3 Hand Anthropometry-Based Joint CoR Estimation

This study established CoR estimation formulas using CoRs estimated based on CT scans and hand anthropometric data. For the x coordinate of a joint CoR, a formula

based on the sine rule for a right-angled triangle was developed. Segment length between CMC and MCP joints and angle between the CMC-MCP segment of the middle finger and the CMC-MCP segment of another finger were used as independent variables in the formula for x coordinate calculation. For the y coordinate of the joint CoR, a regression formula was established using the perpendicular length from the joint to the horizontal line going through the CMC joint. For the z coordinate of the joint CoR, a regression formula was established using the joint depth.

The formula for calculation of the x coordinate of a CoR can provide an exact solution, and the regression formulas for estimation of y and z coordinates showed high adjusted R^2 values (0.996 and 0.814) and low standard errors (2.0 mm and 1.0 mm). A consistent relationship between y coordinate and the perpendicular length from a joint to the horizontal line going through the CMC joint was found at different joints, as shown in Figure 5.3.a. However, a large variation of the relationship between z coordinate and a joint depth was found at the MCP joint, as shown in Figure 5.3.b. The reason of the large variation can be explained by the effect of fat tissue at the palm on the measurement of joint depth. For example, a small hand with a lot of fat tissue at the palm can result in an over measurement of joint depth. A further study is needed to reduce the effect of fat tissue on joint depth measurement by various methods such as squeezing the palm during measurement.

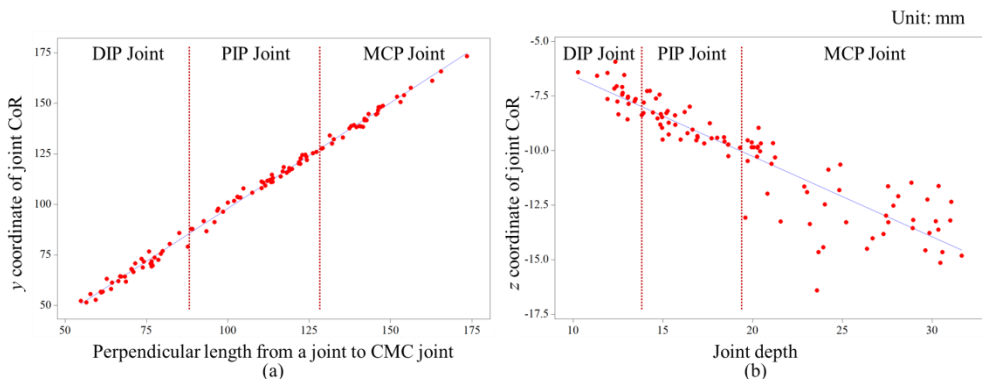


Figure 5.3. Relationship between dependent variable and independent variable for joint center of rotation (CoR) estimation at different joints including the distal interphalangeal (DIP), proximal interphalangeal (PIP), and metacarpophalangeal (MCP) joints: (a) y coordinate of a joint CoR with the perpendicular length from the joint to the horizontal line going through the carpometacarpal (CMC) joint and (b) z coordinate of a joint CoR with the joint depth

5.4 Applications

The established formulas can be applied for practitioners to efficiently and practically find CoRs of a person's finger joints by measuring the person's hand dimensions within a reasonable accuracy level. The estimated CoRs of the person's finger joints can be used to build a digital link model for the person. Then a digital hand model of the person can be established by combining the digital link model and a skin model generated by a 3D scanner. The digital hand model can be used for computer-aided

ergonomic hand-held product design and evaluation and finger joint surgery such as artificial finger joint replacement. For ergonomic product design and evaluation, with the help of the link model, an accurate hand posture while using a hand-held product can be predicted and used for design of the shape and size of a product and ergonomic evaluation of the product such as accommodation rate of the product and its fitness to the hand. For artificial finger joint replacement surgery, the accurate location of an artificial finger joint can be decided by the link model so that a natural joint movement as the patient's original joint can be guaranteed after surgery.

5.5 Future Studies

Future studies can extend the applications of the established formulas for hand joint CoR estimation by (1) cross validation of the formulas using different data from the current study, (2) development of formulas for instantaneous joint CoR estimation, and (3) establishment of a hand model template for product design by applying the instantaneous joint CoR estimation formulas. A cross validation should be conducted by estimating the hand joint CoRs of new participants' hand using the established formulas and check the estimated joint CoRs by comparison with the CT-based joint CoRs. For a practical application purpose, an ergonomic analysis that could provide simulated results based on the human hand motion in the sense of real-time processing is highly emphasized in an ergonomic product design. At this point, using the estimated fixed joint CoRs to analyse the desired posture is insufficient and

impossible to simulate the hand motion in real-time. It has been recommended that new formulas for prediction of instantaneous hand joint CoRs should be built by including the hand anthropometry and kinematic measurement information such as the joint angle and applied to form an accurate template hand model for a better and faster hand posture recognition.

Chapter 6 CONCLUSION

The present study achieved three objectives for CoR estimation of hand joints including (1) comparing existing methods for joint CoR estimation based on CT measurement, (2) applying Delonge-Kasa's circle-fitting method for finger joint CoR estimation using motion capture data and check its validity in estimating finger joint CoR, and (3) forming regression models to predict finger joint CoRs using hand anthropometric data.

Firstly, the present study found that Figueroa et al.'s method and Delonge-Kasa's method showed the best performance in estimating instantaneous and fixed joint CoRs, respectively. Figueroa et al.'s method showed significantly lower average mean distances and standard errors (MCP joint: 1.6 ± 0.4 mm, PIP joint: 2.2 ± 0.5 mm, DIP joint: 1.4 ± 0.6 mm) among the estimated joint CoRs of 102 out of 108 hand joints than Reuleaux's method (MCP joint: 5.2 ± 3.1 mm, PIP joint: 3.2 ± 1.2 mm, DIP joint: 1.9 ± 0.6 mm). While Delonge-Kasa's method achieved the smallest mean distance (1.38 ± 1.08 mm) between its estimated fixed CoR to the centroid (measured using the estimated joint CoRs by Figueroa et al.'s, Reuleaux's, bone curvature-based, and Delonge-Kasa's methods) among all the methods.

Secondly, Delonge-Kasa's method showed the best performance in estimating fixed PIP joint CoRs, other than the DIP and MCP joints. 95%, 78%, and 78% of the PIP, DIP, and MCP joints CoRs have been found accurately located close

to the CT-based fixed joint CoR by Delonge-Kasa's method (average mean distance of MCP joints: 3.99 ± 2.3 mm, PIP joints: 2.6 ± 1.5 mm, DIP joints: 2.8 ± 1.3 mm). The accurate joint CoRs were estimated if the ROM at the distal segment $> 60^\circ$. The PIP joints that have achieved the highest number of accurate joint CoR were found have the largest ROM (119°) occurs at its distal segment.

Lastly, three formulas for estimation of the x , y , and z coordinates of joint CoRs were established to practically predict fixed joint CoRs using hand anthropometric data. The x coordinates of CoRs for all the joints were calculated using a deterministic sine rule for the right-angled triangle, while the y and z coordinates of CoRs for all the joints were predicted using two linear regression equations, respectively. The adjusted R^2 values of the regression equations for the y and z coordinates of CoRs were 0.996 and 0.814 with standard errors of 2.0 mm and 1.1 mm, respectively.

REFERENCES

- Abouhossein, A., Weisse, B., Ferguson, S.J. (2013). Quantifying the centre of rotation pattern in a multi-body model of the lumbar spine. *Computer Methods in Biomechanics and Biomedical Engineering*, 16(12), 1362-1373.
- Ahmadi, A., Maroufi, N., Behtash, H., Zekavat, H., Parmianpour, M. (2009). Kinematic analysis of dynamic lumbar motion in patients with lumbar segmental instability using digital videofluoroscopy. *Eur Spine J*, 18(11), 1677-1685.
- Al-Sharadqah, A., Chernov, N. (2009). Error analysis for circle fitting algorithms. *Electron. J. Statist*, 3, 886-911.
- An, K.N., Ueba, Y., Chao, E.Y., Cooney, W.P., Linscheid, R.L. (1983). Tendon Excursion and Moment Arm of Index Finger Muscles. *J. Biomechanics*, 16(6), 419-425.
- Besl, P.J., McKay, N.D. (1992). A method for registration of 3-D shapes. *IEEE Transactions on Pattern Analysis and Machine Intelligence*, 14(2), 239-256.
- Cai, Y. (2008). Digital Human Modeling: Trends in Human Algorithms. *Springer-Verlag*. Berlin Heidelberg.
- Cerveri, P., Lopomo, N., Pedotti, A., Ferrigno, G. (2005). Derivation of Centers and Axes of Rotation for Wrist and Fingers in a Hand Kinematic Model: Methods and Reliability Results. *Annals of Biomedical Engineering*, 33(3), 402-412.
- Chaffin, D.B. (2008). Digital Human Modeling for Workspace Design. *Reviews of Human Factors and Ergonomics*, 4(1), 41-74.
- Challis, J.H. (2001). Estimation of the finite center of rotation in planar movements. *Medical Engineering & Physics*, 23(3), 227-233.
- Claessens, T. (2017). Finding the location of the instantaneous center of rotation using a particle image velocimetry algorithm. *American Journal of Physics*, 185-192.
- Cobos, S., Ferre, M., Uran, M.A.S., Ortego, J., Pena, C. (2008). Efficient Human Hand Kinematics for Manipulation Tasks. *IEEE/RSJ International Conference on Intelligent Robots and Systems*, 2246-2251.
- Ehrig, R.M., Taylor, W.R., Duda, G.N., Heller, M.O. (2006). A survey of formal methods for determining the centre of rotation of ball joints. *Journal of Biomechanics*, 2798-809.
- Figueroa, R., Armstrong, T., Sun L., Zhou, W., Woolley, C. (2016). Determining instantaneous centers of rotation for finger through different postures using the iterative closest point algorithm (ICP). *Proceedings of the Human Factors and Ergonomics Society Annual Meeting*, 60(1), 1470-1474.
- Frederick, L.J., Armstrong, T.J. (1995). Effect of friction and load on pinch force in a hand transfer task. *Ergonomics*, 2447-2454.
- Fowler, N.K. (2001). Method of determination of three dimensional index finger moment arms and tendon lines of action using high resolution MRI scans. *Journal of Biomechanics*, 34(6), 791-797.

- Gamage, S.S., Lasenby, J. (2002). New least squares solutions for estimating the average centre of rotation and the axis of rotation. *Journal of Biomechanics*, 35(1), 87-93.
- Halvorsen, K., Lesser, M., Lundberg, A. (1999). A new method for estimating the axis of rotation and the center of rotation. *Journal of Biomechanics*, 32(11), 1221-1227.
- Hamill, J., Knutzen, K. (2015). Biomechanical Basis of Human Movement (4th Edition). *Massachusetts: Wolters Kluwer*. ISBN 978-1-4511-7730-5.
- Hollerbach, K., Ashby, A.E., Logan, C., Martz, H., Bossart, P.L., Rikard, D. (1996). High resolution hand dataset for joint modeling [CT images]. *IEEE Engineering in Medicine and Biology Society*, 676-677.
- Houglum, P.A., Bertoti, D.B. (2012). Brunnstrom's Clinical Kinesiology (6th Edition). *F. A. Davis Company*. ISBN 978-0-8036-2352-1.
- Kanungo, T., Mount, D.M., Netanyahu, N.S., Silverman, R., Piatko, C.D., Wu, A.Y. (2002). An Efficient k-Means Clustering Algorithm: Analysis and Implementation. *IEEE TRANSACTIONS ON PATTERN ANALYSIS AND MACHINE INTELLIGENCE*, 24(7), 881-892.
- KASA. (1976). A Circle Fitting Procedure and Its Error Analysis. *IEEE TRANSACTIONS ON INSTRUMENTATION AND MEASUREMENT*, 8-14.
- Kasban, H. (2015). A Comparative Study of Medical Imaging Techniques. *International Journal of Information Science and Intelligent System*, 4(2), 37-58.
- Kinzel, G.L., Gutkowski L.J. (1983). Joint models, degrees of freedom, and anatomical motion measurement. *Journal of Biomechanical Engineering*, 105(1), 55-62.
- Knight J.K., Semwal S.K. (2009). Unbiased Closed-Form Solutions for Center of Rotation. *VISIGRAPP 2009*, 73-88.
- Kurihara, T., Miyata, N. (2004). Modeling Deformable Human Hands from Medical Images. *Eurographics/ACM SIGGRAPH Symposium on Computer Animation*, 355-363.
- Lim, S.J., Park, Y.S., Moon, Y.W., Jung, S.M., Ha, H.C., Seo, J.G. (2009). Modular Cementless Total Hip Arthroplasty for Multiple Epiphyseal Dysplasia. *The Journal of Arthroplasty*, 24(1), 77-82.
- Lin J., Wu, Y., Huang, T.S. (2000). Modeling the Constraints of Human Hand Motion. *IEEE*, 121-126.
- Liu, H., Iberall, T., Bekey, G.A. (1989). The multi-dimensional quality of task requirements for dextrous robot hand control. *Proceedings of IEEE Int. Con Robotics Automat.*, 1989, 452–457.
- Marin, F., Mannel, H., Clases, L., Durselen, L. (2003) Accurate Determination of a Joint Rotation Center Based on the Minimal Amplitude Point Method. *Computer Aided Surgery*, 8(1), 30-4
- Miyata, N., Kouchi, M., Kurihara, T., and Mochimaru, M. (2004). Modeling of Human Hand Link Structure from Optical Motion Capture Data. *Proc. IROS'04*, 2129-2135.

- Muggleton, J.M., Allen, R. (1998). Insights into the measurement of vertebral translation in the sagittal plane. *Medical Engineering & Physics*, 20, 21–32.
- Piazza, S.J., Erdemir, A., Okita, N., Cavanagh, P.R. (2004). Assessment of the functional method of hip joint center location subject to reduced range of hip motion. *Journal of Biomechanics*, 37(3), 349-356.
- Petit, Y., Aubin, C., Labelle, H. (2004). Spinal shape changes resulting from scoliotic spine surgical instrumentation expressed as intervertebral rotations and centers of rotation. *Journal of Biomechanics*, 37, 173-180.
- Pratt, V.R., 1987. Direct least-squares fitting of algebraic surfaces. *Computer Graphics*, 21, 145–152.
- Reuleaux's F. (1875). Theretische Kinematik. Braunschweig.
- Silva, S.N., Mattar, R.Jr., Neto, R.B., Pereira, C.A. (2005). Measurement of the flexing force of the fingers by a dynamic splint with a dynamometer. *CLINICS*, 60(5), 381-388.
- Seo, N. J., Armstrong, T. J., Ashton-Miller, J. A., Chaffin, D. B. (2007). The effect of torque direction and cylindrical handle diameter on the coupling between the hand and a cylindrical handle. *Journal of Biomechanics*, 40(14), 3236–3243.
- Soudan, K., Van Audekercke, R., Martens, M. (1979) Methods, difficulties and inaccuracies in the study of human joint kinematics and pathokinematics by the instant axis concept. Example: the knee joint. *J. Biomechanics*, 12, 27-33.
- Supuk, T.G., Harwin, W., Zanchi. V. (2004). CALCULATING POSITIONS OF THE FINGER JOINTS CENTERS OF ROTATIONS IN FLEXION-EXTENSION MOVEMENT FROM REFLECTIVE MARKERS. *IMEKO, IEEE, SICE*, 363-366.
- Staub, B.N., Holman, P.J., Reitman, C.A., Hipp, J. (2015). Sagittal plane lumbar intervertebral motion during seated flexion-extension radiographs of 658 asymptomatic nondegenerated levels. *J Neurosurg Spine*, 23(6), 731-738.
- Stillfried G., Smagt P.V. (2010). Movement model of a human hand based on magnetic resonance imaging (MRI). *1st International Conference on Applied Bionics and Biomechanics*.
- Taylor C.L., Schwarz R.J. (1955). The Anatomy and Mechanics of the Human Hand. *Artif Limbs*, 2(2), 22-35.
- Wu, G., van der Helm, F.C., Veeger, H.E., Makhsous, M., Van Roy, P., Anglin, C., Nagels, J., Karduna, A.R., McQuade, K., Wang, X., Werner, F.W., Buchholz, B. (2005). ISB recommendation on definitions of joint coordinate systems of various joints for the reporting of human joint motion—Part II: shoulder, elbow, wrist and hand. *Journal of Biomechanics*, 38(5), 981-992.
- Zatsiorsky, V.M. (1998). Kinematics of human motion. United State of America: Human Kinetics.
- Zhang, X., Lee, S.W., Braido, P. (2003). Determining finger segmental centers of rotation in flexion–extension based on surface marker measurement. *Journal of Biomechanics*, 36(8), 1097-1102.

APPENDICES

Appendix A: Institutional Review Board Certification and Documents

	결과통지서				
파제번호	37100475-201802-HR-001		관리번호	2	

귀하께서 2018년 03월 02일에 신청한 수정 후 신속실의 연구과제에 대하여 에스포항병원기관생명윤리위원회에서 심의하여 다음과 같이 결정하였음을 통지합니다.

연구과제명	동작분석 데이터 및 CT-Scan Image를 이용한 손가락 관절 회전 중심 추정 방법 개발 및 검증				
연구책임자	성명	박 덕호	소속	재활의학과	직위
					진료과장
심의 대상	<input type="checkbox"/> 연구계획서(신규)			<input checked="" type="checkbox"/> 연구계획서(시정/보완)	
	2018년03월02 일		심의 장소	에스포항병원 5 층 책임심사위원 연구실	
심의 종류	<input type="checkbox"/> 정규심의		<input checked="" type="checkbox"/> 신속심의	<input type="checkbox"/> 심의면제	
	<input checked="" type="checkbox"/> 승인		<input type="checkbox"/> 수정후승인	<input type="checkbox"/> 수정후신속심의	<input type="checkbox"/> 보완
승인 인자	2018년03월02 일	승인 유효기간	2018.03.02 – 2019.03.01		
승인 번호	37100475-201802-HR-001				
심의 의견	2018.02.23 위원회가 검토한 심의내용이 반영되도록 연구대상자용 설명문이 수정되어 연구과제를 승인합니다.				
	심의의견에 대한 답변서, 변경대비표, 수정된 연구대상자용 설명문				
심의된 서류					

본 확인서에 기재된 사항은 에스포항병원 기관생명윤리위원회에 기록된 내용과 일치함을 증명합니다.

본 기관생명윤리위원회는 생명 윤리 및 안전에 관한 법률과 관련 법규를 준수합니다.

본 연구와 이해 상충(Conflict of Interest)이 있는 위원이 있을 경우 연구의 심의에서 배제합니다.

본 통지서의 사본은 에스포항병원 기관생명윤리위원회에서 보관합니다.

에스포항병원 기관생명윤리위원회 [별지 제 9-1 호 서식]

※ 모든 연구자들은 아래의 사항을 준수하여야 합니다.

- 1) 승인된 계획서에 따라 연구를 수행하여야 합니다.
- 2) 위원회의 승인을 받은 동의서를 사용하여야 합니다.
- 3) 모국어가 한국어가 아닌 연구대상자들에게는 승인된 동의서를 연구대상자의 모국어로 인증된 번역본을 사용할 것이며 이러한 동의서 번역본은 반드시 위원회의 승인을 받아야 합니다.
- 4) 연구진행에 있어 연구대상자를 보호하기 위해 불가피한 경우를 제외하고 연구의 어떠한 변경이든 위원회의 사전 승인을 받고 수행하여야 하며 연구대상자들의 보호를 위해 취해진 어떠한 응급상황에서의 변경도 즉각 위원회에 보고하여야 합니다.
- 5) 위원회에서 승인된 계획서에 따라 등록된 어떠한 연구대상자라도 사망, 입원, 심각한 질병에 대하여는 위원회에 서면으로 보고하여야 합니다.
- 6) 연구 또는 연구대상자의 안전에 대해 유해한 영향을 미칠 수 있는 어떠한 새로운 정보도 즉각적으로 위원회에 보고하여야 합니다.
- 7) 위원회의 요구가 있을 때에는 연구의 진행과 관련된 보고를 위원회에 제출하여야 합니다.
- 8) 위원회가 심의한 과제에 대해 조사 및 감독 차원에서 현장점검을 실시할 시 원활한 점검절차 진행을 위해 연구자는 연구진행과 관련된 서류를 준비하고 협조하여야 합니다.
- 9) 연구대상자 모집광고를 사용할 시에는 사용 전에 위원회의 승인을 받아야 합니다.
- 10) 동의는 강제 혹은 부당한 영향이 없는 상태에서 충분한 설명에 근거하여 수행되어야 하며, 잠재적인 연구대상자에게 연구에 참여여부를 고려할 수 있도록 충분히 기회를 제공하여야 합니다.
- 11) 연구자와 그밖에 이해당사자는 연구계획서 승인을 광고나 홍보, 상업적 목적으로 사용할 수 없습니다.
- 12) 위원회의 심의결과 시경요구에 대해 모두 이행 및 쟁족될 경우에만 연구를 진행할 수 있습니다.
- 13) 위원회가 시정 및 보완을 요구한 경우 시정·보완 계획을 1개월 이내에 본 위원회에 제출하여야 합니다. 심의일로부터 1년 이내에 시정·보완 계획을 제출하지 않은 경우 심의가 투표화될 수 있습니다.
- 14) 시정계획은 신속심의로 진행되고 보완계획은 정규심의로 진행되며, 승인일과 승인 유효기간은 심의 결과에 따라 결정됩니다.
- 15) 승인기간 이후에도 연구를 지속하기 위해서는 적어도 승인 만료 2개월 전까지 연구의 진행상황에 대하여 중간보고를 하여야 합니다.
- 16) 연구 종료 후 3개월 이내에 종료보고를 하여야 합니다.
- 17) 연구와 관련된 기록은 연구가 종료된 시점을 기준으로 최소 3년간 보관하여야 합니다.

2018년 03월 02일



에스포항병원 기관생명윤리위원장 (인)

본 확인서에 기재된 사항은 에스포항병원 기관생명윤리위원회에 기록된 내용과 일치함을 증명합니다.
본 기관생명윤리위원회는 생명 윤리 및 안전에 관한 법률과 관련 법규를 준수합니다.

본 연구와 이해상충(Conflict of Interest)이 있는 위원이 있을 경우 연구의 심의에서 배제합니다.
본 통지서의 사본은 에스포항병원 기관생명윤리위원회에서 보관합니다.

Appendix B: Informed Consent for Participants

실험 참여 동의서

1. 실험기관: 1) 포항공과대학교 산업경영공학과 인간공학설계기술 연구실

2) 에스포항병원

2. 실험개요

- 목적: 손가락 관절 회전 중심(joint center of rotation) 추정을 위한 자연스러운 손 그립 동작의 motion capture, CT scan, 그리고 손 측정
- 실험 내용
 - (1) 실험에 대한 전반적인 설명 청취 및 실험참여 동의서 작성 (5분).
 - (2) CT scan 시 활용될 손 자세 고정 도구 제작 (10분)
 - (3) 에스포항병원에서 10단계의 손 그립 구분 동작 CT scan 수행 (25분)
 - A. 손등면에 24개의 steel marker를 부착한 뒤 그립 자세 연습 수행 (10분)
 - B. 편 자세에서 주먹을 편 자세까지 10가지 그립 동작 시 자세 CT Scan (15분)

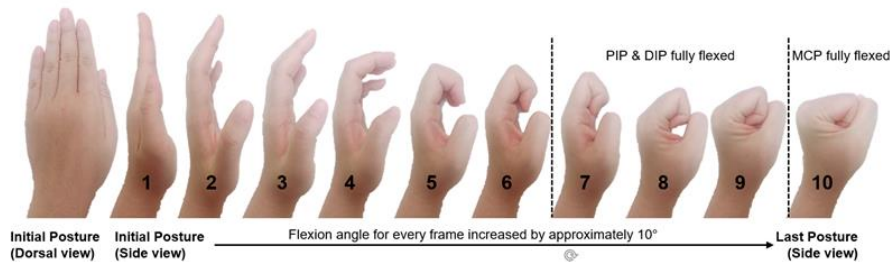


그림1. CT scan을 위한 10가지 손 그립 자세



그림2. Marker 부착 및 손 자세 고정 도구와 CT scanning 예시

※ 요청 사항

- 4공학관 208호에 CT scan 실험 하루 전 방문하여 손길이 측정 및 손 자세 고정

※ 요청 사항

- 4공학관 208호에 CT scan 실험 하루 전 방문하여 손길이 측정 및 손 자세 고정 도구 제작을 위한 협조 요청

(4) 실험실 환경에서 손 동작 측정 실험 (15분)

- A. 손 등에 적외선 반사용 marker를 부착하고 손 그립 동작 연습 수행 (10분)

- i. 동작 1: DIP 편 상태에서 DIP 관절의 최대 굴곡
- ii. 동작 2: PIP 편 상태에서 PIP 관절의 최대 굴곡
- iii. 동작 3: MCP 편 상태에서 MCP 관절의 최대 굴곡

- B. 손 그립 동작 수행 및 측정 (5분)

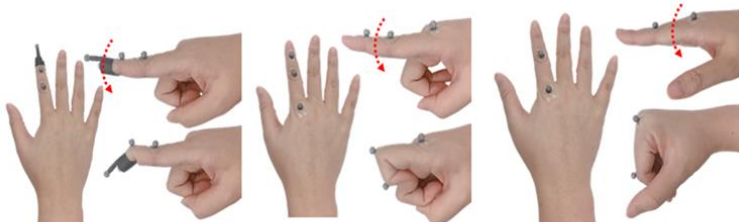


그림3. 손 동작에 따라 부착된 24개의 적외선 반사 marker

※ 요청 사항

- 평가 중 추가 설명이 필요한 경우 실험 진행자에게 설명을 요청합니다.

3. 소요시간: 약 1.5 시간

4. 참가 사례비: 60,000원

※ 본 연구는 에스포항병원 임상시험심사위원회(IRB)로부터 제반 연구의 승인을 받음 (IRB No:
37100475-201802-HR-001)

※ 실험 참여자로서 상기 내용을 충분히 숙지한 후 실험에 자발적으로 참여함을 확인합니다.

2018 년 월 일

실험 참여자: _____ 서명: _____

실험 진행자: _____ 서명: _____

Appendix C: MATLAB Codes for Joint CoR Estimation by CT Scan

Determine the centerline of segment

```
% Select the range of bone shaft
L = -10.5; R = 15;

posture = 1; % CT scan frame: 1~10
bone = 'MCP'; % Bone segment: MCP, PIP, DIP
Digit = 5; % Finger: 2~5

%% DO NOT CHANGE THE FOLLOWING CODE
% Read file
col2 = posture + 10;
if bone == 'PIP'; col1 = 'A'; end % Define column to read from excel file
if bone == 'DIP'; col1 = 'E'; end % Define column to read from excel file

F1 = sprintf('%s%d', col1, posture); % A,E,I (PIP, DIP, TP)
F2 = sprintf('%s%d', col1, col2); % A,E,I (PIP, DIP, TP)
ptCloud = pcread(sprintf("%s_0%d_%d.ply", bone, Digit, posture));
pg = Digit-1;

%% Select bone shaft and save in a new storage
[eigenvectors, score] = pca(ptCloud.Location, 'Algorithm','eig', 'Centered',true); % apply PCA on bone

a = max(score(:,1))-min(score(:,1))
% Select only specific region
idx = 0;
for i = 1: length(score)
    if score(i, 1) > L && score(i, 1) < R
        idx = idx + 1;
        Shaft(idx,:) = score(i,:);
    end
end
plane = 0.05;
% Find points lie at plane every interval of 0.05
idx1 = 0; idx2 = 1; idx3 = 0; idx4 = 0;
for x = L:plane:R
    for i = 1:length(Shaft)
        if Shaft(i,1) >= x-0.2 && Shaft(i,1) <= x+0.2
            idx1 = idx1 + 1;
            Frame(idx1, idx2:idx2+2) = Shaft(i,:);
        end
    end
    idx2 = idx2 + 3;
end

% Determine midpoint & plot
% Draw linear line using midpoint
P_xy = polyfit(Midpoint1(:,1),Midpoint1(:,2),1);
P_xz = polyfit(Midpoint1(:,1),Midpoint1(:,3),1);
N = length(score(:,1));
xx = linspace(min(score(:,1))-15, max(score(:,1))+15,N);
yy = polyval(P_xy, xx);
zz = polyval(P_xz, xx);
axis_line = zeros(length(xx), 3);
axis_line(:,1) = xx';
axis_line(:,3) = zz';
```

```

axis_line(:,2) = yy';

%% PCA reconstruction
% PCA reconstruction=PC scores.Eigenvectors'+Mean
nComp = 3;
mu = mean(ptCloud.Location);

Landmark_1_re = Landmark_1(:,1:nComp) * eigenvectors(:,1:nComp)';
Landmark_1_re = bsxfun(@plus, Landmark_1_re, mu);

Landmark_1_extend_re = Landmark_extend(:,1:nComp) * eigenvectors(:,1:nComp)';
Landmark_1_extend_re = bsxfun(@plus, Landmark_1_extend_re, mu);

```

Estimate the instantaneous joint CoR using Figueroa and Reuleaux methods

```

%% Define input
Digit      = 5;          % 1~5
CoR_Joint   = 'DIP';      % MCP / PIP / DIP
Sheet       = 12;         % 1:MCP2 MCP3 MCP4 4:MCP5 || 5:PIP2 PIP3 PIP4 8:PIP5 || 9:DIP2 DIP3
DIP4 12:DIP5 || 13:PIP1 14:MCP1

%% DO NOT CHANGE THE FOLLOWING CODE
% Read file
name    = sprintf('Digit 0%d', Digit);
ptCloud = pcread(sprintf('%s_All_0%d.ply', Distal_Joint, Digit));           % Read Distal bone
ptCloud_MCP = pcread(sprintf('%s_0%d_1.ply', CoR_Joint, Digit));             % Read Proximal bone

% Read centerline of bone from excel (Input of Figueroa method)
axis_pt = xlsread('PCA_Reconstructed.xlsx', name);
% Read selected landmark A (Input of Reuleaux method)
Landmark1 = xlsread('Landmark_Reuleaux_down.xlsx', name);
% Read selected landmark B (Input of Reuleaux method)
Landmark2 = xlsread('Landmark_Reuleaux_up.xlsx', name);

slope = @(line) (line(2,2) - line(1,2))/(line(2,1) - line(1,1));      % Slope of a line,m = (y2-y1)/(x2-x1)
intercept = @(line,m) line(1,2) - m*line(1,1);                      % Intercept of 2 lines = y1 - m*x1

idxx = 0; idx = 0;
for posture1 = 1:10          % Posture 1: 1~10
    for posture2 = posture1+1:10 % Posture 2: 2~10

        pt_cloud = ptCloud.Location; % get XYZ coordinate of bone point cloud

        % Add PCA axis line (start & end point of the line) to end of bone point cloud
        pt_cloud(end+1,1:3) = axis_pt(posture1,col:col+2);    % posture 1 start point
        pt_cloud(end+1,1:3) = axis_pt(posture2,col:col+2);    % posture 2 start point
        pt_cloud(end+1,1:3) = axis_pt(posture1+10,col:col+2); % posture 1 end point
        pt_cloud(end+1,1:3) = axis_pt(posture2+10,col:col+2); % posture 2 end point
        % Add Reuleaux Landmark A & B to end of bone point cloud
        pt_cloud(end+1,1:3) = Landmark1(posture1,col:col+2);  % posture 1 Landmark A
        pt_cloud(end+1,1:3) = Landmark1(posture2,col:col+2);  % posture 2 Landmark A'
        pt_cloud(end+1,1:3) = Landmark2(posture1,col:col+2);  % posture 1 Landmark B
        pt_cloud(end+1,1:3) = Landmark2(posture2,col:col+2);  % posture 2 Landmark B'
        % PCA for reduction of dimensionality, score = principal component(XYZ)
        [eigenvectors, score] = pca(pt_cloud, 'Algorithm','eig', 'Centered',true);
    end
end

```

```

%% PCA method

n = 2; % defined plane to view: 2 is XY view plane, 3 is XZ view plane
% Line = [ X_start Y_start ; X_end Y_end ];
line1 = [score(end-7,1) score(end-7,n); score(end-5,1) score(end-5,n)]; % Posture 1
line2 = [score(end-6,1) score(end-6,n); score(end-4,1) score(end-4,n)]; % Posture 2
% Find slope of 2 lines for determining intercept
m1 = slope(line1);
m2 = slope(line2);
% Find intercept between 2 line using slopes
b1 = intercept(line1,m1);
b2 = intercept(line2,m2);
xintersect = (b2-b1)/(m1-m2); % COR_X (local)
yintersect = m1*xintersect + b1; % COR_Y (local)

% COR = [xintersect, 0, yintersect];
if n == 2; COR_PCA = [xintersect, yintersect, 0]; end
if n == 3; COR_PCA = [xintersect, 0, yintersect]; end

% Find rotation angle between 2 vectors (using slope)
line3 = [xintersect yintersect; score(end-7,1) score(end-7,2)];
line4 = [xintersect yintersect; score(end-6,1) score(end-6,2)];
m3 = slope(line3);
m4 = slope(line4);
angle = atand(m3) - atand(m4); % angle = tan^-1(slope1) - tan^-1(slope2)
% To handle acute & obtuse angle (angle with -ve number & angle that is larger than
perpendicular)
if angle < 0 , angle = -angle; end
if angle >90, angle = 180-angle; end
% Realeaux

% Find midpoint between A-A' & B-B'
A1 = [score(end-3,1), score(end-3,2)]; % Landmark A
A2 = [score(end-2,1), score(end-2,2)]; % Landmark A'
B1 = [score(end-1,1), score(end-1,2)]; % Landmark B
B2 = [score(end,1), score(end,2)]; % Landmark B'
mid_A = (A1(:) + A2(:)).'/2; % Midpoint of line A-A'
mid_B = (B1(:) + B2(:)).'/2; % Midpoint of line B-B'

% Line = [ X_start Y_start ; X_end Y_end ];
line5 = [score(end-3,1) score(end-3,2); score(end-2,1) score(end-2,2)];
line6 = [score(end-1,1) score(end-1,2); score(end,1) score(end,2)];
% Find perpendicular slope, per_slope = -1/slope
m5 = -1/slope(line5);
m6 = -1/slope(line6);

% Create Perpendicular line using per_slope and midpoint, [X,Y] = drawline(Midpoint,
per_slope, line length)
[xLine_1, yLine_1] = drawline1(mid_A,m5, 15); % MCP:45 PIP:15
[xLine_2, yLine_2] = drawline1(mid_B,m6, 7); % MCP:40 PIP:7

% Arrange coordinate of Perpendicular line to [X, Y, Z]
perp_line1 = zeros(length(xLine_1),3);
perp_line1(:,1) = xLine_1';
perp_line1(:,2) = yLine_1';
perp_line2 = zeros(length(xLine_2),3);
perp_line2(:,1) = xLine_2';
perp_line2(:,2) = yLine_2';

```

```

% Find intersection from A-A' & B-B' (Using Perpendicular line)
line7 = [perp_line1(1,1) perp_line1(1,n); perp_line1(end,1) perp_line1(end,n)];
line8 = [perp_line2(1,1) perp_line2(1,n); perp_line2(end,1) perp_line2(end,n)];
m7 = slope(line7);
m8 = slope(line8);
b3 = intercept([line7,m7]);
b4 = intercept([line8,m8]);
xintersect = (b4-b3)/(m7-m8); % COR_X (local)
yintersect = m7*xintersect + b3; % COR_Y (local)

if n == 2; COR_Realeaux = [xintersect, yintersect, 0]; end
if n == 3; COR_Realeaux = [xintersect, 0, yintersect]; end

end
end

%% PCA reconstruction of instantaneous CORs
% PCA reconstruction = score* Eigenvectors + Mean

nComp = 3; % Dimension: XYZ
mu = mean(pt_cloud); % Find mean of bone point cloud

% Figueroa instantaneous CORs
CoR_P_re = C_P(:,1:nComp) * eigenvectors(:,1:nComp)';
CoR_P_re = bsxfun(@plus, CoR_P_re, mu);

% Reuleaux instantaneous CORs
CoR_R_re = C_R(:,1:nComp) * eigenvectors(:,1:nComp)';
CoR_R_re = bsxfun(@plus, CoR_R_re, mu);

```

Estimate the fixed joint CoR using Bone curvature method

```

%% Define input
Digit      = 5; % 2~5
CoR_Joint = 'MCP'; % MCP / PIP / DIP

% Select contact point
Initial_contact_pt = 24; % initial contact point (X coordinate)
Last_contact_pt   = 17.8; % Last contact point (X coordinate)
smoothing_window = 19; % Gaussian smoothing window

ptCloud_1 = pcread(sprintf('%s_%s_0%d_1.ply', CoR_Joint, Distal_Joint, Digit)); % Distal bone
ptCloud_2 = pcread(sprintf('%s_0%d_1.ply', CoR_Joint, Digit)); % Proximal bone

% Apply PCA to get local coordinate
[eigenvectors1, score1] = pca(ptCloud_1.Location, 'Algorithm','eig', 'Centered',true);

% bone head is selected separately in 2 parts using X-plane
% 1st part: X coordinate of Bone point cloud > initial contact point
idx = 0;
for i = 1: length(score1(1:no_score2,1))
    if S02(i, 1) > Initial_contact_pt
        idx = idx + 1;
        Head1(idx,:) = S02(i,:);
    end
end

```

```

end

% 2nd part: Last contact point < X coordinate of Bone point cloud < Initial contact point
idx = 0;
for i = 1: length(score1(1:no_score2,1))
    if S02(i, 1) > Last_contact_pt && S02(i,1) <= Initial_contact_pt
        idx = idx + 1;
        Head2(idx,:)= S02(i,:);
    end
end

% Get outer point cloud from 1st part bone: Find X-maximum in every plane from 1st storage
idx1 = 1;
for i = length(storage(1,:))-2:-3:1
    a = find(storage(:,i) == max(storage(:,i)));
    point(idx1,:)= storage(a,i:i+2);
    idx1 = idx1 + 1;
end

% Get outer point cloud from 2nd part bone: Find Z-minimum in every plane from 2nd storage
for i = length(storage2(1,:))-3:-3
    a = find(storage2(:,i) == min(storage2(:,i)));
    point(idx1,:)= storage2(a,i-2:i);
    idx1 = idx1 + 1;
end

% Apply Gaussian filter
XY = [Filtered_point(:,1) Filtered_point(:,3)];
smoothed_XY = smoothdata(XY,'gaussian', smoothing_window);
Idx_crv_pt = LineCurvature2D(pt); % Curvature unit of all points

% Find tangent of landmark A
dy1 = diff(pt(:,2))./diff(pt(:,1)); % Find dy
k = find(abs(Idx_crv_pt) == max(abs(Idx_crv_pt))); % index of landmark A = index that contains largest curv. unit
tang1 = (pt(:,1)-pt(k,1))*dy1(k)+pt(k,2); % Find tangent (Y)
pt_A = [pt(k,1) pt(k,2)]; % Coordinate of landmark A

% Draw perpendicular bisectors using tangent line and landmark A
slope = @(line) (line(2,2) - line(1,2))/(line(2,1) - line(1,1)); % Find slope
line1 = [pt(1,1) tang1(1); pt(end,1) tang1(end)]; % Tangent line of landmark A
m1 = -1/slope(line1); % perpendicular slope of tangent line of landmark A
[xLine_1, yLine_1] = drawline(pt_A,m1, 8); % Draw perpendicular tangent line

% Find intercept of Landmark A
line4 = [xLine_1(1) yLine_1(1); xLine_1(end) yLine_1(end)];
intercept = @(line,m) line(1,2) - m*line(1,1);
b4 = intercept(line4,m1);

% Find all intercept of all landmark B: points that located at left side of A
idx = 0;
for i = k:5:length(pt)
    idx = idx + 1;
    k1 = i; % Index of random landmark

    if k1 < length(pt)
        tang2=(pt(:,1)-pt(k1,1))*dy1(k1)+pt(k1,2);
        pt_B = [pt(k1,1) pt(k1,2)];
        Landmark(idx,:)= [pt(k1,1) 0 pt(k1,2)];
    end
end

```

```

line2 = [pt(1,1) tang2(1); pt(end,1) tang2(end)];
m2 = -1/slope(line2);
[xLine_2, yLine_2] = drawline1(pt_B,m2, 8);
line5 = [xLine_2(1) yLine_2(1); xLine_2(end) yLine_2(end)];
m5(idx) = slope(line5);
b5(idx) = intercept(line5,m5(idx));
end
end

% Find intersection of line(Landmark A) and line(Landmark B)
% CoR2 = CoRs that found only from pair of line(Landmark A) and all lines(landmark B)
idx = 0;idx1 = 0;
for i = 1:length(b5)
    for j = i+1:length(b5)
        idx = idx + 1;
        xintersect1 = (b5(j)-b5(i))/(m5(i)-m5(j));
        yintersect1 = m5(i)*xintersect1 + b5(i);
        pair(idx,:) = [i j];
        if i == length(b5) || j == length(b5)
            idx1 = idx1 + 1;
            CoR2(idx1,:) = [xintersect1 0 yintersect1];
        end
    end
end

% Find centroid using CoR1 and CoR2
[idxx,C] = kmeans(CoR2(:,1:2:3),1);

%% PCA reconstruction: Transform COR back to global coordinate system

nComp = 3; % Dimension: XYZ
mu = mean(ptCloud_2.Location); % Find mean of bone point cloud

CoR1_curv_re = New_Cor(:,1:nComp) * eigenvectors2(:,1:nComp)';
CoR1_curv_re = bsxfun(@plus, CoR1_curv_re, mu) % Global centroid CoR

```

Estimate the fixed joint CoR using Delonge-Kasa method

```

%% Define input
Digit      = 5; % 2~5
CoR_Joint = 'MCP'; % MCP / PIP / DIP
name      = sprintf('Digit 0%d', Digit);
ptCloud = pcread(sprintf('%s_All_0%d.ply', Distal_Joint, Digit)); % Distal bone
ptCloud_MCP = pcread(sprintf('%s_0%d_1.ply', CoR_Joint, Digit)); % Proximal bone
Landmark1      = xlsread('Landmark_Kasa.xlsx', name); % Landmark of motion

% PCA to determine principal component (score)
[eigenvectors, score] = pca(pt_cloud, 'Algorithm', 'eig', 'Centered', true);

% Use PCA component to undergo delonge-kasa
YZ = score(end-N+1:end,1:2); % Use YZ data

COR = Kasa(YZ) % Delonge-Kasa

nComp = 3; % Dimension: XYZ
mu = mean(pt_cloud); % Find mean of bone point cloud

```

```
% PCA reconstruction = score* Eigenvectors + Mean
COR_re = Cor(:,1:nComp) * eigenvectors(:,1:nComp)';
COR_re = bsxfun(@plus, COR_re, mu)
```

Validate the motion-based estimated joint CoR

```
%% Define input
Digit      = 5; % 1~5
CoR_Joint  = 'DIP'; % MCP / PIP / DIP

name = sprintf('%s%d', CoR_Joint, Digit);
name1 = sprintf('Digit %d', Digit);
Raw   = xlsread('DH_of_Global_coordinate.xlsx', name);
PCA_line = xlsread('PCA_Reconstructed.xlsx', name1);

%% Fine Rotation 1: PCA line align to MCP marker
% fine-rotate: Align axis line to initial marker (X_marker = 0, X_pca1 = 0, Y_marker_pip = 0)
fun1 = @(x)Processing1(x, translated_PCA1(1),translated_PCA1(2),translated_PCA1(3),
initial_marker_PIP(1),initial_marker_PIP(2),initial_marker_PIP(3),initial_marker(1),initial_marker(2),initial_marker(3));
% fun1 = @(x)Processing1(x, translated_PCA1(1),translated_PCA1(2),translated_PCA1(3),
% translated_PCA2(1),translated_PCA2(2),translated_PCA2(3),initial_marker(1),initial_marker(2),initial_marker(3));
x1 = fsolve(fun1,[0,0,0]);
OO = x1(1); PP = x1(2); KK = x1(3);
M2 = [cosd(PP)*cosd(KK)    (cosd(OO)*sind(KK))+(sind(OO)*sind(PP)*cosd(KK))
((sind(OO)*sind(KK))-(cosd(OO)*sind(PP)*cosd(KK))) ; ...
       -(cosd(PP)*sind(KK)) ((cosd(OO)*cosd(KK))-(sind(OO)*sind(PP)*sind(KK)))
((sind(OO)*cosd(KK))+(cosd(OO)*sind(PP)*sind(KK))) ; ...
       sind(PP)           -(sind(OO)*cosd(PP))
cosd(OO)*cosd(PP)];
idx = 0;
for i = 1:length(score)
    idx=idx+1;
    C1 = [S02(1,i);S02(2,i);S02(3,i)];
    S03(:,idx) = M2*C1;
end

% Project motion data into 2D by rotation
[val, idx_DIP] = min(TP_01(:,2));
fun = @(x)Processing(x, TP_01(1,1),TP_01(1,2),TP_01(1,3),
TP_01(idx_DIP,1),TP_01(idx_DIP,2),TP_01(idx_DIP,3));
% fun = @Rot_S1;
idx = 0;
x = fsolve(fun,[0,0,0])
O = x(1); P = x(2); K = x(3);
M2 = [cosd(P)*cosd(K)    (cosd(O)*sind(K))+(sind(O)*sind(P)*cosd(K))    ((sind(O)*sind(K))-...
(cosd(O)*sind(P)*cosd(K))) ; ...
       -(cosd(P)*sind(K)) ((cosd(O)*cosd(K))-(sind(O)*sind(P)*sind(K)))
((sind(O)*cosd(K))+(cosd(O)*sind(P)*sind(K))) ; ...
       sind(P)           -(sind(O)*cosd(P))           cosd(O)*cosd(P)];
for i = 1:length(DIP)
    idx=idx+1;
    TP_02(:,idx) = M2*TP_01t(:,i);
```

```
DIP_02(:,idx) = M2*DIP_01t(:,i);  
end  
  
CT_link_length_MCP_PIP = S04(end-2,2) - S04(end-3,2)  
Motion_link_length_MCP_PIP = PIP_01(1,2) - Motion_data_TP(1,2)  
Error_distance_y = CT_link_length_MCP_PIP - Motion_link_length_MCP_PIP  
idx = 0;  
for i = 1:length(Motion_data_TP)  
    idx = idx + 1;  
    y(idx,:) = Motion_data_TP(i,2) - Error_distance_y;  
end  
  
%% Delonge-Kasa  
COR_PIP = Kasa(New_distal_motion(:,2:3))
```

Appendix D: Mean distances of instantaneous joint CoRs

MCP joint

	Digit 02		Digit 03		Digit 04		Digit 05	
	Figueroa	Reuleaux	Figueroa	Reuleaux	Figueroa	Reuleaux	Figueroa	Reuleaux
P1	1.6±1.2	7.8±15.4	1.1±0.9	1.6±1.3	1.1±0.8	1.3±1.0	1.3±1.2	1.8±1.4
P2	1.7±1.3	5.6±4.9	0.7±0.6	1.4±1.8	2.5±3.2	3.5±8.7	3.7±4.9	5.3±5.3
P3	1.0±1.2	1.3±1.3	0.4±0.4	1.2±1.6	1.0±1.4	1.2±1.7	1.8±2.1	5.0±12.2
P4	2.7±2.8	51±213	1.1±1.0	3.5±4.4	1.2±1.6	2.3±2.5	2.9±6.7	10.2±25
P5	0.8±1.0	1.2±1.5	1.0±0.7	2.0±2.2	2.0±1.3	2.2±2.7	2.0±1.8	23.5±77
P6	1.8±1.5	4.7±14.1	3.2±7.4	3.5±6.5	1.5±1.1	2.7±2.1	1.8±2.6	4.8±8.7
P7	1.4±1.6	4.7±3.9	0.7±1.1	2.1±3.6	0.8±0.6	2.8±5.8	0.8±1.0	2.2±3.5
P8	1.7±4.0	4.1±6.8	0.±0.5	1.5±1.2	0.9±1.4	1.9±1.5	4.5±7.1	9.0±28.9
P9	1.5±1.9	2.3±2.7	2.2±6.5	2.2±6.0	0.8±0.8	1.4±1.6	1.1±2.8	2.9±3.7

PIP joint

	Digit 02		Digit 03		Digit 04		Digit 05	
	Figueroa	Reuleaux	Figueroa	Reuleaux	Figueroa	Reuleaux	Figueroa	Reuleaux
P1	2.7±3.6	4.1±8.6	5.8±13.3	10.7±25	4.3±5.3	4.0±6.6	8.9±32.4	4.6±10.5
P2	0.8±1.1	2.6±8.2	1.3±1.6	1.3±1.6	1.4±1.5	1.4±1.9	1.1±1.6	3.2±8.5
P3	0.9±1.4	1.2±3.2	0.8±1.6	1.0±1.7	1.2±1.6	1.1±1.6	3.9±11.9	4.1±11.6
P4	2.2±3.3	2.0±3.3	6.7±23.4	7.2±24.6	4.2±1.4	8.3±26.2	3.1±8.9	6.7±25.3
P5	0.9±1.1	1.0±1.1	1.8±4.5	1.9±4.2	1.1±1.7	1.2±1.8	0.6±0.7	1.1±1.6
P6	1.1±1.6	1.0±1.3	3.3±6.9	3.2±7.6	1.7±1.5	1.5±1.5	3.2±7.8	14.3±47
P7	0.9±0.6	0.6±0.5	1.4±3.0	7.3±27.4	1.4±2.3	1.2±2.3	0.8±0.8	1.2±1.5
P8	0.5±0.3	0.2±0.1	1.1±1.8	1.1±1.9	0.8±1.1	0.9±1.1	1.4±3.1	1.5±3.4
P9	2.9±5.2	3.4±6.1	1.2±2.2	2.8±4.0	1.4±2.7	1.6±3.4	1.4±2.2	4.5±16.6

DIP joint

	Digit 02		Digit 03		Digit 04		Digit 05	
	Figueroa	Reuleaux	Figueroa	Reuleaux	Figueroa	Reuleaux	Figueroa	Reuleaux
P1	0.7±0.8	1.1±1.1	0.5±0.7	0.6±0.7	0.7±1.3	0.8±1.5	2.0±3.9	1.8±3.2
P2	1.2±2.2	1.4±2.1	0.8±1.1	1.0±1.3	1.7±4.8	2.1±4.9	0.4±0.5	0.8±0.7
P3	0.6±0.5	0.6±0.6	1.0±2.2	2.8±9.5	0.4±0.3	0.5±0.6	0.4±0.5	0.5±0.5
P4	1.3±3.4	4.6±8.6	1.3±1.9	1.3±2.2	7.0±18.9	8.8±24.8	0.6±0.9	2.3±4.6
P5	1.0±0.8	0.9±0.7	2.4±5.5	1.5±1.4	9.1±30.9	8.6±28.4	0.9±2.1	1.2±1.2
P6	1.5±2.3	2.4±3.6	1.2±2.6	1.6±3.6	1.0±1.3	1.3±1.5	2.1±3.1	2.7±4.8
P7	0.4±0.4	0.7±0.7	0.7±0.7	0.8±1.3	0.6±1.2	0.7±0.8	0.3±0.7	0.4±0.7
P8	0.7±1.6	2.3±7.2	1.4±3.2	2.2±6.1	0.4±0.5	0.6±1.0	1.2±2.0	1.3±2.0
P9	1.8±3.6	5.9±14.7	0.8±1.0	1.1±1.2	1.0±1.2	1.4±2.2	1.0±1.6	1.1±1.2

Appendix E: Instantaneous joint CoRs

Participant 1: Instantaneous Joint CoRs by Figueroa et al.'s method

Posture	Index												Middle												Ring												Little											
	MCP joint				PIP joint				DIP joint				MCP joint				PIP joint				DIP joint				MCP joint				PIP joint				DIP joint				MCP joint				PIP joint							
	First	Second	X	Y	Z	X	Y	Z	X	Y	Z	X	Y	Z	X	Y	Z	X	Y	Z	X	Y	Z	X	Y	Z	X	Y	Z	X	Y	Z	X	Y	Z	X	Y	Z	X	Y	Z	X	Y	Z				
1	2	-4.1	0.9	131.2	-0.1	12.6	85.0	-0.9	14.9	57.0	-26.3	0.3	131.8	-19.8	15.1	80.7	-18.5	15.6	47.7	-45.9	5.8	137.7	-39.6	15.3	89.8	-38.3	18.8	58.3	-61.9	18.2	141.4	-57.1	19.1	108.2	-56.3	20.6	85.2											
1	3	-4.1	0.9	131.5	-0.1	12.6	85.0	-0.9	14.8	56.5	-26.2	0.0	132.8	-19.8	15.2	80.6	-18.5	15.4	46.9	-45.9	5.7	138.3	-39.6	15.3	89.6	-38.3	18.8	58.0	-61.5	17.6	145.5	-57.1	19.0	108.9	-56.3	20.6	84.8											
1	4	-3.9	1.0	130.7	-0.1	12.6	84.9	-0.9	14.9	57.0	-26.2	0.1	132.3	-19.8	15.3	80.4	-18.5	15.6	47.7	-45.9	5.6	138.7	-39.6	15.4	88.5	-38.3	18.8	58.3	-61.5	17.6	145.2	-57.1	19.1	107.7	-56.3	20.6	84.4											
1	5	-3.5	1.1	129.6	-0.1	12.6	84.7	-0.9	14.9	57.1	-26.0	0.7	130.1	-19.6	15.0	78.8	-18.5	15.6	47.9	-45.7	6.3	135.4	-39.6	15.6	85.7	-38.3	18.9	58.5	-61.7	17.8	143.7	-57.1	19.2	107.1	-56.3	20.6	84.3											
1	6	-3.4	1.2	129.3	-0.1	12.6	84.6	-0.9	14.9	57.2	-26.0	0.6	130.6	-19.6	15.0	78.5	-18.5	15.6	47.9	-45.6	6.1	136.1	-39.6	15.6	85.3	-38.3	18.9	58.4	-61.4	17.5	146.2	-57.2	19.2	107.3	-56.3	20.6	84.3											
1	7	-3.3	1.3	128.9	-0.1	12.6	84.6	-0.9	14.9	57.1	-26.0	0.6	130.6	-19.6	15.0	78.5	-18.5	15.6	47.8	-45.7	6.2	135.7	-39.6	15.6	85.6	-38.3	18.9	58.4	-61.5	17.6	145.5	-57.2	19.2	107.3	-56.3	20.6	84.3											
1	8	-3.3	1.2	129.0	-0.1	12.6	84.3	-0.9	14.9	57.1	-26.0	0.6	130.3	-19.6	15.0	78.6	-18.5	15.6	47.9	-45.7	6.1	135.9	-39.6	15.5	85.4	-38.3	18.8	58.4	-61.5	17.6	145.3	-57.2	19.2	107.2	-56.3	20.6	84.4											
1	9	-3.3	1.3	129.0	-0.1	12.6	84.3	-0.9	14.9	57.2	-26.0	0.7	130.2	-19.6	15.0	78.7	-18.5	15.6	47.9	-45.7	6.2	135.9	-39.6	15.5	85.6	-38.3	18.9	58.5	-61.5	17.7	144.8	-57.1	19.2	107.2	-56.3	20.6	84.9											
1	10	-3.0	1.4	128.0	-0.1	12.6	84.0	-0.9	14.9	57.2	-26.0	0.7	130.3	-19.7	15.0	79.2	-18.5	15.6	48.0	-45.6	6.0	136.5	-39.6	15.5	86.9	-38.3	18.9	58.6	-61.5	17.5	145.5	-57.1	19.1	107.3	-56.3	20.7	84.8											
2	3	-4.1	0.9	131.4	-0.1	13.0	84.8	-0.9	14.7	57.4	-26.2	0.0	130.9	-19.6	16.2	80.2	-18.8	15.1	49.5	-45.7	5.7	138.5	-39.6	15.6	89.9	-38.4	18.8	58.6	-60.9	17.7	147.4	-56.7	19.8	107.6	-56.2	20.7	84.3											
2	4	-3.0	1.8	128.8	-0.1	13.0	84.7	-0.9	14.7	57.4	-26.2	0.1	130.2	-19.8	16.4	80.1	-18.5	15.6	47.8	-45.7	5.7	139.2	-39.3	17.0	88.4	-38.3	18.8	58.1	-60.9	17.7	146.7	-56.7	19.7	107.6	-56.2	20.7	84.3											
2	5	-3.1	1.8	128.8	-0.1	13.0	84.7	-0.9	14.7	57.4	-26.0	0.5	130.7	-19.7	16.4	80.4	-18.5	15.6	47.8	-45.7	5.6	139.2	-39.3	17.0	88.4	-38.3	18.8	58.1	-60.9	17.7	146.7	-56.7	19.7	107.6	-56.2	20.7	84.3											
2	6	-3.0	1.8	128.8	-0.1	13.0	84.8	-0.9	14.8	57.3	-26.1	0.5	130.7	-19.7	16.4	80.4	-18.5	15.6	47.8	-45.8	5.6	139.4	-39.3	17.0	88.3	-38.3	18.8	58.1	-60.9	17.7	146.7	-56.7	19.7	107.6	-56.2	20.7	84.3											
2	7	-3.1	1.8	128.8	-0.1	13.1	84.7	-0.9	14.8	57.3	-26.1	0.5	130.7	-19.7	16.4	80.4	-18.5	15.6	47.8	-45.8	5.6	139.4	-39.3	17.0	88.4	-38.3	18.8	58.1	-60.9	17.7	146.7	-56.7	19.7	107.6	-56.2	20.7	84.3											
2	8	-3.1	1.8	128.8	-0.1	13.2	84.6	-0.9	14.8	57.3	-26.1	0.5	130.6	-19.6	16.4	80.5	-18.5	15.6	47.8	-45.8	5.6	139.5	-39.3	17.0	88.3	-38.3	18.8	58.1	-60.9	17.7	146.7	-56.7	19.7	107.6	-56.2	20.7	84.3											
2	9	-2.8	2.0	128.8	-0.1	13.3	84.5	-0.9	14.9	57.4	-26.0	0.4	130.6	-19.6	16.4	80.5	-18.5	15.6	47.9	-45.8	5.6	139.5	-39.3	17.0	88.4	-38.3	18.8	58.1	-60.9	17.7	146.7	-56.7	19.7	107.6	-56.2	20.7	84.3											
2	10	-0.0	0.8	131.1	-0.1	12.6	84.9	-0.9	14.8	57.2	-26.0	0.4	130.7	-19.7	16.4	80.6	-18.6	15.6	48.0	-45.9	5.9	139.5	-39.2	17.0	88.5	-38.4	18.8	58.2	-60.9	17.7	146.5	-56.7	19.7	107.6	-56.2	20.7	84.5											
3	4	-3.8	0.7	130.2	-0.1	12.9	84.7	-0.9	14.7	57.3	-26.2	0.0	131.0	-19.6	16.3	80.7	-18.5	15.7	48.2	-45.6	6.0	139.6	-39.3	17.0	88.6	-38.4	18.8	58.2	-60.9	17.7	146.7	-56.7	19.7	107.6	-56.2	20.7	84.4											
3	5	-3.7	0.7	129.7	-0.1	13.0	84.7	-0.9	14.7	57.2	-26.2	0.2	131.0	-19.6	16.3	80.8	-18.7	15.7	48.1	-45.6	5.6	139.7	-39.2	17.0	88.2	-38.4	18.8	58.2	-60.9	17.7	146.7	-56.7	19.7	107.6	-56.2	20.7	84.3											
3	6	-3.5	0.7	129.7	-0.1	13.0	84.7	-0.9	14.7	57.3	-26.3	0.3	131.4	-19.6	16.4	80.8	-18.7	15.7	48.1	-45.6	5.5	139.7	-39.2	17.0	88.2	-38.4	18.8	58.2	-60.9	17.7	146.7	-56.7	19.7	107.6	-56.2	20.7	84.3											
3	7	-3.5	0.7	129.7	-0.1	13.2	84.5	-0.9	14.7	57.2	-26.3	0.3	131.6	-19.6	16.5	80.9	-18.7	15.7	48.0	-45.6	5.5	139.7	-39.2	17.0	88.2	-38.4	18.8	58.2	-60.9	17.7	146.7	-56.7	19.7	107.6	-56.2	20.7	84.3											
3	8	-3.5	0.7	129.7	-0.1	13.2	84.5	-0.9	14.7	57.3	-26.3	0.3	131.6	-19.6	16.5	80.9	-18.7	15.7	48.0	-45.6	5.5	139.7	-39.2	17.0	88.2	-38.4	18.8	58.2	-60.9	17.7	146.7	-56.7	19.7	107.6	-56.2	20.7	84.3											
3	9	-3.1	1.7	129.0	-0.1	13.2	84.5	-0.9	14.7	57.4	-26.3	0.3	131.6	-19.6	16.5	80.9	-18.7	15.7	48.0	-45.6	5.5	139.7	-39.2	17.0	88.2	-38.4	18.8	58.2	-60.9	17.7	146.7	-56.7	19.7	107.6	-56.2	20.7	84.3											
3	10	-2.9	2.1	128.1	-0.1	13.6	84.5	-0.9	14.9	57.1	-26.0	0.0	130.3	-19.6	16.5	80.6	-18.6	15.6	48.0	-45.6	5.9	139.5	-39.4	17.0	88.4	-38.4	18.8	58.4	-60.9	17.7	146.7	-56.7	19.7	107.6	-56.2	20.7	84.3											
4	5	-3.5	0.5	129.0	-0.1	12.9	85.1	-0.9	14.4	56.6	-24.8	0.3	131.9	-19.6	16.3	80.4	-18.7	15.7	47.5	-44.3	9.5	139.3	-39.3	17.0	88.3	-38.3	18.8	58.3	-60.9	17.7	146.7	-56.7	19.7	107.6	-56.2	20.7	84.5											
4	7	-3.7	2.9	128.3	-0.1	12.9	85.0	-0.9	14.4	56.6	-25.0	0.3	131.9	-19.6	16.3	80.4	-18.7	15.7	47.5	-44.3	9.5	139.3	-39.3	17.0	88.3	-38.3	18.8	58.3	-60.9	17.7	146.7	-56.7	19.7	107.6	-56.2	20.7	84.5											
4	8	-3.6	3.2	128.2	-0.1	13.0	84.9	-0.9	14.5	56.6	-25.0	0.3	131.9	-19.7	16.3	80.5	-18.8	15.8	47.6	-44.8	9.4	139.3	-39.3	17.0	88.4	-38.4	18.8	58.4	-60.9	17.7	146.7	-56.7	19.7	107.6	-56.2	20.7	84.5											
4	9	-3.6	3.3	128.2	-0.1	13.0	84.9	-0.9	14.5	56.6	-25.0	0.3	131.7	-19.7	16.3	80.5	-18.8	15.8	47.6	-44.8	9.4	139.3	-39.3	17.0	88.4	-38.4	18.8	58.4	-60.9	17.7	146.7	-56.7	19.7	107.6	-56.2	20.7	84.5											
4	10	-3.4	3.7	128.1	-0.1	13.0	84.9	-0.9	14.5	56.7	-25.1	0.3	131.9	-19.7	16.4	80.5	-18.8	15.8	47.6	-44.8	9.4	139.3	-39.3	17.0	88.4	-38.4	18.8	58.4	-60.9	17.7	146.7	-56.7	19.7	107.6	-56.2	20.7	84.5											
4	2	-3.9	3.0	130.3	-0.1	13.2	85.2	-0.1	15.3	56.8	-25.8	0.3	131.6	-19.7	16.4	80.5	-18.6	15.6	48.8	-45.3	7.3	138.6	-39.6	17.0	88.4	-38.6	18.8	58.4	-60.9	17.7	147.5	-56.7	19.7	107.5	-56.2	20.7	84.0											
4	3	-3.4	2.9	130.3	-0.1	13.2	85.2	-0.1	15.3	56.8	-25.8	0.3	131.6	-19.6	16.3	80.5	-18.6	15.6	48.5	-45.3	7.3	138.6	-39.6	17.0	88.4	-38.6	18.8	58.4	-60.9	17.7	147.5	-56.7	19.7	107.5	-56.2	20.7	84.0											
4</td																																																

Participant 2: Instantaneous Joint CoRs by Figueroa et al.'s method

Posture	Index												Middle												Ring												Little											
	MCP joint				PIP joint				DIP joint				MCP joint				PIP joint				DIP joint				MCP joint				PIP joint				DIP joint				MCP joint				PIP joint				DIP joint			
First	Second	X	Y	Z	X	Y	Z	X	Y	Z	X	Y	Z	X	Y	Z	X	Y	Z	X	Y	Z	X	Y	Z	X	Y	Z	X	Y	Z	X	Y	Z	X	Y	Z	X	Y	Z	X	Y	Z	X	Y	Z		
1	2	17.7	68.8	64.7	15.2	56.6	19.3	13.1	-51.2	-7.9	-4.4	-66.4	61.7	-4.4	-57.2	12.4	-4.7	-52.2	-19.6	-24.2	-63.0	-56.5	18.4	23.6	-51.6	-10.7	-38.1	-58.7	95.6	-41.0	55.0	41.6	-41.7	-49.5	14.2													
1	3	17.7	68.8	64.7	15.1	56.5	18.7	13.4	-51.2	-6.5	-4.4	-66.3	61.2	-4.4	-57.0	10.5	-4.8	-52.2	-20.0	-24.2	-63.2	-67.3	-22.5	-55.6	19.3	23.6	-51.6	-10.3	-41.8	-58.6	74.6	-41.2	53.9	35.0	-41.7	-49.6	13.7											
1	4	17.5	69.2	66.8	15.1	56.5	18.6	13.4	-51.2	-6.6	-4.4	-66.4	62.0	-4.5	-57.0	9.9	-4.9	-52.2	-20.1	-24.1	-63.3	-67.7	-22.5	-55.6	18.9	23.6	-51.6	-10.5	-41.7	-56.8	75.2	-41.2	53.4	34.7	-41.7	-49.6	13.7											
1	5	17.5	69.1	66.5	15.1	56.4	18.3	13.4	-51.2	-6.5	-4.4	-66.4	62.1	-4.5	-56.9	9.4	-4.7	-52.2	-19.9	-24.3	-62.1	-69.2	-22.6	-55.6	18.4	23.6	-51.6	-10.4	-41.1	-51.1	78.3	-41.2	53.8	34.3	-41.7	-49.6	13.8											
1	6	17.6	68.9	65.6	15.1	56.4	18.3	13.4	-51.2	-6.6	-4.4	-66.4	61.9	-4.5	-56.9	9.3	-4.7	-52.2	-19.9	-24.2	-62.7	-63.7	-22.6	-55.6	18.3	23.6	-51.6	-10.4	-40.4	-51.2	57.1	-41.2	53.8	34.3	-41.7	-49.6	13.8											
1	7	17.7	68.9	65.4	15.1	56.4	18.3	13.4	-51.2	-6.6	-4.4	-66.4	61.6	-4.5	-56.9	8.8	-4.7	-52.2	-19.9	-24.2	-63.1	-66.4	-22.6	-55.5	17.8	23.6	-51.6	-10.5	-41.9	-56.7	73.8	-41.2	53.7	33.7	-41.7	-49.6	13.7											
1	8	17.7	68.8	64.8	15.1	56.4	18.2	13.4	-51.2	-6.6	-4.4	-66.3	61.2	-4.5	-56.9	8.8	-4.7	-52.2	-19.9	-24.2	-63.0	-65.6	-22.6	-55.4	17.0	23.6	-51.7	-10.7	-42.2	-56.6	72.3	-41.2	53.7	33.6	-41.7	-49.6	13.6											
1	9	17.8	68.8	64.6	15.1	56.4	18.1	13.4	-51.2	-6.6	-4.4	-66.3	61.0	-4.5	-56.8	8.7	-4.8	-52.2	-20.1	-24.2	-63.0	-65.6	-22.6	-55.4	17.0	23.6	-51.7	-10.5	-41.9	-56.7	73.8	-41.2	53.7	33.6	-41.7	-49.6	13.6											
1	10	17.8	68.8	64.5	15.1	56.4	18.1	13.4	-51.2	-6.7	-4.4	-66.3	61.2	-4.5	-56.9	9.2	-4.8	-52.2	-20.2	-24.2	-63.0	-65.6	-22.6	-55.5	17.5	23.6	-51.7	-10.8	-42.2	-56.5	72.1	-41.2	53.7	33.6	-41.7	-49.6	13.5											
2	3	17.7	68.8	64.7	15.1	56.5	18.7	13.4	-51.2	-6.4	-4.4	-66.3	61.2	-4.4	-57.0	10.5	-4.8	-52.2	-20.1	-24.2	-63.2	-67.2	-22.5	-55.6	19.3	23.6	-51.6	-10.2	-41.7	-56.9	74.8	-41.2	54.0	35.1	-41.7	-49.6	13.6											
2	4	17.6	69.0	65.5	15.1	56.5	18.6	13.4	-51.2	-6.5	-4.4	-66.4	61.5	-4.5	-56.9	9.4	-4.7	-52.2	-19.9	-24.3	-62.5	-62.0	-22.6	-55.6	18.4	23.6	-51.6	-10.4	-41.7	-57.2	78.0	-41.2	53.8	34.3	-41.7	-49.6	13.7											
2	5	17.6	69.0	65.3	15.1	56.4	18.3	13.4	-51.2	-6.5	-4.4	-66.4	61.4	-4.5	-56.9	9.1	-4.8	-52.2	-19.9	-24.2	-63.0	-66.4	-22.6	-55.5	17.8	23.6	-51.6	-10.5	-41.7	-56.9	74.9	-41.2	53.8	33.8	-41.7	-49.6	13.7											
2	6	17.7	68.8	64.8	15.1	56.4	18.1	13.4	-51.2	-6.6	-4.4	-66.3	61.2	-4.5	-56.9	8.8	-4.7	-52.2	-19.9	-24.2	-63.0	-65.6	-22.6	-55.5	17.4	23.6	-51.6	-10.5	-41.9	-56.8	74.0	-41.2	53.7	33.7	-41.7	-49.6	13.6											
2	7	17.7	68.8	64.6	15.1	56.4	18.1	13.4	-51.2	-6.6	-4.4	-66.3	61.0	-4.5	-56.8	8.7	-4.8	-52.2	-20.1	-24.2	-63.0	-65.6	-22.6	-55.4	17.0	23.6	-51.7	-10.7	-42.2	-56.6	72.3	-41.2	53.7	33.6	-41.7	-49.6	13.6											
2	8	17.7	68.8	64.6	15.1	56.4	18.1	13.4	-51.2	-6.7	-4.4	-66.3	61.0	-4.5	-56.9	9.2	-4.8	-52.2	-20.2	-24.2	-63.0	-65.6	-22.6	-55.5	17.5	23.6	-51.6	-10.8	-42.2	-56.5	72.1	-41.2	53.7	33.6	-41.7	-49.6	13.5											
3	4	18.4	66.8	62.8	15.1	56.5	18.3	13.4	-51.2	-6.6	-4.4	-66.0	60.3	-4.5	-56.9	9.4	-4.8	-52.2	-19.9	-24.2	-63.5	-67.8	-22.5	-55.6	18.7	23.6	-51.6	-10.5	-41.8	-56.8	74.6	-41.2	53.4	34.1	-41.7	-49.6	13.8											
3	5	18.2	67.4	63.4	15.1	56.5	18.3	13.4	-51.2	-6.6	-4.4	-66.0	60.3	-4.5	-56.9	9.4	-4.8	-52.2	-19.9	-24.2	-63.5	-67.8	-22.5	-55.6	18.7	23.6	-51.6	-10.5	-41.8	-56.8	74.7	-41.2	53.4	34.1	-41.7	-49.6	13.8											
3	6	18.2	67.4	63.4	15.1	56.5	18.3	13.4	-51.2	-6.6	-4.4	-66.0	60.3	-4.5	-56.9	9.4	-4.8	-52.2	-19.9	-24.2	-63.5	-67.8	-22.5	-55.6	18.7	23.6	-51.6	-10.5	-41.8	-56.8	74.7	-41.2	53.4	34.1	-41.7	-49.6	13.8											
3	7	18.4	66.8	62.8	15.1	56.5	18.3	13.4	-51.2	-6.6	-4.4	-66.0	60.3	-4.5	-56.9	9.4	-4.8	-52.2	-19.9	-24.2	-63.5	-67.8	-22.5	-55.6	18.7	23.6	-51.6	-10.5	-41.8	-56.8	74.7	-41.2	53.4	34.1	-41.7	-49.6	13.8											
3	8	18.2	67.4	63.4	15.1	56.5	18.3	13.4	-51.2	-6.6	-4.4	-66.0	60.3	-4.5	-56.9	9.4	-4.8	-52.2	-19.9	-24.2	-63.5	-67.8	-22.5	-55.6	18.7	23.6	-51.6	-10.5	-41.8	-56.8	74.7	-41.2	53.4	34.1	-41.7	-49.6	13.8											
3	9	18.1	67.4	63.4	15.1	56.5	18.3	13.4	-51.2	-6.6	-4.4	-66.0	60.3	-4.5	-56.9	9.4	-4.8	-52.2	-19.9	-24.2	-63.5	-67.8	-22.5	-55.6	18.7	23.6	-51.6	-10.5	-41.8	-56.8	74.7	-41.2	53.4	34.1	-41.7	-49.6	13.8											
3	10	18.1	67.4	63.4	15.1	56.5	18.3	13.4	-51.2	-6.6	-4.4	-66.0	60.3	-4.5	-56.9	9.4	-4.8	-52.2	-19.9	-24.2	-63.5	-67.8	-22.5	-55.6	18.7	23.6	-51.6	-10.5	-41.8	-56.8	74.7	-41.2	53.4	34.1	-41.7	-49.6	13.8											
4	9	17.8	68.4	62.8	15.1	56.5	18.3	13.4	-51.2	-6.6	-4.4	-66.0	60.3	-4.5	-56.9	9.4	-4.8	-52.2	-19.9	-24.2	-63.5	-67.8	-22.5	-55.6	18.7	23.6	-51.6	-10.5	-41.8	-56.8	74.7	-41.2	53.4	34.1	-41.7	-49.6	13.8											
4	10	18.1	67.4	63.4	15.1	56.5	18.3	13.4	-51.2	-6.6	-4.4	-66.0	60.3	-4.5	-56.9	9.5	-4.8	-52.2	-19.9	-24.2	-63.5	-67.8	-22.5	-55.6	18.7	23.6	-51.6	-10.5	-41.8	-56.8	74.7	-41.2	53.4	34.1	-41.7	-49.6	13.8											
4	11	17.7	68.8	64.8	15.1	56.9	18.5	13.4	-51.2	-6.7	-4.2	-66.4	64.4	-4.5	-57.0	10.5	-4.8	-52.2	-19.9	-24.2	-63.9	-68.8	-22.5	-55.5	19.4	23.6	-51.6	-10.7	-42.0	-57.0	81.6	-41.2	53.8	34.1	-41.7	-49.6	13.7											
4	12	4	16.8	71.7	66.2	15.0	57.0	18.1	13.4	-51.2	-6.7	-4.2	-66.1	64.4	-4.5	-57.0	9.9	-5.1	-52.2	-20.4	-23.7	-60.9	-68.8	-22.5	-55.3	19.4	23.6	-51.6	-10.7	-41.6	-57.5	76.5	-41.2	53.8	34.1	-41.7	-49.6	13.7										
4	13	5	15.7	74.8	70.5	15.0	56.7	18.3	13.4	-51.2	-6.8	-4.1	-66.1	64.4	-4.5	-56.7	9.6	-5.1	-52.2	-20.4	-23.7	-60.3	-68.8	-22.5	-55.3	18.4	23.6	-51.6	-10.7	-41.6	-57.5	76.5	-41.2	53.8	34.1	-41.7	-49.6	13.7										
4	14	6	15.9	71.2	67.0	15.0	56.7	18.3	13.4	-51.2	-6.8	-4.1	-66.1	64.4	-4.5	-56.8	9.6	-5.1	-52.2	-20.4	-23.7	-60.3	-68.8	-22.5	-55.3	18.4	23.6	-51.6	-10.7	-41.6	-57.5	76.5	-41.2	53.8	34.1	-41.7	-49.6	13.7										
4	15	7	15.3	74.3	64.3	15.1	56.7	18.3	13.4	-51.2	-6.8	-4.1	-66.1	64.4	-4.5	-56.8	9.3	-5.0	-52.2	-20.4	-23.7	-60.3	-68.8	-22.5	-55.3	18.4	23.6	-51.6	-10.7	-41.6	-57.5	76.5	-41.2	53.8	34.1	-41.7	-49.6	13.7										
4	16	8	15.3	74.3	64.3	15.1	56.7	18.3	13.4	-51.2	-6.8	-4.1	-66.1	64.4	-4.5	-56.8	9.3	-5.0	-52.2	-20.4	-23.7	-60.3	-68.8	-22.5	-55.3	18.4	23.6	-51.6	-10.7	-41.6	-57.5	76.5	-41.2	53.8	34.1	-41.7	-49.6	13.7										
4	17	9	15.3	74.3	64.3	15.1	56.7	18.3	13.4	-51.2	-6.8	-4.1	-66.1	64.4	-4.5	-56.8	9.3	-5.0	-52.2	-20.4	-23.7	-60.3	-68.8	-22.5	-55.3	18.4	23.6	-51.6	-10.7	-41.6	-57.5	76.5	-41.2	53.8	34.1	-41.7	-49.6	13.7										
4	18	10	15.3	74																																												

Participant 3: Instantaneous Joint CoRs by Figueroa et al.'s method

Posture	Index						Middle						Ring						Little						DIP joint												
	MCP joint			PIP joint			DIP joint			MCP joint			PIP joint			DIP joint			MCP joint			PIP joint			DIP joint			DIP joint									
First	Second	X	Y	Z	X	Y	Z	X	Y	Z	X	Y	Z	X	Y	Z	X	Y	Z	X	Y	Z	X	Y	Z	X	Y	Z	X	Y	Z						
1	2	21.4	-84.3	43.9	20.7	-72.9	-1.1	18.4	71.6	-28.0	-2.7	-81.6	45.6	-1.8	-74.2	-4.1	2.8	-72.8	-34.6	-22.4	-79.5	54.8	-20.3	-71.7	9.0	-19.8	-72.6	20.1	39.5	-71.7	59.4	-39.0	-66.4	25.6	39.1	-68.6	4.4
1	3	21.4	-84.3	44.0	20.7	-72.9	-1.2	18.8	71.6	-26.5	-2.7	-81.6	45.2	-1.8	-74.2	-4.1	2.8	-72.8	-34.4	-22.4	-79.2	52.9	-20.3	-71.7	8.8	-19.8	-72.7	20.3	36.9	-73.7	60.1	-39.0	-66.4	25.5	39.0	-68.7	3.8
1	4	21.4	-84.3	44.0	20.7	-72.9	-1.1	18.2	71.5	-29.3	-2.7	-81.6	45.2	-1.8	-74.2	-4.2	2.8	-72.8	-34.4	-22.4	-79.3	53.5	-20.3	-71.8	8.7	-19.8	-72.6	20.1	38.6	-72.4	62.8	-39.0	-66.4	25.5	39.0	-68.6	4.0
1	5	21.4	-84.3	44.0	20.7	-72.9	-1.4	18.2	71.5	-29.2	-2.7	-81.6	45.2	-1.8	-74.2	-4.3	2.8	-72.8	-34.4	-22.4	-79.3	53.7	-20.3	-71.8	8.3	-19.8	-72.6	19.8	38.8	-72.2	62.1	-39.0	-66.4	25.5	39.0	-68.6	4.0
1	6	21.4	-84.4	44.3	20.7	-72.9	-1.5	18.4	71.6	-28.0	-2.7	-81.6	45.1	-1.8	-74.2	-4.7	2.8	-72.8	-34.5	-22.4	-79.2	53.0	-20.3	-71.8	8.2	-19.8	-72.6	19.9	38.9	-72.3	61.5	-39.0	-66.4	25.4	39.0	-68.6	3.9
1	7	21.4	-84.4	44.3	20.6	-72.9	-1.6	18.5	71.6	-27.8	-2.7	-81.5	45.0	-1.8	-74.2	-4.2	2.8	-72.8	-34.5	-22.4	-79.2	53.0	-20.4	-71.8	7.5	-19.8	-72.6	19.8	38.9	-72.2	61.7	-39.1	-66.5	25.1	39.0	-68.7	3.9
1	8	21.4	-84.4	44.5	20.6	-72.9	-1.5	18.4	71.6	-28.2	-2.7	-81.6	45.2	-1.8	-74.2	-4.2	2.8	-72.8	-34.3	-22.4	-79.2	52.8	-20.4	-71.8	7.8	-19.8	-72.6	19.8	38.9	-72.2	61.8	-39.1	-66.5	25.1	39.0	-68.7	3.9
1	9	21.4	-84.4	44.5	20.7	-72.9	-1.5	18.5	71.6	-27.8	-2.7	-81.6	45.1	-1.8	-74.2	-4.8	2.8	-72.8	-34.0	-22.4	-79.2	52.8	-20.4	-71.8	7.8	-19.9	-72.5	19.5	38.9	-72.3	61.6	-39.1	-66.5	25.1	39.0	-68.6	4.0
1	10	21.4	-84.4	44.5	20.7	-72.9	-1.5	18.5	71.6	-27.9	-2.7	-81.5	45.0	-1.8	-74.2	-4.8	2.8	-72.8	-34.5	-22.4	-79.3	53.3	-20.4	-71.8	7.9	-19.9	-72.5	19.5	38.7	-72.3	62.3	-39.0	-66.4	25.3	39.0	-68.6	4.0
2	3	21.3	-84.5	44.1	20.7	-72.6	-1.8	18.3	71.5	-28.3	-2.7	-81.3	43.8	-1.7	-73.9	-4.3	2.8	-73.0	-33.8	-22.4	-79.3	53.3	-20.3	-71.2	63.3	-39.0	-66.2	25.5	38.8	-68.6	2.8						
2	4	21.3	-84.4	44.1	20.7	-72.6	-1.8	18.3	71.5	-28.6	-2.7	-81.4	43.9	-1.7	-73.9	-4.3	2.8	-72.9	-34.0	-22.4	-79.3	53.7	-20.2	-71.1	8.0	-19.8	-72.0	20.1	38.7	-72.0	62.0	-39.0	-66.2	25.4	39.0	-68.6	3.9
2	5	21.3	-84.6	44.2	20.7	-72.8	-1.5	18.3	71.5	-28.3	-2.7	-81.4	43.9	-1.7	-73.8	-4.2	2.8	-72.9	-34.2	-22.4	-79.4	53.8	-20.2	-70.9	8.8	-19.8	-72.6	20.4	38.9	-71.9	61.5	-39.0	-66.1	25.1	39.0	-68.6	3.9
2	6	21.2	-85.0	44.6	20.7	-72.8	-1.4	18.4	71.6	-28.0	-2.7	-81.4	43.0	-1.7	-73.7	-4.5	2.8	-72.8	-34.4	-22.4	-79.3	53.0	-20.2	-70.9	8.4	-19.8	-72.6	19.8	38.9	-72.1	61.4	-39.0	-66.1	25.3	39.0	-68.6	3.8
2	7	21.2	-84.9	44.5	20.7	-72.7	-1.5	18.5	71.5	-27.8	-2.7	-81.4	43.4	-1.7	-73.7	-4.5	2.8	-72.8	-34.5	-22.4	-79.3	53.2	-20.2	-70.7	8.3	-19.8	-72.6	19.8	38.9	-72.1	61.6	-39.0	-66.0	25.3	39.0	-68.6	4.0
2	8	21.2	-84.9	44.6	20.7	-72.8	-1.4	18.5	71.5	-27.8	-2.7	-81.4	43.5	-1.7	-73.7	-4.5	2.8	-72.9	-34.0	-22.4	-79.3	53.2	-20.2	-70.8	8.4	-19.9	-72.6	19.5	38.7	-72.0	62.3	-39.0	-66.2	25.4	39.0	-68.6	4.0
2	9	21.2	-84.8	44.6	20.7	-72.7	-1.5	18.4	71.5	-27.9	-2.7	-81.4	43.6	-1.7	-73.7	-4.5	2.8	-72.9	-34.2	-22.4	-79.3	53.4	-20.2	-70.7	8.5	-19.9	-72.6	19.5	38.7	-72.0	62.5	-39.0	-66.2	25.4	39.0	-68.6	4.0
2	10	21.2	-84.8	44.6	20.7	-72.7	-1.5	18.5	71.5	-27.9	-2.7	-81.4	43.6	-1.7	-73.7	-4.5	2.8	-72.9	-34.2	-22.4	-79.3	53.4	-20.2	-70.7	8.5	-19.9	-72.6	19.5	38.7	-72.0	62.5	-39.0	-66.2	25.4	39.0	-68.6	4.0
3	5	21.5	-83.8	43.6	20.7	-72.8	-1.4	18.3	71.5	-28.0	-2.7	-81.5	43.0	-1.7	-73.8	-4.4	2.8	-72.8	-34.3	-22.4	-79.4	53.4	-20.2	-70.6	8.5	-19.8	-72.6	20.2	38.7	-72.0	62.0	-39.0	-66.7	25.1	39.0	-68.7	4.1
3	6	20.9	-85.9	45.1	20.7	-72.8	-1.4	18.4	71.5	-28.1	-2.7	-81.5	43.1	-1.7	-73.7	-4.5	2.8	-72.9	-34.5	-22.4	-79.4	53.0	-20.2	-70.7	8.8	-19.8	-72.6	19.9	38.9	-71.6	61.2	-39.0	-66.1	25.1	39.0	-68.7	3.9
3	7	21.1	-85.3	45.1	20.7	-72.8	-1.5	18.5	71.5	-27.9	-2.7	-81.4	43.0	-1.7	-73.7	-4.5	2.8	-72.7	-34.4	-22.4	-79.3	53.0	-20.2	-70.7	8.5	-19.8	-72.6	19.8	38.9	-71.7	61.5	-38.9	-65.9	25.3	39.0	-68.7	4.1
3	8	21.1	-85.2	45.6	20.7	-72.8	-1.4	18.4	71.5	-28.2	-2.7	-81.5	43.2	-1.7	-73.7	-4.5	2.8	-72.8	-34.4	-22.4	-79.3	53.2	-20.2	-70.7	8.8	-19.8	-72.6	19.8	38.9	-71.7	61.6	-38.9	-65.9	25.3	39.0	-68.7	3.9
3	9	21.1	-85.2	45.6	20.7	-72.8	-1.5	18.5	71.5	-27.9	-2.7	-81.5	43.2	-1.7	-73.7	-4.5	2.8	-72.8	-34.4	-22.4	-79.3	53.2	-20.2	-70.7	8.5	-19.9	-72.6	19.8	38.9	-71.7	61.5	-38.9	-65.9	25.3	39.0	-68.7	4.0
3	10	21.2	-84.9	44.4	20.7	-72.8	-1.4	18.5	71.4	-28.1	-2.7	-81.4	43.0	-1.7	-73.6	-4.5	2.8	-72.9	-34.5	-22.4	-79.3	53.4	-20.2	-70.7	8.5	-19.9	-72.6	19.5	38.8	-71.6	61.2	-39.0	-66.2	25.4	39.0	-68.6	4.0
4	6	20.9	-85.1	45.1	20.7	-72.8	-1.5	18.5	71.5	-28.0	-2.7	-81.4	43.1	-1.7	-73.6	-4.5	2.8	-72.9	-34.5	-22.4	-79.3	53.0	-20.2	-70.8	8.5	-19.9	-72.6	19.5	38.8	-71.6	61.3	-39.0	-66.2	25.4	39.0	-68.6	3.7
4	7	21.1	-84.7	44.6	20.7	-72.8	-1.3	18.4	71.6	-27.8	-2.7	-81.4	43.5	-1.7	-73.6	-4.5	2.8	-72.8	-34.5	-22.4	-79.3	53.0	-20.2	-70.8	8.5	-19.9	-72.6	19.5	38.8	-71.6	61.3	-39.0	-66.2	25.4	39.0	-68.6	3.5
4	8	21.1	-84.9	44.6	20.7	-72.8	-1.5	18.5	71.6	-27.8	-2.7	-81.4	43.5	-1.7	-73.6	-4.5	2.8	-72.8	-34.5	-22.4	-79.3	53.0	-20.2	-70.8	8.5	-19.9	-72.6	19.5	38.8	-71.6	61.4	-39.0	-66.2	25.4	39.0	-68.6	3.5
4	9	21.1	-84.9	44.6	20.7	-72.7	-1.7	18.5	71.6	-28.2	-2.7	-81.4	43.5	-1.7	-73.6	-4.5	2.8	-72.8	-34.5	-22.4	-79.3	53.0	-20.2	-70.7	8.5	-19.9	-72.6	19.5	38.7	-71.6	61.4	-39.0	-66.2	25.4	39.0	-68.6	3.8
4	10	21.1	-84.9	44.6	20.7	-72.7	-1.7	18.5	71.6	-28.2	-2.7	-81.4	43.5	-1.7	-73.6	-4.5	2.8	-72.8	-34.5	-22.4	-79.3	53.0	-20.2	-70.7	8.5	-19.9	-72.6	19.5	38.7	-71.6	61.4	-39.0	-66.2	25.4	39.0	-68.6	3.8
5	7	21.2	-84.5	44.2	20.6	-72.6	-1.8	18.2	71.2	-28.1	-2.7	-80.4	46.1	-1.7	-73.9	-4.3	2.8	-72.7	-34.5	-22.4	-79.4	54.0	-20.3	-71.3	8.7	-19.8	-72.9	19.3	38.8	-71.3	62.0	-39.0	-66.2	25.4	38.9	-68.6	3.9
5	8	21.2	-84.5	44.2	20.6	-72.6	-1.8	18.2	71.2	-28.1	-2.7	-80.4	46.1	-1.7	-73.9	-4.3	2.8	-72.7	-34.5	-22.4	-79.4	54.0	-20.3	-71.2	8.7	-19.8	-72.9	19.3	38.8	-71.3	62.0	-39.0	-66.2	25.4	38.9	-68.6	3.9
5	9	21.2	-84.5	44.2	20.6	-72.7	-1.8	18.3	71.2	-28.2	-2.7	-80.4	46.1	-1.7	-73.9	-4.3	2.8	-72.7	-34.5	-22.4	-79.4	54.0	-20.3	-71.2	8.7	-19.8	-72.9	19.3	38.8	-71.3	62.0	-39.0	-66.2	25.4	38.9	-68.6	3.9
5	10	21.2	-84.5	44.2	20.6	-72.7	-1.8	18.3	71.2	-28.2	-2.7	-80.4	46.1	-1.7	-73.9	-4.3	2.8	-72.7	-34.5	-22.4	-79.4	54.0	-20.3	-71.2	8.7	-19.8	-72.9	19.3	38.8	-71.3	62.0	-39.0	-66.2	25.4	38.9	-68.6	3.9
6	8	21.2	-84.5	44.2	20.6	-72.7	-1.8	18.3	71.2	-28.2	-2.7	-80.4	46.1	-1.7	-73.9	-4.3	2.8	-72.7	-34.5	-22.4	-79.4	54.0	-20.3	-71.2	8.7	-19.8	-72.9	19.3	38.8	-71.3	62.0	-39.0	-66.2	25.4	38.9	-68.6	3

Participant 4: Instantaneous Joint CoRs by Figueroa et al.'s method

Posture	Index			Middle			Ring			Little																											
	MCP joint	PIP joint	DIP joint	MCP joint	PIP joint	DIP joint	MCP joint	PIP joint	DIP joint	MCP joint	PIP joint	DIP joint																									
First	X	Y	Z	X	Y	Z	X	Y	Z	X	Y	Z																									
Second	X	Y	Z	X	Y	Z	X	Y	Z	X	Y	Z																									
1	2	25.7	-82.7	24.9	20.6	-67.7	-16.7	20.5	-63.3	-41.5	0.1	-79.6	27.4	2.7	-66.0	-20.1	4.0	-61.6	-48.1	-18.4	-72.7	33.7	-14.6	-64.0	-10.8	-15.8	-60.8	-38.8	31.5	-59.7	40.6	-30.2	-59.1	7.7	32.2	-57.8	-13.1
1	3	25.8	-82.7	24.8	20.6	-67.7	-16.7	20.5	-63.4	-41.4	0.1	-79.6	27.7	2.7	-66.0	-20.2	4.0	-61.6	-48.0	-18.4	-72.7	33.6	-14.6	-64.0	-11.0	-15.8	-60.8	-38.7	31.5	-59.7	40.4	-30.2	-59.1	7.6	32.2	-57.8	-13.0
1	4	26.0	-82.3	23.5	20.6	-67.7	-16.8	20.5	-63.4	-41.5	0.1	-79.7	27.7	2.7	-66.0	-20.4	4.0	-61.6	-48.0	-18.4	-72.7	33.8	-14.6	-64.0	-11.1	-15.8	-60.8	-38.5	26.7	-61.9	52.9	-30.2	-59.1	7.4	32.2	-57.8	-13.0
1	5	26.4	-81.7	22.0	20.6	-67.7	-16.7	20.5	-63.4	-41.5	0.1	-79.2	28.3	2.7	-66.0	-20.3	4.0	-61.6	-48.0	-18.4	-72.7	33.7	-14.6	-64.0	-11.1	-15.8	-60.8	-38.6	28.8	-61.0	47.4	-30.2	-59.1	7.6	32.2	-57.8	-13.0
1	6	26.3	-81.9	22.4	20.6	-67.7	-16.7	20.5	-63.4	-41.4	0.2	-78.9	24.9	2.7	-66.0	-20.4	4.0	-61.6	-48.0	-18.4	-72.4	32.5	-14.6	-64.0	-11.1	-15.8	-60.8	-38.4	30.3	-60.3	43.7	-30.2	-59.1	7.5	32.2	-57.8	-12.9
1	7	26.3	-81.9	22.4	20.6	-67.7	-17.0	20.5	-63.3	-41.6	0.2	-78.8	24.3	2.7	-65.9	-21.2	4.0	-61.6	-48.1	-18.4	-72.4	32.2	-14.7	-64.0	-12.3	-15.8	-60.8	-38.8	30.9	-60.0	42.0	-30.3	-59.1	7.1	32.2	-57.8	-13.0
1	8	26.3	-81.8	22.4	20.6	-67.7	-17.1	20.5	-63.3	-41.7	0.2	-78.8	24.4	2.7	-65.9	-21.2	4.0	-61.6	-48.3	-18.4	-72.3	31.6	-14.7	-64.0	-12.3	-15.8	-60.8	-38.8	30.9	-59.7	41.8	-30.1	-58.6	7.2	32.2	-57.8	-13.0
1	9	26.5	-81.7	21.7	20.6	-67.7	-17.0	20.5	-63.3	-41.8	0.2	-78.8	24.3	2.7	-65.9	-21.0	3.9	-61.6	-48.4	-18.4	-72.2	31.3	-14.7	-64.0	-11.8	-15.8	-60.8	-38.8	30.9	-60.0	42.0	-30.2	-59.1	7.2	32.2	-57.8	-13.1
1	10	26.5	-81.7	21.7	20.6	-67.7	-16.7	20.5	-63.3	-41.6	0.2	-78.9	24.8	2.7	-65.9	-21.0	3.9	-61.6	-47.6	-18.4	-72.9	31.7	-14.6	-64.0	-12.8	-15.8	-60.8	-38.2	30.9	-60.0	42.1	-30.2	-59.1	7.6	32.2	-57.8	-12.9
2	3	24.8	-82.2	29.0	20.6	-67.5	-16.7	20.5	-63.6	-41.2	0.4	-69.1	60.8	2.7	-64.9	-20.2	4.0	-61.7	-47.9	-17.4	-70.9	36.9	-14.5	-62.8	-10.8	-15.8	-60.8	-38.6	29.7	-59.6	44.0	-30.1	-58.8	7.4	32.2	-57.8	-13.1
2	4	25.6	-82.6	25.6	20.6	-67.4	-16.8	20.5	-63.5	-41.4	0.1	-79.7	26.9	2.7	-65.1	-48.0	0.3	-64.5	-43.0	-10.8	-61.0	-38.4	-30.5	-59.6	42.4	-30.1	-58.8	7.4	32.2	-57.9	-12.9						
2	5	25.9	-82.8	24.3	20.6	-67.6	-16.7	20.5	-63.5	-41.4	0.1	-79.7	27.2	2.7	-65.6	-20.4	4.0	-61.6	-48.1	-18.4	-72.7	33.6	-14.6	-64.0	-10.8	-15.8	-61.0	-38.5	30.3	-59.6	42.8	-30.2	-58.9	7.5	32.2	-57.8	-12.9
2	6	26.0	-82.9	24.6	20.6	-67.5	-16.7	20.5	-63.5	-41.3	0.1	-79.9	26.4	2.7	-65.4	-20.1	4.0	-61.7	-47.9	-18.5	-72.8	33.3	-14.4	-64.0	-10.7	-15.8	-61.0	-38.3	30.5	-59.6	42.6	-30.1	-58.8	7.4	32.2	-57.9	-12.9
2	7	26.1	-83.0	23.3	20.6	-67.3	-16.8	20.5	-63.5	-40.9	0.1	-80.1	25.7	2.7	-64.8	-20.2	4.0	-61.6	-48.0	-18.6	-73.1	32.9	-14.4	-64.0	-10.8	-15.8	-61.0	-38.4	30.9	-59.7	41.9	-30.1	-58.7	7.3	32.2	-57.8	-13.1
2	8	26.3	-83.2	23.0	20.6	-67.2	-16.8	20.5	-63.5	-40.5	0.2	-80.3	25.2	2.7	-64.8	-20.2	4.0	-60.8	-49.3	-18.8	-73.3	32.4	-14.4	-64.0	-12.7	-15.8	-60.8	-38.8	30.9	-59.7	41.8	-30.1	-58.6	7.2	32.2	-57.8	-13.0
2	9	26.3	-83.1	22.2	20.6	-67.2	-16.8	20.5	-63.4	-40.6	0.2	-80.4	24.9	2.7	-65.0	-20.2	4.3	-55.0	-56.6	-18.9	-73.6	31.9	-14.5	-62.8	-10.8	-15.8	-60.8	-38.8	30.8	-59.7	41.9	-30.1	-58.7	7.3	32.2	-57.7	-13.2
2	10	26.4	-82.4	23.0	20.6	-67.1	-16.8	20.5	-63.3	-41.7	0.2	-80.3	25.0	2.7	-65.4	-20.1	4.0	-61.4	-47.5	-18.5	-73.4	32.3	-14.3	-64.0	-12.7	-15.8	-61.0	-38.6	30.7	-59.7	42.1	-30.2	-59.1	7.5	32.2	-57.9	-12.8
3	4	25.6	-82.6	25.4	20.6	-67.3	-16.7	20.5	-63.2	-41.2	0.1	-79.7	27.5	2.7	-65.4	-20.2	4.0	-61.4	-48.2	-18.5	-72.8	33.3	-14.5	-64.1	-10.8	-15.8	-61.2	-38.2	30.6	-59.6	42.4	-30.1	-58.8	7.4	32.3	-58.1	-12.8
3	5	25.9	-82.8	24.2	20.6	-67.6	-16.7	20.5	-63.5	-41.0	0.1	-79.9	26.6	2.7	-65.6	-20.2	4.0	-61.6	-47.8	-18.5	-72.7	33.4	-14.6	-64.0	-10.8	-15.8	-61.0	-38.5	30.3	-59.6	42.8	-30.2	-58.9	7.5	32.2	-57.8	-12.9
3	6	26.0	-82.8	23.8	20.6	-67.6	-16.7	20.5	-63.5	-41.1	0.1	-80.0	26.6	2.7	-65.6	-20.2	4.0	-61.8	-47.8	-18.5	-72.8	33.4	-14.6	-64.0	-10.8	-15.8	-61.2	-38.1	30.5	-59.6	42.8	-30.2	-58.9	7.4	32.2	-57.8	-12.9
3	7	26.1	-82.9	23.6	20.6	-67.2	-16.7	20.5	-63.8	-41.1	0.1	-80.2	25.7	2.7	-64.8	-20.2	4.0	-61.9	-47.3	-18.6	-73.0	33.4	-14.4	-64.0	-10.7	-15.7	-61.5	-38.3	30.9	-59.7	41.9	-30.1	-58.7	7.3	31.9	-56.9	-13.8
3	8	26.2	-82.9	22.5	20.6	-67.1	-16.7	20.5	-63.8	-41.2	0.1	-80.2	25.3	2.7	-64.8	-20.2	4.0	-61.9	-47.3	-18.6	-73.3	32.4	-14.4	-64.0	-10.7	-15.7	-61.5	-38.3	30.9	-59.7	41.9	-30.1	-58.7	7.3	32.2	-57.8	-13.2
3	9	26.3	-83.0	22.2	20.6	-67.1	-16.7	20.5	-63.9	-41.0	0.2	-80.2	25.0	2.7	-65.0	-20.2	4.0	-61.9	-47.3	-18.6	-73.4	31.9	-14.5	-64.0	-10.7	-15.8	-61.6	-38.3	30.7	-59.6	42.0	-30.2	-59.1	7.4	32.2	-57.8	-12.9
3	10	26.3	-82.1	22.0	20.6	-67.0	-16.7	20.5	-63.8	-41.0	0.1	-79.9	25.0	2.7	-64.9	-20.2	4.0	-61.9	-47.3	-18.6	-73.4	31.8	-14.5	-64.0	-10.7	-15.8	-61.6	-38.3	30.7	-59.5	42.0	-30.2	-59.1	7.5	32.2	-57.8	-12.9
4	8	26.3	-82.1	22.4	20.6	-67.0	-16.7	20.5	-63.8	-41.2	0.1	-79.9	25.0	2.7	-64.7	-20.2	4.0	-61.9	-47.7	-18.7	-73.2	31.7	-14.6	-64.0	-10.7	-15.8	-61.6	-38.3	30.7	-59.5	41.8	-30.1	-58.6	7.4	32.2	-57.8	-12.8
4	9	26.4	-82.0	21.8	20.6	-66.9	-16.6	20.5	-63.8	-40.9	0.1	-79.9	24.9	2.7	-64.7	-20.2	4.0	-61.9	-47.7	-18.7	-73.2	31.7	-14.6	-64.0	-10.7	-15.8	-61.6	-38.3	30.7	-59.5	41.8	-30.1	-58.6	7.3	32.2	-57.8	-12.8
4	10	26.5	-81.9	21.6	20.6	-66.8	-16.6	20.5	-63.8	-40.7	0.2	-79.8	24.8	2.7	-64.5	-20.1	4.0	-61.9	-47.7	-18.7	-73.2	31.6	-14.6	-64.0	-10.7	-15.8	-61.6	-38.3	30.7	-59.5	41.8	-30.1	-58.6	7.3	32.2	-57.8	-12.8
4	11	26.5	-81.8	21.4	20.6	-66.7	-16.6	20.5	-63.8	-40.5	0.2	-79.8	24.7	2.7	-64.5	-20.1	4.0	-61.9	-47.7	-18.7	-73.2	31.5	-14.6	-64.0	-10.7	-15.8	-61.6	-38.3	30.7	-59.5	41.8	-30.1	-58.6	7.3	32.2	-57.8	-12.8
4	12	26.5	-81.7	21.2	20.6	-66.7	-16.6	20.5	-63.8	-40.3	0.2	-79.8	24.6	2.7	-64.5	-20.1	4.0	-61.9	-47.7	-18.7	-73.2	31.4	-14.6	-64.0	-10.7	-15.8	-61.6	-38.3	30.7	-59.5	41.8	-30.1	-58.6	7.3	32.2	-57.8	-12.8
4	13	26.5	-81.6	21.0	20.6	-66.7	-16.6	20.5	-63.8	-40.1	0.2	-79.8	24.5	2.7	-64.5	-20.1	4.0	-61.9	-47.7	-18.7	-73.2	31.3	-14.6	-64.0	-10.7	-15.8	-61.6	-38.3	30.7	-59.5	41.8	-30.1	-58.6	7.3	32.2	-57.8	-12.8
4	14	26.5	-81.5	20.8	20.6	-66.7	-16.6	20.5	-63.8	-40.0	0.2	-79.8	24.4	2.7	-64.5	-20.1	4.0	-61.9	-47.7	-18.7	-73.2	31.2	-14.6	-64.0	-10.7	-15.8	-61.6	-38.3	30.7	-59.5	41.8	-30.1	-58.6	7.3	32.2	-57.8	-12.8
4	15	26.5	-81.4	20.6	20.6	-66.7	-16.6	20.5	-63.8	-39.9	0.2	-79.8	24.3	2.7	-64.5	-20.1	4.0	-61.9	-47.7	-18.7	-73.2	31.1	-14.6	-64.0	-10.7	-15.8	-61.6	-38.3	30.7	-59.5	41.8	-30.1	-58.6	7.3	32.2	-57.8	-12.8
4	16	26.5	-81.3	20.4	20.6	-66.7	-16.6	20.5	-63.8	-39.8	0.2	-79.8	24.2	2.7	-64.5	-20.1	4.0	-61.9	-47.7	-18.7	-73.2	31.0	-14.6	-64.0	-10.7	-15.8	-61.6	-38.3	30.7	-59.5	41.8	-30.1	-58.6	7.3	32.2	-57.8	-12.8
4	17	26.5	-81.2	20.2	20.6	-66.7	-16.6	20.5	-63.8	-39.7	0.2	-79.8	24.1	2.7	-64.5	-20.1	4.0	-61.9	-47.7	-18.7	-73.2	30.9	-14.6	-64.0	-10.7	-15.8	-61.6	-38.3	30.7	-59.5	41.8	-30.1	-58.6	7.3	32.2	-57.8	-12.8
4	18	26.5	-81.1	20.0	20.6	-66.7	-16.6	20.5	-63.8</td																												

Participant 5: Instantaneous Joint CoRs by Figueroa et al.'s method

Posture	Index			Middle									Ring									Little															
	MCP joint			PIP joint			DIP joint			MCP joint			PIP joint			DIP joint			MCP joint			PIP joint			DIP joint			MCP joint			PIP joint						
First	Second	X	Y	Z	X	Y	Z	X	Y	Z	X	Y	Z	X	Y	Z	X	Y	Z	X	Y	Z	X	Y	Z	X	Y	Z	X	Y	Z						
1	2	-13.7	4.0	85.5	-10.8	22.4	47.0	-11.8	27.2	21.2	-35.9	11.6	90.2	-31.6	25.7	43.5	-31.0	32.3	13.9	-53.1	21.5	98.3	-51.6	31.4	54.3	-52.5	33.7	24.7	-68.7	33.1	105.0	-67.8	35.4	71.4	-69.8	34.7	50.9
1	3	-13.5	4.3	84.9	-10.8	22.4	47.0	-11.7	27.3	21.5	-35.9	11.6	90.1	-31.6	25.7	43.4	-30.9	32.3	14.2	-53.1	21.4	98.5	-51.6	31.4	54.3	-52.5	33.8	24.8	-68.7	33.1	105.0	-67.8	35.4	71.6	-69.8	34.8	51.0
1	4	-13.5	4.9	83.1	-10.8	22.4	47.2	-11.7	27.3	21.5	-35.9	11.5	90.1	-31.5	25.8	43.3	-30.8	32.4	14.5	-53.1	21.4	98.5	-51.6	31.4	54.4	-52.4	33.8	25.0	-69.2	33.1	105.0	-67.8	35.4	71.8	-69.8	34.8	51.1
1	5	-15.7	4.0	94.6	-10.8	22.4	47.2	-11.7	27.3	21.6	-35.9	11.6	89.1	-31.5	25.7	43.3	-30.8	32.4	14.5	-53.1	21.4	97.4	-51.6	31.4	54.4	-52.4	33.9	25.3	-69.2	33.1	105.0	-67.8	35.4	71.8	-69.8	34.8	51.2
1	6	-13.7	4.0	85.5	-10.8	22.3	46.6	-11.7	27.3	21.6	-35.9	11.7	90.0	-31.5	25.8	43.0	-30.8	32.4	14.5	-53.1	21.4	97.4	-51.6	31.4	54.4	-52.4	33.9	25.3	-69.2	33.1	105.0	-67.8	35.4	71.8	-69.8	34.8	51.2
1	7	-14.1	3.2	87.5	-10.8	22.3	46.1	-11.7	27.3	21.8	-35.9	11.1	92.0	-31.5	25.8	43.0	-30.7	32.4	14.9	-53.1	21.3	97.3	-51.5	31.4	54.4	-52.4	33.9	25.3	-69.2	33.1	105.0	-67.8	35.4	71.8	-69.8	34.8	51.3
1	8	-13.6	4.2	85.0	-10.8	22.3	47.8	-11.7	27.3	21.8	-35.9	11.6	90.2	-31.5	26.0	43.2	-30.9	32.5	15.2	-53.1	21.5	98.4	-51.6	31.5	54.4	-52.4	34.0	25.8	-68.5	33.0	105.9	-67.7	35.4	72.0	-69.8	34.9	51.2
1	9	-13.5	4.4	84.6	-10.8	22.3	48.0	-11.7	27.3	21.9	-35.9	11.6	90.1	-31.6	25.8	42.9	-30.7	32.5	15.1	-53.2	21.6	97.7	-51.5	31.4	54.6	-52.4	34.0	25.8	-68.5	33.0	105.9	-67.7	35.4	72.0	-69.8	34.9	51.2
1	10	-13.3	4.7	83.8	-10.8	22.3	46.1	-11.7	27.3	21.5	-35.9	11.2	91.5	-31.6	25.7	43.3	-30.7	32.5	14.9	-53.2	21.7	97.5	-51.5	31.4	54.5	-52.4	33.9	25.4	-68.5	33.0	106.2	-67.7	35.4	72.2	-69.8	34.9	51.2
2	3	-13.8	3.9	86.3	-10.8	22.1	47.2	-11.7	27.3	21.8	-35.9	11.2	90.1	-31.5	25.9	43.4	-31.0	32.5	15.3	-53.1	21.5	98.7	-51.7	31.6	54.2	-52.3	33.7	24.9	-69.1	33.0	103.9	-67.9	35.2	71.7	-69.8	34.8	51.2
2	4	-13.8	3.9	86.3	-11.0	21.9	47.3	-11.8	27.0	21.7	-35.9	11.6	90.2	-31.5	26.0	43.3	-30.9	32.2	14.8	-53.2	21.5	98.2	-51.6	31.6	54.4	-52.3	33.8	25.1	-67.4	33.8	108.7	-67.8	35.1	71.8	-69.8	34.8	51.0
2	5	-13.8	4.0	86.2	-11.0	21.9	47.3	-11.7	27.0	21.8	-35.9	11.6	90.4	-31.6	26.0	43.3	-30.9	32.1	15.1	-53.0	21.6	99.1	-51.6	31.3	54.4	-52.3	33.8	25.4	-67.9	33.5	107.3	-67.9	35.1	71.8	-69.8	34.8	51.1
2	6	-13.7	4.0	85.6	-11.0	21.8	47.4	-11.7	26.9	22.0	-35.9	11.6	90.2	-31.5	26.0	43.2	-30.9	32.5	15.4	-53.1	21.5	98.4	-51.6	31.5	54.4	-52.3	33.8	25.7	-68.3	33.4	106.2	-67.9	35.1	71.8	-69.8	34.9	51.3
2	7	-13.8	3.9	86.6	-11.2	21.8	47.7	-11.7	27.0	21.9	-35.9	11.6	90.9	-31.6	25.6	43.6	-30.9	32.3	15.2	-53.1	21.5	98.5	-51.8	31.0	54.8	-52.3	33.8	25.7	-68.2	33.4	106.4	-67.9	35.0	71.9	-69.8	34.9	51.3
2	8	-13.6	4.1	85.1	-11.0	21.6	47.5	-11.7	27.0	21.9	-35.9	11.6	90.2	-31.6	26.0	43.2	-30.9	32.1	15.4	-53.2	21.5	98.2	-51.6	31.3	54.8	-52.3	33.8	25.9	-68.3	33.3	106.0	-67.9	35.1	71.9	-69.8	34.9	51.4
2	9	-13.6	4.1	84.8	-11.0	21.6	47.7	-11.7	27.0	21.8	-35.9	11.6	90.1	-31.5	26.1	43.2	-30.9	32.1	15.3	-53.1	21.5	98.0	-51.7	31.4	54.6	-52.3	33.8	25.6	-68.5	33.3	105.5	-67.9	35.1	71.8	-69.8	34.8	51.3
2	10	-13.5	4.2	84.1	-11.0	21.5	47.6	-11.7	27.0	21.7	-35.9	11.6	90.1	-31.5	26.0	43.2	-30.9	32.1	15.3	-53.1	21.5	97.9	-51.7	31.4	54.6	-52.3	33.8	25.5	-68.3	33.3	106.0	-67.9	35.0	71.8	-69.8	34.8	51.2
3	1	-13.8	3.9	86.3	-10.8	21.8	47.3	-11.7	27.3	21.5	-35.9	11.7	90.0	-31.4	26.4	43.2	-30.9	32.1	15.4	-53.1	21.5	98.6	-51.7	31.4	54.5	-52.3	33.7	24.9	-69.1	33.0	107.8	-67.8	35.1	71.8	-69.8	34.8	51.1
3	2	-13.6	4.2	85.3	-10.8	21.8	47.8	-11.7	27.3	21.8	-35.9	11.6	90.1	-31.5	26.5	43.3	-30.9	32.1	15.5	-53.2	21.5	98.7	-51.7	31.5	54.6	-52.3	33.8	25.6	-68.2	33.1	107.3	-67.8	35.1	71.8	-69.8	34.8	51.1
3	3	-13.6	4.2	85.0	-10.8	21.8	47.8	-11.7	27.3	21.8	-35.9	11.6	90.2	-31.5	26.5	43.3	-30.9	32.1	15.5	-53.2	21.5	98.7	-51.7	31.5	54.6	-52.3	33.8	25.6	-68.2	33.1	107.3	-67.8	35.1	71.8	-69.8	34.8	51.1
3	4	-13.6	4.2	84.8	-10.8	21.8	47.8	-11.7	27.3	21.8	-35.9	11.6	90.1	-31.4	26.4	43.2	-30.9	32.1	15.4	-53.2	21.5	98.6	-51.7	31.5	54.5	-52.3	33.8	25.6	-68.2	33.1	107.3	-67.8	35.1	71.8	-69.8	34.8	51.1
3	5	-13.6	4.2	84.5	-10.8	21.8	47.8	-11.7	27.3	21.8	-35.9	11.6	90.1	-31.4	26.4	43.2	-30.9	32.1	15.4	-53.2	21.5	98.6	-51.7	31.5	54.5	-52.3	33.8	25.6	-68.2	33.1	107.3	-67.8	35.1	71.8	-69.8	34.8	51.1
3	6	-13.6	4.2	84.3	-10.8	21.8	47.8	-11.7	27.3	21.8	-35.9	11.6	90.1	-31.4	26.4	43.2	-30.9	32.1	15.4	-53.2	21.5	98.6	-51.7	31.5	54.5	-52.3	33.8	25.6	-68.2	33.1	107.3	-67.8	35.1	71.8	-69.8	34.8	51.1
3	7	-13.6	3.9	86.7	-10.8	21.7	47.4	-11.7	27.3	21.8	-35.9	11.6	90.1	-31.5	26.5	43.3	-30.9	32.1	15.5	-53.1	21.7	98.7	-51.7	31.6	54.6	-52.3	33.8	25.7	-68.2	33.1	107.3	-67.8	35.1	71.8	-69.8	34.8	51.1
3	8	-13.0	4.2	85.9	-10.8	21.7	47.8	-11.7	27.3	21.8	-35.9	11.6	90.1	-31.5	26.5	43.3	-30.9	32.1	15.5	-53.1	21.7	98.7	-51.7	31.6	54.6	-52.3	33.8	25.7	-68.2	33.1	107.3	-67.8	35.1	71.8	-69.8	34.8	51.1
3	9	-13.6	4.2	85.7	-10.8	21.7	47.8	-11.7	27.3	21.8	-35.9	11.6	90.1	-31.5	26.5	43.3	-30.9	32.1	15.5	-53.1	21.7	98.7	-51.7	31.6	54.6	-52.3	33.8	25.7	-68.2	33.1	107.3	-67.8	35.1	71.8	-69.8	34.8	51.1
3	10	-13.6	4.2	85.5	-10.8	21.7	47.8	-11.7	27.3	21.8	-35.9	11.6	90.1	-31.5	26.5	43.3	-30.9	32.1	15.5	-53.1	21.7	98.7	-51.7	31.6	54.6	-52.3	33.8	25.7	-68.2	33.1	107.3	-67.8	35.1	71.8	-69.8	34.8	51.1
3	11	-13.6	4.2	85.3	-10.8	21.7	47.8	-11.7	27.3	21.8	-35.9	11.6	90.1	-31.5	26.5	43.3	-30.9	32.1	15.5	-53.1	21.7	98.7	-51.7	31.6	54.6	-52.3	33.8	25.7	-68.2	33.1	107.3	-67.8	35.1	71.8	-69.8	34.8	51.1
3	12	-13.6	4.2	85.1	-10.8	21.7	47.8	-11.7	27.3	21.8	-35.9	11.6	90.1	-31.5	26.5	43.3	-30.9	32.1	15.5	-53.1	21.7	98.7	-51.7	31.6	54.6	-52.3	33.8	25.7	-68.2	33.1	107.3	-67.8	35.1	71.8	-69.8	34.8	51.1
3	13	-13.6	4.2	84.9	-10.8	21.7	47.8	-11.7	27.3	21.8	-35.9	11.6	90.1	-31.5	26.5	43.3	-30.9	32.1	15.5	-53.1	21.7	98.7	-51.7	31.6	54.6	-52.3	33.8	25.7	-68.2	33.1	107.3	-67.8	35.1	71.8	-69.8	34.8	51.1
3	14	-13.6	4.2	84.7	-10.8	21.7	47.8	-11.7	27.3	21.8	-35.9	11.6	90.1	-31.5	26.5	43.3	-30.9	32.1	15.5	-53.1	21.7	98.7	-51.7	31.6	54.6	-52.3	33.8	25.7	-68.2	33.1	107.3	-67.8	35.1	71.8	-69.8	34.8	51.1
3	15	-13.6	4.2	84.5	-10.8	21.7	47.8	-11.7	27.3	21.8	-35.9	11.6	90.1	-31.5	26.5	43.3	-30.9	32.1	15.5	-53.1	21.7	98.7	-51.7	31.6	54.6	-52.3	33.8	25.7	-68.2	33.1	107.3	-67.8	35.1				

Participant 6: Instantaneous Joint CoRs by Figueroa et al.'s method

Posture	Index												Middle												Ring												Little											
	MCP joint			PIP joint			DIP joint			MCP joint			PIP joint			DIP joint			MCP joint			PIP joint			DIP joint			MCP joint			PIP joint			DIP joint			MCP joint			PIP joint			DIP joint					
First	Second	X	Y	Z	X	Y	Z	X	Y	Z	X	Y	Z	X	Y	Z	X	Y	Z	X	Y	Z	X	Y	Z	X	Y	Z	X	Y	Z	X	Y	Z	X	Y	Z	X	Y	Z	X	Y	Z	X	Y	Z		
1	2	0.5	-29.7	-11.4	0.5	-13.7	51.8	-1.6	-9.0	-76.3	-20.1	26.9	-6.4	-20.8	-16.6	54.4	21.8	-8.9	-82.1	35.9	-20.4	1.9	-40.2	-13.4	-43.3	-42.8	-8.3	-70.1	-53.2	-11.1	5.0	60.2	-10.4	-25.6	-65.4	-6.3	-44.3											
1	3	0.6	-29.6	-11.7	0.5	-13.7	51.8	-1.6	-9.0	-76.3	-20.1	26.9	-6.4	-20.8	-16.5	54.6	21.7	-8.9	-81.8	35.9	-20.4	2.0	-40.2	-13.4	-43.5	-42.8	-8.3	-70.1	-53.2	-11.2	8.0	60.3	-10.3	-26.2	-65.4	-6.3	-44.3											
1	4	0.6	-29.4	-12.2	0.5	-13.7	51.8	-1.6	-9.0	-76.2	-20.1	26.9	-6.5	-20.8	-16.5	54.7	21.7	-8.9	-81.8	35.8	-20.4	2.1	-40.2	-13.4	-43.6	-42.8	-8.3	-69.8	-53.0	-11.1	5.7	60.4	-10.3	-26.3	-65.4	-6.3	-44.4											
1	5	0.5	-29.7	-11.4	0.5	-13.7	51.8	-1.5	-9.0	-76.1	-20.2	26.7	-7.7	-20.8	-16.5	54.9	21.8	-8.8	-82.6	36.1	-20.2	0.3	-40.3	-13.3	-44.2	-42.8	-8.3	-70.1	-52.7	-11.2	6.6	60.5	-10.2	-26.6	-65.4	-6.3	-44.5											
1	6	0.5	-29.7	-11.4	0.5	-13.7	51.8	-1.5	-9.0	-76.1	-20.2	26.7	-7.7	-20.8	-16.5	54.9	21.8	-8.8	-82.6	36.1	-20.2	0.4	-40.3	-13.3	-44.2	-42.8	-8.3	-69.9	-53.5	-11.1	4.3	60.4	-10.2	-26.5	-65.4	-6.3	-44.5											
1	7	0.6	-29.6	-11.6	0.5	-13.7	51.9	-1.6	-9.0	-76.3	-20.2	26.8	-8.2	-20.8	-16.4	55.0	21.8	-8.8	-82.3	36.2	-20.1	-0.4	-40.3	-13.3	-44.3	-42.8	-8.3	-70.3	-52.7	-11.2	6.6	60.5	-10.2	-26.6	-65.4	-6.3	-44.4											
1	8	0.6	-29.6	-11.8	0.5	-13.7	52.0	-1.7	-9.0	-76.8	-20.2	26.5	-8.3	-20.8	-16.4	55.0	21.8	-8.9	-81.7	36.4	-19.9	-1.6	-40.3	-13.3	-44.3	-42.8	-8.3	-70.1	-52.3	-11.2	7.6	60.5	-10.2	-26.6	-65.4	-6.3	-44.5											
1	9	0.6	-29.5	-11.9	0.5	-13.7	52.0	-1.7	-9.0	-76.6	-20.2	26.5	-8.5	-20.8	-16.4	55.1	21.7	-8.9	-81.7	36.4	-19.9	-1.6	-40.3	-13.3	-44.3	-42.8	-8.3	-70.1	-52.3	-11.2	8.0	60.5	-10.2	-26.6	-65.4	-6.3	-44.5											
1	10	0.6	-29.6	-11.6	0.5	-13.7	51.8	-1.6	-9.0	-76.0	-20.2	26.5	-8.5	-20.8	-16.4	55.1	21.7	-8.9	-81.6	35.9	-20.4	1.7	-40.1	-13.0	-43.8	-42.8	-8.4	-70.0	-52.0	-11.2	8.5	60.3	-10.0	-26.5	-65.4	-6.3	-44.4											
2	3	0.5	-29.7	-11.1	0.5	-13.8	51.8	-1.6	-8.9	-76.6	-20.1	26.9	-6.5	-20.6	-15.8	55.0	21.8	-9.1	-81.8	35.9	-20.4	1.7	-40.1	-13.0	-43.8	-42.8	-8.4	-70.0	-52.0	-11.2	8.5	60.3	-10.0	-26.5	-65.4	-6.3	-44.3											
2	4	0.5	-29.7	-10.8	0.5	-13.7	51.8	-1.6	-9.1	-76.2	-20.1	26.9	-6.3	-20.7	-16.0	54.9	21.8	-8.7	-82.3	35.9	-20.4	1.6	-40.1	-12.9	-43.8	-42.8	-8.5	-69.9	-52.8	-11.1	6.3	60.3	-10.0	-26.5	-65.4	-6.3	-44.3											
2	5	0.5	-29.7	-11.1	0.5	-14.0	51.7	-1.6	-8.9	-76.4	-20.1	26.9	-6.6	-20.7	-16.2	54.7	19.3	-7.8	-103.1	35.8	-20.3	2.4	-40.1	-12.9	-43.9	-42.8	-8.4	-69.9	-53.5	-11.1	4.3	60.3	-9.9	-26.7	-65.4	-6.2	-44.6											
2	6	0.5	-29.7	-11.4	0.5	-13.7	51.8	-1.6	-9.1	-76.1	-20.2	27.0	-7.0	-20.7	-16.1	54.8	21.7	-8.6	-82.6	36.0	-20.4	1.3	-40.1	-12.7	-44.0	-42.8	-8.3	-70.1	-52.7	-11.1	6.5	60.3	-10.0	-26.5	-65.4	-6.3	-44.5											
2	7	0.5	-29.7	-11.5	0.5	-13.6	51.9	-1.6	-9.0	-76.3	-20.3	27.1	-7.7	-20.7	-16.1	54.9	21.7	-8.3	-82.6	36.2	-20.6	0.3	-40.1	-12.7	-44.0	-42.8	-8.3	-70.4	-52.7	-11.1	6.5	60.3	-10.0	-26.6	-65.4	-6.3	-44.4											
2	8	0.5	-29.7	-11.7	0.5	-13.5	51.9	-1.5	-8.9	-76.4	-20.4	27.1	-8.1	-20.7	-16.0	54.8	21.8	-8.7	-81.7	36.5	-20.7	0.4	-40.1	-12.7	-43.9	-42.8	-8.2	-70.4	-52.5	-11.1	7.3	60.3	-10.0	-26.5	-65.4	-6.3	-44.5											
2	9	0.6	-29.7	-11.9	0.5	-13.5	51.9	-1.5	-8.8	-76.3	-20.3	26.9	-8.4	-20.7	-16.1	54.9	21.8	-8.8	-81.6	36.6	-20.8	1.5	-40.1	-12.7	-43.9	-42.8	-8.3	-69.7	-52.3	-11.2	7.6	60.3	-9.9	-26.6	-65.4	-6.2	-44.6											
2	10	0.5	-29.7	-11.6	0.5	-13.7	51.8	-1.6	-9.1	-76.0	-20.4	27.1	-8.3	-20.7	-16.2	54.7	22.5	-9.2	-81.7	36.6	-20.8	1.4	-40.1	-12.7	-43.9	-42.8	-8.2	-70.9	-52.1	-11.2	3.0	60.2	-9.3	-26.9	-65.3	-5.9	-44.6											
3	4	0.3	-30.4	-7.7	0.6	-13.6	51.6	-1.6	-9.2	-76.1	-20.2	26.9	-6.0	-20.7	-16.2	54.8	22.0	-9.6	-81.6	36.0	-20.4	1.5	-40.1	-12.8	-43.9	-42.8	-8.6	-69.8	-51.8	-11.1	9.0	60.3	-9.9	-26.5	-65.3	-6.1	-44.6											
3	5	0.5	-29.7	-11.1	0.4	-14.3	51.6	-1.6	-9.2	-76.2	-20.2	26.9	-6.0	-20.7	-16.2	54.8	22.1	-9.7	-81.9	36.0	-20.4	1.7	-40.1	-12.7	-43.9	-42.8	-8.7	-70.1	-52.6	-11.3	6.9	60.3	-9.9	-26.5	-65.3	-6.1	-44.5											
3	6	0.6	-29.6	-11.5	0.5	-13.6	51.6	-1.6	-9.1	-76.2	-20.2	26.9	-6.2	-20.7	-16.1	54.8	22.1	-9.8	-81.9	36.0	-20.4	1.2	-40.1	-12.6	-44.0	-42.8	-8.7	-70.1	-52.6	-11.3	6.9	60.3	-9.9	-26.5	-65.3	-6.1	-44.5											
3	7	0.6	-29.6	-11.8	0.5	-13.5	51.6	-1.4	-7.6	-76.1	-20.3	26.8	-8.2	-20.7	-16.1	54.8	22.2	-10.2	-81.6	36.4	-20.5	0.8	-40.1	-12.7	-43.9	-42.8	-8.6	-69.7	-52.5	-11.3	7.3	60.3	-9.9	-26.5	-65.3	-5.9	-44.7											
3	8	0.6	-29.6	-11.8	0.5	-13.5	51.6	-1.5	-8.3	-76.3	-20.3	26.8	-8.4	-20.7	-16.3	54.9	21.9	-9.5	-81.7	36.6	-20.5	1.5	-40.1	-12.7	-43.9	-42.8	-8.6	-69.7	-52.1	-11.2	7.7	60.3	-9.9	-26.6	-65.2	-5.7	-45.0											
3	9	0.6	-29.6	-11.6	0.5	-13.7	51.6	-1.6	-9.3	-76.2	-20.2	26.8	-8.4	-20.7	-16.4	54.9	21.9	-9.6	-81.7	36.5	-20.5	1.6	-40.1	-12.7	-43.9	-42.8	-8.7	-69.7	-52.1	-11.2	8.0	60.3	-9.9	-26.6	-65.3	-5.9	-44.6											
3	10	0.7	-29.3	-12.0	0.5	-13.7	51.6	-1.7	-9.3	-76.2	-20.2	26.8	-8.5	-20.7	-16.4	54.9	21.9	-9.7	-81.7	36.5	-20.5	1.7	-40.1	-12.7	-43.9	-42.8	-8.8	-70.0	-52.1	-10.9	8.0	60.4	-10.0	-26.6	-65.3	-5.9	-44.6											
4	1	0.6	-29.5	-11.8	0.5	-13.7	51.8	-1.6	-9.2	-76.0	-20.2	26.8	-8.6	-20.7	-16.5	54.8	21.9	-9.8	-81.7	36.5	-20.4	1.8	-40.1	-12.7	-43.9	-42.8	-8.9	-69.7	-52.1	-11.2	7.7	60.3	-9.9	-26.7	-65.4	-6.1	-44.6											
4	2	0.6	-29.5	-11.5	0.5	-13.7	51.8	-1.6	-9.2	-76.0	-20.2	26.8	-8.6	-20.7	-16.5	54.8	21.9	-9.8	-81.7	36.5	-20.4	1.9	-40.1	-12.7	-43.9	-42.8	-8.9	-69.7	-52.1	-11.2	7.7	60.3	-9.9	-26.7	-65.4	-6.1	-44.6											
4	3	0.6	-29.5	-11.5	0.5	-13.7	51.8	-1.6	-9.2	-76.0	-20.2	26.8	-8.6	-20.7	-16.5	54.8	21.9	-9.8	-81.7	36.5	-20.4	1.9	-40.1	-12.7	-43.9	-42.8	-8.9	-69.7	-52.1	-11.2	7.7	60.3	-9.9	-26.7	-65.4	-6.1	-44.6											
4	4	0.6	-29.5	-11.5	0.5	-13.7	51.8	-1.6	-9.2	-76.0	-20.2	26.8	-8.6	-20.7	-16.5	54.8	21.9	-9.8	-81.7	36.5	-20.4	1.9	-40.1	-12.7	-43.9	-42.8	-8.9	-69.7	-52.1	-11.2	7.7	60.3	-9.9	-26.7	-65.4	-6.1	-44.6											
4	5	0.6	-29.5	-11.5	0.5	-13.7	51.8	-1.6	-9.2	-76.0	-20.2	26.8	-8.6	-20.7	-16.5	54.8	21.9	-9.8	-81.7	36.5	-20.4	1.9	-40.1	-12.7	-43.9	-42.8	-8.9	-69.7	-52.1	-11.2	7.7	60.3	-9.9	-26.7	-65.4	-6.1	-44.6											
4	6	0.6	-29.5	-11.5	0.5	-13.7	51.8	-1.6	-9.2	-76.0	-20.2	26.8	-8.6	-20.7	-16.5	54.8	21.9	-9.8	-81.7	36.5	-20.4	1.9	-40.1	-12.7	-43.9	-42.8	-8.9	-69.7	-52.1	-11.2	7.7	60.3	-9.9	-26.7	-65.4	-6.1	-44.6											
4	7	0.6	-29.5	-11.5	0.5	-13.7	51.8	-1.6	-9.2	-76.0	-20.2	26.8	-8.6	-20.7	-16.5	54.8	21.9	-9.8	-81.7	36.5	-20.4	1.9	-40.1	-12.7	-43.9	-42.8	-8.9	-69.7	-52.1	-11.2	7.7	60.3	-9.9	-26.7	-65.4	-6.1	-44.6											
4	8	0.6	-29.5	-11.5	0.5	-13.7	51.8	-1.6	-9.2	-76.0	-20.2	26.8	-8.6	-20.7	-16.5	54.8	21.9	-9.8	-81.7	36.5	-20.4	1.9	-40.1	-12.7	-43.9	-42.8	-8.9	-69.7	-52																			

Participant 7: Instantaneous Joint CoRs by Figueroa et al.'s method

Posture	First	Second	Index						Middle						Ring						Little										
			MCP joint			PIP joint			DIP joint			MCP joint			PIP joint			DIP joint			MCP joint			PIP joint			DIP joint				
			X	Y	Z	X	Y	Z	X	Y	Z	X	Y	Z	X	Y	Z	X	Y	Z	X	Y	Z	X	Y	Z	X	Y	Z		
1	2	19.6	55.1	27.9	24.3	-46.6	-15.0	28.0	-43.9	-39.6	-1.8	56.8	27.5	8.1	-46.1	-20.4	12.8	-43.3	-49.9	-19.8	-51.0	26.7	-9.6	-47.3	-15.1	-4.3	-44.9	-43.3	29.4	-44.3	74.7
1	3	19.8	54.9	26.7	24.3	-46.6	-15.0	28.0	-43.9	-40.2	-0.8	55.6	23.0	8.2	-46.1	-20.7	12.9	-43.2	-50.5	-19.4	-50.9	24.5	-9.4	-47.2	-16.2	-4.5	-44.9	-42.8	35.8	-46.5	32.7
1	4	19.9	54.8	26.0	24.3	-46.6	-15.1	28.0	-43.9	-39.8	-0.8	55.6	23.0	8.2	-46.1	-20.7	12.6	-42.7	-47.0	-19.6	-51.0	25.4	-9.5	-47.3	-15.5	-3.9	-45.1	-44.7	36.0	-46.6	31.6
1	5	19.8	54.9	26.3	24.3	-46.5	-15.2	28.0	-43.9	-39.4	-0.8	55.6	23.1	8.3	-46.1	-21.2	12.8	-43.0	-49.6	-19.6	-51.0	25.6	-9.4	-47.2	-16.1	-4.4	-44.9	-43.1	36.0	-46.6	31.5
1	6	19.8	54.9	26.8	24.5	-46.5	-16.0	28.0	-43.9	-39.3	-0.8	55.6	23.0	8.6	-46.0	-22.8	12.8	-43.0	-49.1	-19.5	-51.0	25.5	-9.3	-47.2	-16.8	-4.5	-44.9	-42.9	36.0	-46.6	31.7
1	7	19.8	54.9	26.5	24.5	-46.5	-16.2	28.0	-43.9	-39.4	-0.8	55.6	23.1	8.6	-46.0	-22.7	12.8	-43.0	-49.1	-19.5	-50.9	25.1	-9.2	-47.2	-16.9	-4.5	-44.9	-42.9	36.1	-46.6	31.1
1	9	19.8	54.9	26.4	24.4	-46.5	-16.1	28.0	-43.9	-39.5	-0.8	55.6	23.2	8.5	-46.0	-22.7	12.8	-43.0	-49.1	-19.5	-50.9	25.0	-9.2	-47.2	-17.0	-4.5	-44.9	-43.0	36.0	-46.6	31.0
1	10	19.9	54.8	26.1	24.4	-46.5	-16.0	28.0	-43.9	-39.4	-0.8	55.6	23.1	8.5	-46.0	-22.5	12.8	-43.0	-49.3	-19.5	-50.9	25.0	-9.2	-47.2	-17.0	-4.5	-44.9	-43.0	36.2	-46.7	30.4
2	3	19.9	54.9	26.3	24.3	-46.5	-15.8	28.0	-43.9	-39.7	-0.8	55.8	23.5	8.2	-46.2	-21.0	12.8	-43.1	-50.1	-19.6	-51.1	25.5	-9.3	-46.1	-16.1	-4.3	-44.9	-43.3	36.2	-46.0	30.5
2	4	20.0	54.5	25.8	24.3	-46.5	-15.8	28.0	-43.9	-39.7	-0.9	55.8	23.2	8.3	-46.6	-21.0	12.8	-43.1	-50.1	-19.6	-51.1	25.5	-9.3	-46.3	-16.5	-4.5	-45.0	-42.9	30.4	-30.5	45.7
2	5	20.0	54.6	26.1	24.3	-46.4	-15.8	28.0	-43.9	-39.8	-0.9	55.8	23.3	8.3	-46.2	-21.3	12.8	-43.1	-50.1	-19.6	-51.1	25.5	-9.2	-46.2	-16.5	-4.5	-45.0	-42.9	30.7	-30.7	45.7
2	6	19.9	54.7	26.5	24.4	-45.7	-15.7	28.0	-43.8	-39.7	-1.2	56.4	24.4	8.4	-44.5	-21.5	12.8	-43.1	-49.1	-19.6	-51.1	25.8	-10.1	-45.4	-16.5	-4.5	-44.9	-42.9	36.0	-30.6	45.7
2	7	19.9	54.7	26.5	24.4	-45.6	-15.8	28.0	-43.8	-39.7	-0.9	55.8	23.4	8.4	-44.8	-21.7	12.8	-43.2	-49.0	-19.6	-51.1	25.8	-9.5	-45.0	-16.5	-4.5	-45.0	-42.9	36.2	-46.0	30.5
2	9	20.0	54.6	26.1	24.4	-45.6	-15.8	28.0	-43.8	-39.4	-0.9	55.8	23.4	8.4	-44.9	-21.7	12.7	-43.2	-49.0	-19.6	-51.1	25.3	-9.2	-46.0	-16.1	-4.5	-45.0	-42.9	36.2	-46.0	30.5
2	10	20.0	54.5	26.0	24.4	-45.6	-15.8	28.0	-43.8	-39.3	-0.9	55.8	23.2	8.4	-44.9	-21.7	12.7	-43.2	-49.1	-19.5	-50.8	25.1	-9.2	-46.2	-16.9	-4.5	-45.0	-42.9	36.2	-46.0	30.1
3	4	20.2	53.9	25.5	24.2	-47.4	-14.8	28.1	-43.8	-39.3	-0.3	55.6	23.0	8.4	-44.2	-21.6	12.9	-43.2	-49.3	-19.6	-51.0	25.5	-9.2	-45.8	-16.1	-4.0	-45.0	-44.3	36.2	-46.0	30.4
3	5	20.0	54.0	25.8	24.3	-45.6	-15.8	28.0	-43.8	-39.4	-0.8	55.7	23.2	8.4	-44.7	-21.6	12.8	-43.3	-49.4	-19.6	-51.0	25.3	-9.2	-45.8	-16.1	-4.5	-45.0	-42.9	36.2	-46.0	30.3
3	6	18.7	54.7	29.6	24.4	-45.7	-15.7	28.0	-43.8	-39.4	-1.2	56.4	24.4	8.4	-44.5	-21.5	12.8	-43.1	-49.1	-19.6	-51.1	25.8	-9.2	-45.8	-16.1	-4.5	-45.0	-42.9	36.0	-30.6	45.8
3	7	20.0	54.5	26.3	24.4	-45.7	-15.7	28.0	-43.8	-39.5	-1.2	56.4	24.4	8.4	-44.5	-21.5	12.8	-43.1	-49.1	-19.6	-51.1	25.8	-9.2	-45.8	-16.1	-4.5	-45.0	-42.9	36.2	-46.0	30.2
3	9	20.0	54.4	26.0	24.4	-45.8	-15.8	28.0	-43.8	-39.5	-0.9	55.7	23.1	8.4	-44.5	-21.5	12.8	-43.1	-49.1	-19.6	-51.1	25.8	-9.2	-45.8	-16.1	-4.5	-45.0	-42.9	36.2	-46.0	30.2
3	10	20.1	54.1	26.3	24.4	-45.8	-15.7	28.0	-43.8	-39.5	-1.0	56.2	23.1	8.4	-44.6	-21.5	12.8	-43.1	-49.1	-19.6	-51.0	25.8	-9.2	-45.8	-16.1	-4.5	-45.0	-42.9	36.2	-46.0	30.1
4	10	19.7	55.3	26.3	24.4	-45.8	-15.8	28.0	-43.8	-39.5	-0.9	55.7	23.1	8.4	-44.5	-21.5	12.8	-43.1	-49.1	-19.6	-50.4	25.8	-9.2	-45.8	-16.1	-4.5	-45.0	-42.9	36.2	-46.0	30.2
4	6	20.1	54.1	26.3	24.4	-45.8	-15.8	28.0	-43.8	-39.5	-0.9	55.7	23.1	8.4	-44.5	-21.5	12.8	-43.1	-49.1	-19.6	-50.4	25.8	-9.2	-45.8	-16.1	-4.5	-45.0	-42.9	36.2	-46.0	30.2
4	7	20.1	54.2	25.9	24.4	-45.7	-15.7	28.0	-43.8	-39.6	-0.9	55.7	23.1	8.4	-44.5	-21.5	12.8	-43.1	-49.1	-19.6	-50.4	25.8	-9.2	-45.8	-16.1	-4.5	-45.0	-42.9	36.2	-46.0	30.2
4	8	20.1	54.2	25.9	24.4	-45.7	-15.7	28.0	-43.8	-39.6	-0.9	55.7	23.1	8.4	-44.5	-21.5	12.8	-43.1	-49.1	-19.6	-50.4	25.8	-9.2	-45.8	-16.1	-4.5	-45.0	-42.9	36.2	-46.0	30.2
4	9	20.1	54.1	25.8	24.4	-45.7	-15.7	28.0	-43.8	-39.6	-0.9	55.7	23.1	8.4	-44.5	-21.5	12.8	-43.1	-49.1	-19.6	-50.4	25.8	-9.2	-45.8	-16.1	-4.5	-45.0	-42.9	36.2	-46.0	30.2
4	10	20.1	54.1	25.8	24.3	-45.7	-15.7	28.0	-43.8	-39.6	-0.9	55.7	23.0	8.4	-44.5	-21.5	12.8	-43.1	-49.1	-19.6	-50.4	25.8	-9.2	-45.8	-16.1	-4.5	-45.0	-42.9	36.2	-46.0	30.2
5	10	20.1	54.1	25.8	24.3	-45.7	-15.7	28.0	-43.8	-39.6	-0.9	55.7	23.0	8.4	-44.5	-21.5	12.8	-43.1	-49.1	-19.6	-50.4	25.8	-9.2	-45.8	-16.1	-4.5	-45.0	-42.9	36.2	-46.0	30.2
5	11	20.1	54.1	25.8	24.3	-45.7	-15.7	28.0	-43.8	-39.6	-0.9	55.7	23.0	8.4	-44.5	-21.5	12.8	-43.1	-49.1	-19.6	-50.4	25.8	-9.2	-45.8	-16.1	-4.5	-45.0	-42.9	36.2	-46.0	30.2
5	12	20.1	54.1	25.8	24.3	-45.7	-15.7	28.0	-43.8	-39.6	-0.9	55.7	23.0	8.4	-44.5	-21.5	12.8	-43.1	-49.1	-19.6	-50.4	25.8	-9.2	-45.8	-16.1	-4.5	-45.0	-42.9	36.2	-46.0	30.2
5	13	20.1	54.1	25.8	24.3	-45.7	-15.7	28.0	-43.8	-39.6	-0.9	55.7	23.0	8.4	-44.5	-21.5	12.8	-43.1	-49.1	-19.6	-50.4	25.8	-9.2	-45.8	-16.1	-4.5	-45.0	-42.9	36.2	-46.0	30.2
5	14	20.1	54.1	25.8	24.3	-45.7	-15.7	28.0	-43.8	-39.6	-0.9	55.7	23.0	8.4	-44.5	-21.5	12.8	-43.1	-49.1	-19.6	-50.4	25.8	-9.2	-45.8	-16.1	-4.5	-45.0	-42.9	36.2	-46.0	30.2
5	15	20.1	54.1	25.8	24.3	-45.7	-15.7	28.0	-43.8	-39.6	-0.9	55.7	23.0	8.4	-44.5	-21.5	12.8	-43.1	-49.1	-19.6	-50.4	25.8	-9.2	-45.8	-16.1	-4.5	-45.0	-42.9	36.2	-46.0	30.2
5	16	20.1	54.1	25.8	24.3	-45.7	-15.7	28.0	-43.8	-39.6	-0.9	55.7	23.0	8.4	-44.5	-21.5	12.8	-43.1	-49.1	-19.6	-50.4	25.8	-9.2	-45.8	-16.1	-4.5	-45.0	-42.9	36.2	-46.0	30.2
5	17	20.1	54.1	25.8	24.3	-45.7	-15.7	28.0	-43.8	-39.6	-0.9	55.7	23.0	8.4	-44.5	-21.5	12.8	-43.1	-49.1	-19.6	-50.4	25.8	-9.2	-45.8	-16.1	-4.5	-45.0	-42.9	36.2	-46.0	30.2
5	18	20.1	54.1	25.8	24.3	-45.7	-15.7	28.0	-43.8	-39.6	-0.9	55.7	23.0	8.4	-44.5	-21.5	12.8	-43.1	-49.1	-19.6	-50.4	25.8	-9.2	-45.8	-16.1	-4.5	-45.0	-42.9	36.2	-46.0	30.2
5	19	20.1	54.1	25.8	24.3	-45.7	-15.7	28.0	-43.8	-39.6	-0.9	55.7	23.0	8.4	-44.5	-21.5	12.8	-43.1	-49.1	-19.6	-50.4	25.8	-9.2	-45.8	-16.1	-4.5	-45.0	-42.9	36.2	-46.0	30.2
5	20	20.1	54.1	25.8	24.3	-45.7	-15.7	28.0	-43.8	-39.6	-0.9	55.7	23.0	8.4	-44.5	-21.5	12.8	-43.1	-49.1	-19.6	-50.4	25.8	-9.2	-45.8	-16.1	-4.5	-45.0	-42.9	36.2	-46.0	30.2
5	21	20.1	54.1	25.8	24.3	-45.7	-15.7	28.0	-43.8	-39.6	-0.9	55.7	23.0	8.4	-44.5	-21.5	12.8	-43.1	-49.1	-19.6	-50.4	25.8	-9.2	-							

Participant 8: Instantaneous Joint CoRs by Figueroa et al.'s method

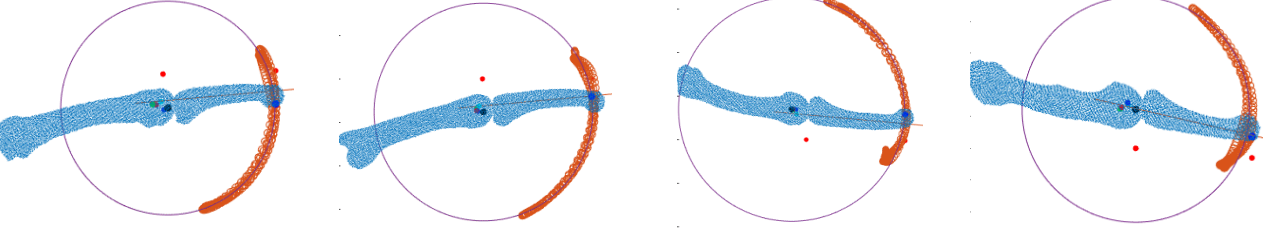
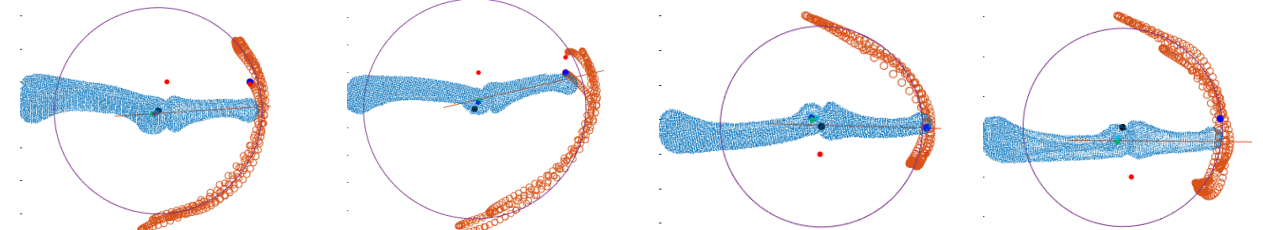
Posture	First	Second	Index			Middle			Ring			Little																									
			MCP joint	PIP joint	DIP joint	MCP joint	PIP joint	DIP joint	MCP joint	PIP joint	DIP joint	MCP joint	PIP joint	DIP joint	MCP joint	PIP joint	DIP joint	MCP joint	PIP joint	DIP joint																	
X	Y	Z	X	Y	Z	X	Y	Z	X	Y	Z	X	Y	Z	X	Y	Z	X	Y	Z																	
1	2	-7.0	9.4	118.1	-8.6	24.7	79.9	-8.7	22.5	56.1	-29.1	8.8	122.0	-25.0	24.4	77.0	-24.5	23.2	49.4	-46.7	14.6	128.6	-42.5	25.5	87.0	-40.6	23.8	61.2	-57.4	25.6	140.0	-58.0	27.1	102.2	57.3	27.7	83.9
1	3	-6.7	9.8	117.0	-8.6	24.7	80.0	-8.7	22.6	56.1	-29.1	8.7	122.3	-25.0	24.4	77.1	-24.5	23.3	49.6	-46.7	14.5	128.8	-42.5	25.5	85.9	-40.7	23.8	61.4	-57.4	25.5	140.2	-58.0	27.1	101.9	57.2	27.7	83.7
1	4	-7.3	8.8	119.8	-8.6	24.8	80.1	-8.7	22.6	56.1	-29.1	8.7	122.2	-25.0	24.4	77.1	-24.5	23.4	49.9	-46.6	15.0	126.6	-42.5	25.5	86.8	-40.7	23.8	61.5	-58.2	26.0	133.9	-58.0	27.1	101.8	57.2	27.6	83.5
1	5	-7.1	9.2	118.7	-8.6	24.8	80.1	-8.7	22.5	55.9	-28.9	9.2	120.4	-25.0	24.4	77.2	-24.5	23.2	49.2	-46.4	16.2	121.8	-42.5	25.5	86.8	-40.6	23.8	61.2	-57.9	25.8	136.6	-58.0	27.1	101.9	57.3	27.7	83.7
1	6	-7.1	9.3	118.6	-8.6	24.8	80.1	-8.7	22.6	56.2	-28.9	9.2	120.5	-25.0	24.4	77.0	-24.5	23.4	49.9	-46.6	14.9	127.2	-42.5	25.5	86.5	-40.7	23.8	61.6	-58.3	26.0	133.4	-58.0	27.1	101.9	57.3	27.8	84.0
1	7	-7.2	9.0	119.3	-8.6	24.8	80.1	-8.7	22.6	56.3	-28.9	9.3	120.3	-25.0	24.4	77.0	-24.5	23.4	50.1	-46.6	15.0	126.7	-42.5	25.4	86.8	-40.7	23.8	61.6	-58.2	26.0	134.1	-58.0	27.1	101.8	57.2	27.6	83.5
1	8	-7.0	9.3	118.4	-8.6	24.8	80.5	-8.7	22.6	56.2	-28.9	9.2	120.7	-25.0	24.3	76.9	-24.4	23.4	50.0	-46.6	14.9	127.6	-42.4	25.4	86.5	-40.7	23.8	61.6	-58.3	26.0	133.9	-58.0	27.1	101.8	57.2	27.6	83.3
1	9	-7.2	9.3	119.2	-8.6	24.8	80.5	-8.6	22.6	56.4	-29.0	9.0	121.1	-25.0	24.4	77.5	-24.5	23.4	50.0	-46.6	14.9	127.5	-42.5	25.5	86.9	-40.7	23.8	61.5	-58.3	26.0	133.9	-58.0	27.1	101.8	57.2	27.6	83.3
1	10	-7.1	9.3	118.3	-8.6	24.8	80.3	-8.7	22.6	56.5	-29.0	8.9	120.5	-25.0	24.4	77.2	-24.5	23.3	50.0	-46.7	14.5	127.7	-42.5	25.5	86.9	-40.7	23.8	61.6	-58.3	26.0	133.6	-58.0	27.1	102.2	57.2	27.6	83.6
2	3	-7.1	9.3	118.8	-8.6	24.3	80.2	-8.7	22.6	56.2	-29.1	8.8	121.8	-25.0	24.2	77.1	-24.5	23.3	49.7	-46.7	14.6	128.4	-42.5	25.5	86.9	-40.7	23.8	61.3	-57.4	25.5	134.5	-58.0	27.3	102.4	57.4	27.8	84.5
2	4	-7.1	9.2	118.9	-8.6	24.3	80.1	-8.7	22.6	56.1	-29.1	8.8	121.9	-25.0	24.3	77.1	-24.5	23.3	49.7	-46.7	14.5	128.1	-42.5	25.5	86.9	-40.7	23.8	61.3	-57.2	25.2	142.2	-57.9	27.3	101.8	57.2	27.7	83.4
2	5	-7.1	9.3	118.5	-8.6	24.3	80.2	-8.7	22.5	55.9	-29.0	8.8	121.4	-25.0	24.2	77.1	-24.5	23.3	49.7	-46.7	14.5	128.0	-42.5	25.5	86.9	-40.6	23.8	61.2	-57.4	26.7	133.4	-57.9	27.3	101.9	57.2	27.7	83.5
2	6	-7.0	9.3	118.5	-8.6	24.3	80.1	-8.7	22.6	56.2	-29.1	8.8	121.3	-25.0	24.3	77.0	-24.5	23.3	50.0	-46.7	14.5	127.6	-42.5	25.5	86.8	-40.7	23.8	61.6	-58.0	26.9	131.8	-57.9	27.4	101.7	57.2	27.7	83.4
2	7	-7.2	9.2	119.1	-8.6	24.4	80.1	-8.7	22.6	56.3	-29.0	8.8	121.3	-25.0	24.4	77.0	-24.5	23.3	50.2	-46.7	14.7	127.9	-42.5	25.7	86.8	-40.7	23.8	61.6	-58.0	26.9	132.3	-57.8	27.4	101.6	57.2	27.7	83.5
2	8	-7.0	9.3	118.8	-8.6	24.4	80.2	-8.7	22.6	56.2	-29.1	8.9	121.0	-25.0	24.5	77.0	-24.5	23.3	50.2	-46.7	14.5	127.6	-42.4	25.4	86.5	-40.7	23.8	61.6	-58.3	26.6	132.6	-57.9	27.2	102.0	57.3	27.7	84.0
2	9	-7.2	9.2	119.1	-8.6	24.2	80.3	-8.6	22.6	56.4	-29.0	8.8	121.3	-25.0	24.0	77.2	-24.5	23.3	50.0	-46.7	14.5	127.7	-42.5	25.5	86.7	-40.7	23.8	61.5	-57.9	26.9	132.9	-58.0	27.3	101.9	57.2	27.6	83.3
2	10	-7.1	9.3	118.5	-8.6	24.1	80.3	-8.7	22.6	56.5	-29.0	8.9	120.5	-25.0	24.0	77.2	-24.5	23.3	50.3	-46.7	14.5	127.8	-42.5	25.5	86.7	-40.7	23.8	61.6	-57.9	26.9	133.0	-58.0	27.1	102.2	57.2	27.7	83.6
3	4	-7.1	9.1	119.1	-8.6	24.4	80.1	-8.7	22.6	55.7	-29.1	8.8	122.0	-25.0	24.3	77.1	-24.5	23.2	49.6	-46.6	14.5	129.5	-42.5	25.5	86.9	-40.3	23.1	59.3	-57.8	26.6	134.3	-58.0	27.3	101.2	57.2	27.7	83.5
3	5	-7.1	9.3	118.8	-8.6	24.4	80.1	-8.7	22.6	56.1	-29.1	8.9	121.3	-25.0	24.1	77.1	-24.5	23.2	49.6	-46.7	14.6	127.4	-42.5	25.5	86.9	-40.7	23.8	61.5	-57.9	26.2	135.0	-57.9	27.2	101.9	57.3	27.7	83.4
3	6	-7.0	9.3	118.5	-8.6	24.4	80.2	-8.7	22.6	56.2	-29.1	8.9	121.0	-25.0	24.3	77.1	-24.5	23.3	50.1	-46.7	14.5	127.8	-42.5	25.5	86.9	-40.7	23.8	61.5	-57.8	26.7	133.4	-58.0	27.2	101.7	57.3	27.6	83.5
3	7	-7.2	9.2	119.4	-8.6	24.4	80.1	-8.7	22.6	56.3	-29.0	8.9	121.3	-25.0	24.4	77.1	-24.5	23.3	50.1	-46.7	14.7	127.9	-42.5	25.7	86.8	-40.7	23.8	61.5	-57.8	26.9	132.3	-57.9	27.2	102.0	57.3	27.6	83.4
3	8	-7.0	9.4	118.7	-8.6	24.1	80.3	-8.7	22.6	56.4	-29.0	9.0	120.5	-25.0	24.3	77.1	-24.5	23.3	50.3	-46.7	14.6	127.8	-42.5	25.5	86.7	-40.7	23.8	61.6	-57.9	26.7	133.5	-58.0	27.1	102.2	57.2	27.7	83.6
3	9	-7.2	9.5	118.8	-8.6	24.4	80.2	-8.7	22.6	56.2	-29.0	9.0	120.9	-25.0	24.2	77.0	-24.5	23.3	50.8	-46.7	14.6	127.5	-42.5	25.5	86.8	-40.7	23.8	61.5	-58.0	26.7	133.4	-58.0	27.3	101.9	57.2	27.6	83.4
3	10	-7.1	9.3	118.7	-8.6	24.4	80.1	-8.7	22.6	56.3	-29.0	8.9	121.3	-25.0	24.1	77.1	-24.5	23.3	50.1	-46.7	14.6	127.7	-42.5	25.5	86.9	-40.7	23.8	61.6	-57.9	26.7	132.4	-58.0	27.1	101.9	57.2	27.6	83.4
4	7	-7.2	9.1	118.9	-8.6	24.4	80.1	-8.7	22.5	55.8	-28.7	8.9	121.3	-25.0	24.1	77.1	-24.5	23.3	49.9	-46.7	14.6	127.8	-42.5	25.5	86.8	-40.7	23.8	61.6	-57.9	26.7	132.4	-58.0	27.1	101.9	57.2	27.6	83.4
4	8	-7.0	9.3	118.8	-8.6	24.4	80.2	-8.7	22.6	55.9	-28.7	8.9	121.2	-25.0	24.2	77.1	-24.5	23.3	50.0	-46.7	14.6	127.9	-42.5	25.5	86.8	-40.7	23.8	61.6	-57.9	26.7	132.3	-58.0	27.1	101.9	57.2	27.6	83.4
4	9	-7.2	9.2	119.0	-8.6	24.4	80.1	-8.7	22.6	56.0	-28.7	8.9	121.2	-25.0	24.3	77.1	-24.5	23.3	50.0	-46.7	14.6	127.8	-42.5	25.5	86.8	-40.7	23.8	61.6	-57.9	26.7	132.2	-58.0	27.1	101.9	57.2	27.6	83.4
4	10	-7.1	9.1	118.7	-8.6	24.4	80.1	-8.7	22.6	56.1	-28.7	8.9	121.3	-25.0	24.4	77.1	-24.5	23.3	50.0	-46.7	14.6	127.7	-42.5	25.5	86.8	-40.7	23.8	61.6	-57.9	26.7	132.1	-58.0	27.1	101.9	57.2	27.6	83.4
5	4	-7.4	11.1	8.6	-24.6	79.3	-9.1	21.3	55.8	-28.7	8.7	120.8	-25.0	24.1	76.8	-24.7	22.7	49.7	-45.7	16.7	129.3	-25.2	24.5	86.9	-40.7	23.1	62.3	-56.9	26.5	101.7	57.4	27.6	84.3				
5	3	-6.7	7.3	118.6	-8.6	24.3	79.3	-8.9	20.8	55.2	-28.5	8.5	121.3	-25.0	24.1	76.7	-24.5	22.7	49.8	-46.4	15.2	129.3	-25.2	24.5	86.8	-40.7	23.1	62.3	-56.5	28.8	101.6	57.4	27.4	84.3			
5	2	-7.2	7.3	119.1	-8.6	24.0	79.3	-9.3	20.3	56.9	-28.7	8.9	121.0	-25.0	24.2	76.9	-24.5	22.7	49.9	-46.7	14.3	129.9	-25.2	24.5	86.7	-40.7	23.1	62.3	-56.5	28.9	101.7	57.3	27.4	83.8			
5	1	-7.0	7.2	119.8	-8.6	24.0	79.4	-8.8	21.3	56.6	-28.7	8.9	121.3	-25.0	24.3	76.8	-24.5	22.7	49.9	-46.7	14.3	129.9	-25.2	24.5	86.7	-40.7	23.1	62.3	-56.5	28.9	101.7	57.3	27.4	83.8			
5	0	-7.0	7.2	119.8	-8.6	24.0	79.3	-8.9	21.3	56.6	-28.7	8.9	121.2	-25.0	24.3	76.7	-24.5	22.7	49.9	-46.7	14.3	129.9	-25.2	24.5	86.7	-40.7	23.1	62.3	-56.5	28.9	101.7	57.3	27.4	83.8			
5	-1	-7.0	7.2	119.8	-8.6	24.0	79.3	-8.9	21.3	56.6	-28.7	8.9	121.2	-25.0	24.3	76.7	-24.5	22.7	49.9	-46.7	14.3	129.9	-25.2	24.5	86.7	-40.7	23.1	62.3	-56.5	28.9							

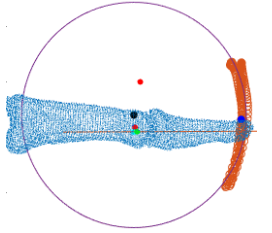
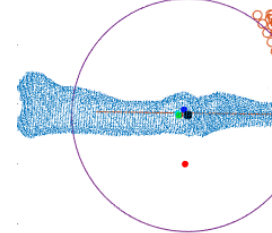
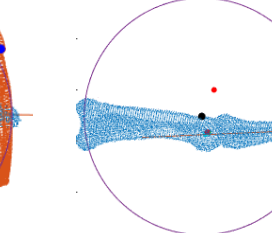
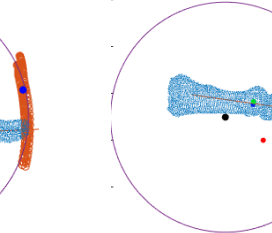
Participant 9: Instantaneous Joint CoRs by Figueroa et al.'s method

Posture	Index												Middle												Ring												Little											
	MCP joint			PIP joint			DIP joint			MCP joint			PIP joint			DIP joint			MCP joint			PIP joint			DIP joint			MCP joint			PIP joint			DIP joint			MCP joint			PIP joint			DIP joint					
First	Second	X	Y	Z	X	Y	Z	X	Y	Z	X	Y	Z	X	Y	Z	X	Y	Z	X	Y	Z	X	Y	Z	X	Y	Z	X	Y	Z	X	Y	Z	X	Y	Z	X	Y	Z	X	Y	Z	X	Y	Z		
1	2	15.6	-68.7	58.1	19.1	-57.2	26.5	20.6	-51.3	5.7	-3.3	-71.2	57.5	4.0	-55.7	17.3	8.1	-52.1	-8.3	-19.9	-65.1	62.6	12.0	-53.0	23.9	-7.4	-51.1	0.0	-33.2	55.8	66.9	-26.0	-49.8	36.6	-24.7	50.2	19.8											
1	3	15.0	-69.5	60.4	19.1	-57.2	26.5	21.0	-50.8	10.0	-3.3	-71.4	57.8	4.0	-55.7	17.3	8.1	-52.0	-7.8	-19.9	-65.1	62.9	12.0	-53.0	24.1	-7.6	-51.1	0.7	-33.1	56.0	67.3	-26.0	-49.7	36.8	-24.7	50.2	20.0											
1	4	15.1	-69.4	60.4	19.1	-57.2	26.3	20.6	-51.3	5.8	-3.2	-71.1	57.2	4.0	-55.7	17.3	8.0	-52.0	-7.5	-19.9	-65.2	62.4	12.0	-53.0	24.1	-7.6	-51.1	0.8	-33.2	55.9	67.2	-26.0	-49.7	36.7	-24.7	50.2	20.1											
1	5	15.0	-69.5	60.2	19.1	-57.2	26.4	20.6	-51.3	5.8	-3.1	-71.0	56.6	4.0	-55.7	17.4	8.0	-52.0	-7.3	-20.0	-65.3	63.4	12.0	-53.0	24.1	-7.7	-51.1	0.9	-30.9	61.4	79.4	-26.0	-49.7	36.7	-24.7	50.2	20.0											
1	6	14.5	-70.1	62.0	19.2	-57.0	25.8	20.6	-51.3	5.8	-3.3	-71.2	57.5	4.0	-55.7	17.5	8.0	-52.0	-7.5	-19.7	-64.7	61.3	12.0	-53.0	24.4	-7.6	-51.1	0.7	-33.3	55.7	66.6	-26.0	-49.7	37.3	-24.7	50.2	20.0											
1	7	14.7	-69.8	61.6	19.2	-57.1	26.2	20.6	-51.3	5.7	-3.2	-71.1	57.1	4.0	-55.7	17.5	8.0	-52.0	-7.7	-19.7	-64.7	61.3	12.0	-53.0	24.3	-7.6	-51.1	0.8	-33.3	55.7	66.6	-26.0	-49.7	37.2	-24.7	50.2	20.1											
1	8	14.8	-69.7	61.0	19.2	-57.1	26.1	20.6	-51.3	5.8	-3.2	-71.0	56.9	4.0	-55.7	17.5	8.0	-52.0	-7.6	-19.7	-64.7	61.2	12.0	-53.0	24.3	-7.6	-51.1	0.8	-33.3	55.7	66.6	-26.0	-49.7	37.3	-24.7	50.2	20.1											
1	9	14.7	-69.8	61.3	19.2	-57.1	26.1	20.6	-51.3	5.8	-3.2	-71.2	57.3	4.0	-55.7	17.6	8.0	-52.0	-7.6	-19.7	-64.7	61.3	12.0	-53.0	24.3	-7.6	-51.1	0.9	-33.3	55.7	66.6	-26.0	-49.7	37.3	-24.7	50.2	20.1											
1	10	14.7	-69.9	61.2	19.2	-57.1	26.2	20.6	-51.3	5.8	-3.3	-71.2	57.4	3.9	-55.7	17.5	8.0	-52.0	-7.6	-19.7	-64.7	61.4	12.0	-53.0	24.3	-7.6	-51.1	0.8	-33.3	55.7	66.6	-26.0	-49.7	37.3	-24.8	50.1	20.2											
2	3	14.9	-69.5	60.4	19.1	-57.3	26.6	20.5	-51.0	6.0	-3.0	-71.1	55.8	4.0	-55.8	17.3	8.0	-52.1	-7.7	-20.0	-65.2	63.3	12.0	-53.1	24.1	-7.6	-51.1	0.9	-33.0	56.1	67.8	-26.0	-49.8	36.8	-24.5	50.3	20.2											
2	4	15.1	-69.4	60.4	19.1	-57.1	26.3	20.6	-51.3	5.9	-3.3	-71.1	57.4	3.7	-55.8	17.4	8.0	-52.1	-7.4	-19.8	-64.9	61.3	12.0	-53.1	24.1	-7.6	-51.1	0.8	-32.9	56.2	68.1	-26.0	-49.8	36.8	-24.7	50.3	20.2											
2	5	15.0	-69.5	60.2	19.1	-57.1	26.4	20.6	-51.3	5.8	-3.2	-71.1	57.2	4.0	-55.9	17.4	8.0	-52.1	-7.3	-19.9	-65.1	62.9	12.0	-53.1	24.1	-7.7	-51.1	1.0	-33.2	55.9	67.1	-26.0	-49.8	36.7	-24.7	50.3	20.1											
2	6	14.5	-70.4	62.0	19.1	-56.5	26.3	20.5	-51.3	5.8	-3.3	-71.3	57.4	3.7	-55.9	17.5	8.0	-52.1	-7.4	-19.8	-64.9	61.5	12.0	-53.2	24.3	-7.6	-51.1	0.7	-33.3	55.8	66.7	-26.0	-49.7	37.2	-24.7	50.3	20.1											
2	7	14.7	-69.8	61.6	19.1	-57.0	26.2	20.6	-51.3	5.7	-3.2	-71.2	57.1	4.0	-55.9	17.4	8.0	-52.1	-7.6	-19.8	-64.9	61.4	12.0	-53.1	24.2	-7.6	-51.1	0.8	-33.3	55.7	66.6	-26.0	-49.7	37.2	-24.7	50.3	20.1											
2	8	14.8	-69.8	61.8	19.1	-57.0	26.2	20.6	-51.3	5.8	-3.2	-71.2	57.3	4.0	-55.9	17.4	8.0	-52.1	-7.6	-19.8	-64.9	61.3	12.0	-53.1	24.2	-7.6	-51.1	0.9	-33.3	55.7	66.6	-26.0	-49.7	37.2	-24.7	50.3	20.1											
2	9	14.7	-69.8	61.3	19.1	-57.0	26.2	20.6	-51.3	5.8	-3.2	-71.3	57.3	4.0	-55.9	17.4	8.0	-52.1	-7.6	-19.8	-64.9	61.4	12.0	-53.2	24.2	-7.6	-51.1	0.9	-33.3	55.8	66.7	-26.0	-49.7	37.3	-24.8	50.3	20.3											
2	10	14.7	-69.9	61.2	19.1	-57.1	26.3	20.5	-51.3	5.9	-3.4	-71.3	57.4	3.7	-55.9	17.5	8.0	-52.1	-7.7	-19.9	-64.7	61.7	12.0	-53.2	24.1	-7.6	-51.1	0.9	-33.0	56.1	67.9	-26.0	-49.5	36.6	-24.7	50.3	20.1											
3	1	14.0	-69.5	61.4	19.1	-56.9	26.3	20.5	-51.3	5.6	-3.2	-71.3	57.5	4.0	-56.0	17.5	8.0	-52.1	-7.6	-19.9	-64.6	61.2	12.0	-53.3	24.1	-7.6	-51.1	0.9	-33.0	55.9	66.6	-26.0	-49.7	36.7	-24.7	50.3	20.1											
3	2	14.0	-69.6	61.2	19.1	-56.9	26.3	20.5	-51.3	5.6	-3.2	-71.3	57.5	4.0	-56.0	17.5	8.0	-52.1	-7.6	-19.9	-64.6	61.1	12.0	-53.3	24.1	-7.6	-51.1	0.9	-33.0	55.9	66.6	-26.0	-49.7	36.7	-24.7	50.3	20.1											
3	3	14.0	-69.7	61.2	19.1	-56.9	26.3	20.5	-51.3	5.6	-3.2	-71.3	57.5	4.0	-56.0	17.5	8.0	-52.1	-7.6	-19.9	-64.6	61.0	12.0	-53.3	24.1	-7.6	-51.1	0.9	-33.0	55.9	66.6	-26.0	-49.7	36.7	-24.7	50.3	20.1											
3	4	14.0	-69.8	61.2	19.1	-56.9	26.3	20.5	-51.3	5.6	-3.2	-71.3	57.5	4.0	-56.0	17.5	8.0	-52.1	-7.6	-19.9	-64.6	60.9	12.0	-53.3	24.1	-7.6	-51.1	0.9	-33.0	55.9	66.6	-26.0	-49.7	36.7	-24.7	50.3	20.1											
3	5	14.0	-69.8	61.3	19.1	-56.9	26.3	20.5	-51.3	5.6	-3.2	-71.3	57.5	4.0	-56.0	17.5	8.0	-52.1	-7.6	-19.9	-64.6	61.2	12.0	-53.3	24.1	-7.6	-51.1	0.9	-33.0	55.9	66.6	-26.0	-49.7	36.7	-24.7	50.3	20.1											
3	6	14.4	-69.4	61.2	19.1	-56.9	26.3	20.5	-51.3	5.6	-3.2	-71.3	57.5	4.0	-56.0	17.5	8.0	-52.1	-7.6	-19.9	-64.6	61.3	12.0	-53.3	24.1	-7.6	-51.1	0.9	-33.0	55.9	66.6	-26.0	-49.7	36.7	-24.7	50.3	20.1											
3	7	14.5	-68.8	61.6	19.2	-57.2	26.3	20.5	-51.5	5.6	-3.3	-71.6	57.6	4.1	-56.1	16.9	7.9	-52.1	-8.0	-19.5	-64.6	61.2	12.0	-53.3	23.6	-7.3	-51.1	0.3	-32.9	54.0	56.0	-26.1	-50.1	37.1	-24.8	50.2	19.8											
3	8	14.5	-68.7	61.7	19.2	-57.1	26.3	20.5	-51.5	5.7	-3.3	-70.8	57.7	4.1	-56.1	16.9	8.0	-52.1	-8.0	-19.4	-64.6	61.1	12.0	-53.3	23.7	-7.3	-51.1	0.2	-32.9	54.0	56.0	-26.1	-50.1	37.1	-24.8	50.2	19.8											
3	9	14.5	-68.9	61.2	19.2	-57.2	26.3	20.5	-51.5	5.7	-3.3	-70.9	57.8	4.1	-56.1	16.9	8.0	-52.1	-8.0	-19.5	-64.5	61.0	12.0	-53.3	23.7	-7.3	-51.1	0.2	-32.9	54.0	56.0	-26.1	-50.1	37.0	-24.8	50.2	19.8											
3	10	14.5	-69.0	61.0	19.2	-57.1	26.3	20.5	-51.5	5.7	-3.3	-70.9	57.9	4.1	-56.1	16.9	8.0	-52.1	-8.0	-19.5	-64.5	60.9	12.0	-53.3	23.7	-7.3	-51.1	0.2	-32.9	54.0	56.0	-26.1	-50.1	37.0	-24.8	50.2	19.8											
3	11	14.5	-69.1	61.0	19.2	-57.1	26.3	20.5	-51.5	5.7	-3.3	-70.9	57.9	4.1	-56.1	16.9	8.0	-52.1	-8.0	-19.5	-64.5	60.8	12.0	-53.3	23.7	-7.3	-51.1	0.2	-32.9	54.0	56.0	-26.1	-50.1	37.0	-24.8	50.2	19.8											
3	12	14.5	-69.2	61.0	19.2	-57.1	26.3	20.5	-51.5	5.7	-3.3	-70.9	57.9	4.1	-56.1	16.9	8.0	-52.1	-8.0	-19.5	-64.5	60.7	12.0	-53.3	23.7	-7.3	-51.1	0.2	-32.9	54.0	56.0	-26.1	-50.1	37.0	-24.8	50.2	19.8											
3	13	14.5	-69.2	61.0	19.0	-56.4	26.3	20.5	-50.4	5.6	-3.2	-71.0	57.8	4.1	-56.1	16.9	8.0	-52.1	-7.7	-19.4	-64.8	61.8	11.9	-11.9	53.3	23.6	-7.2	-50.3	0.5	-33.7	55.7	63.8	-26.1	-50.7	36.0	-24.7	50.2	19.8										
3	14	14.5	-69.2	61.0	19.0	-56.4	26.3	20.5	-50.4	5.6	-3.2	-71.0	57.8	4.1	-56.1	16.9	8.0	-52.1	-7.7	-19.4	-64.8	61.8	11.9	-11.9	53.3	23.6	-7.2	-50.2	0.5	-33.6	55.7	63.8	-26.1	-50.7	36.0	-24.7	50.2	19.8										
3	15	14.5	-69.2	61.0	19.0	-56.4	26.3	20.5	-50.4	5.6	-3.2	-71.0	57.8	4.1																																		

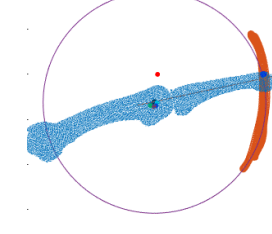
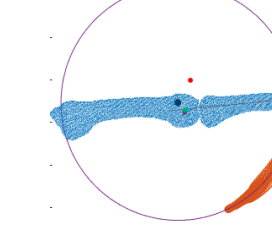
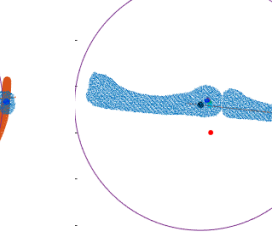
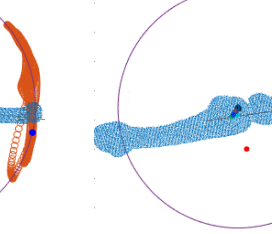
Appendix F: Fixed estimated joint CoRs

Participant 1

Joint (Finger)	MCP (Index finger)	MCP (Middle finger)	MCP (Ring finger)	MCP (Little finger)	
Position of joint CoRs					
M_DK	0.00	2.02	-13.94	0.00	
CT_DK	0.00	-2.75	-12.57	0.00	
Distance CT_DK & M_DK		4.96		3.22	
Rotation angle	94.08		98.13		
Joint (Finger)	PIP (Index finger)	PIP (Middle finger)	PIP (Ring finger)	PIP (Little finger)	
Position of joint CoRs					
M_DK	0.00	-2.63	-8.77	0.00	
CT_DK	0.00	-3.67	-9.76	0.00	
Distance CT_DK & M_DK		1.44		2.67	
Rotation angle	137.66		127.79		

Joint (Finger)	DIP (Index finger)	DIP (Middle finger)	DIP (Ring finger)	DIP (Little finger)								
Position of joint CoRs												
												
M_DK	0.00	-1.15	-5.96	0.00	0.46	8.19	0.00	-2.42	-5.19	0.00	-8.12	4.94
CT_DK	0.00	-0.95	-8.21	0.00	-0.92	8.16	0.00	-1.32	-8.25	0.00	-2.11	7.77
Distance CT_DK & M_DK		2.26		1.38			3.25			6.64		
Rotation angle		71.90		91.51			60.12			58.55		

Participant 2

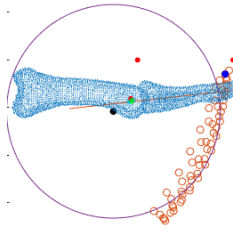
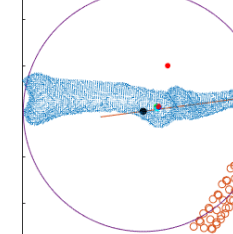
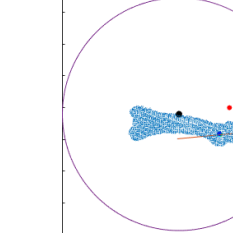
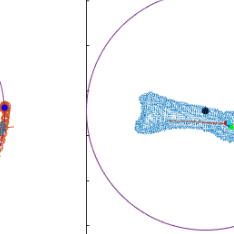
Joint (Finger)	MCP (Index finger)	MCP (Middle finger)	MCP (Ring finger)	MCP (Little finger)								
Position of joint CoRs												
												
M_DK	0.00	-1.37	-12.55	0.00	-5.97	-10.63	0.00	-4.41	11.94	0.00	-2.88	13.98
CT_DK	0.00	-1.63	-14.36	0.00	-2.62	-15.21	0.00	-1.27	14.00	0.00	-3.78	12.82
Distance between CT_DK & M_DK		1.83		5.68			3.76			1.48		
Rotation angle		72.01		81.47			79.44			80.79		

Joint (Finger)	PIP (Index finger)	PIP (Middle finger)	PIP (Ring finger)	PIP (Little finger)
Position of joint CoRs				
M_DK	0.00	-4.10	-7.72	0.00
CT_DK	0.00	-1.87	-9.42	0.00
Distance between CT_DK & M_DK	2.80	2.72	1.00	1.68
Rotation angle	112.92	118.29	108.07	112.91

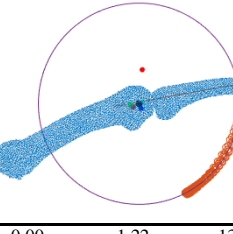
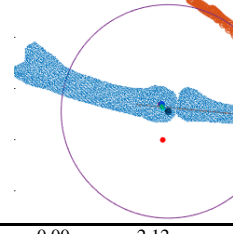
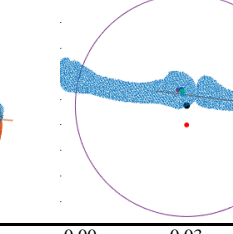
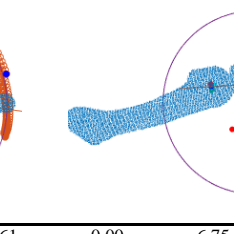
Joint (Finger)	DIP (Index finger)	DIP (Middle finger)	DIP (Ring finger)	DIP (Little finger)
Position of joint CoRs				
M_DK	0.00	-7.27	-13.37	0.00
CT_DK	0.00	-2.85	-7.89	0.00
Distance between CT_DK & M_DK	7.04	1.93	0.77	2.62
Rotation angle	43.41	80.70	78.63	73.26

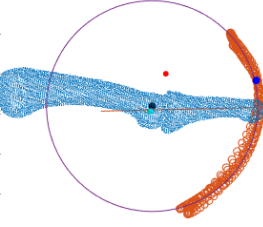
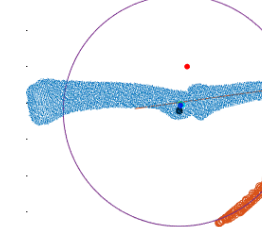
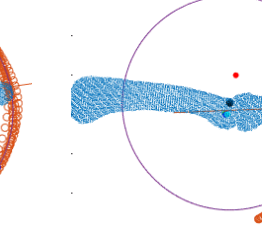
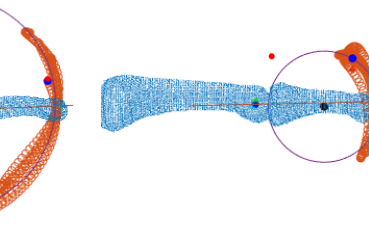
Participant 3

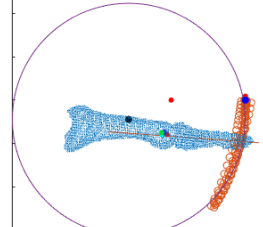
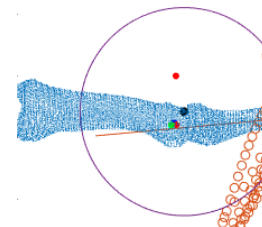
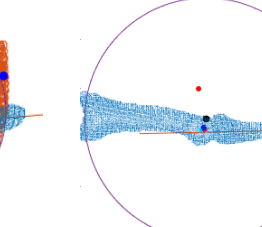
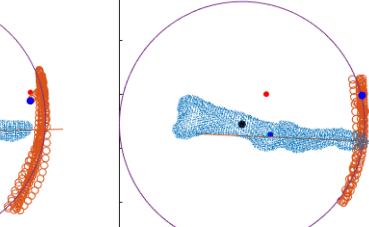
Joint (Finger)	MCP (Index finger)	MCP (Middle finger)	MCP (Ring finger)	MCP (Little finger)								
Position of joint CoRs												
M_DK	0.00	-2.22	6.49	0.00	0.04	15.14	0.00	-1.18	11.27	0.00	-4.48	11.73
CT_DK	0.00	-1.14	15.18	0.00	1.10	15.25	0.00	-0.87	14.30	0.00	-6.93	13.93
Distance between CT_DK & M_DK		8.76		1.06			3.04			3.28		
Rotation angle		71.73		116.80			101.69			97.87		
Joint (Finger)	PIP (Index finger)	PIP (Middle finger)	PIP (Ring finger)	PIP (Little finger)								
Position of joint CoRs												
M_DK	0.00	-3.62	-6.87	0.00	-0.89	-10.51	0.00	-2.14	15.10	0.00	-0.59	14.59
CT_DK	0.00	-2.19	-10.01	0.00	1.30	-9.90	0.00	-0.21	10.10	0.00	-2.50	9.65
Distance between CT_DK & M_DK		3.45		2.27			5.36			5.30		
Rotation angle		106.04		106.39			123.50			113.58		

Joint (Finger)	DIP (Index finger)	DIP (Middle finger)	DIP (Ring finger)	DIP (Little finger)								
Position of joint CoRs												
												
M_DK	0.00	-5.09	-10.79	0.00	-5.35	-9.98	0.00	-15.87	-2.05	0.00	-8.52	-4.50
CT_DK	0.00	-1.41	-8.14	0.00	-1.99	-8.91	0.00	-3.20	-8.23	0.00	-3.90	-7.21
Distance between CT_DK & M_DK		4.54		3.53			14.10			5.36		
Rotation angle		76.75		91.75			52.93			42.88		

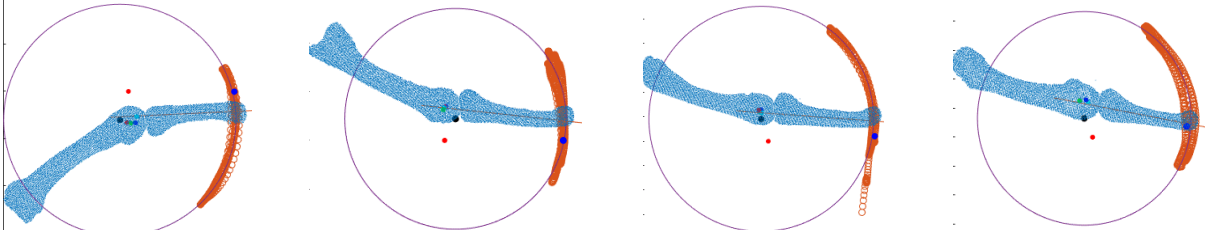
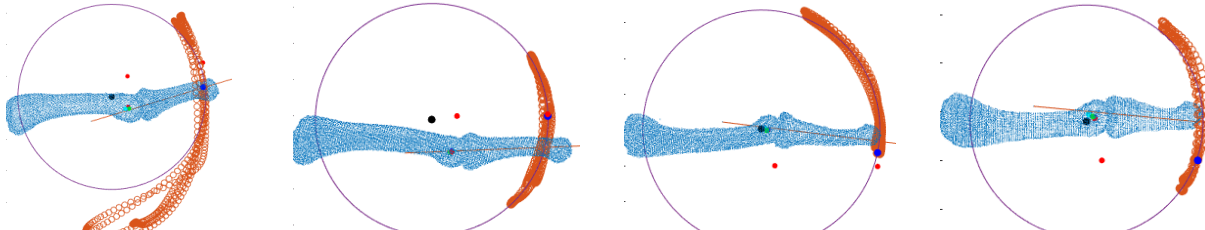
Participant 4

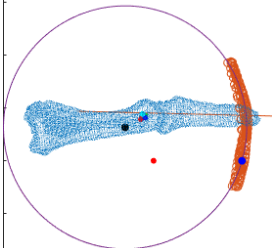
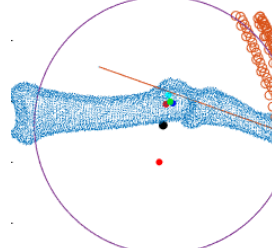
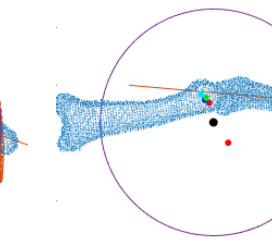
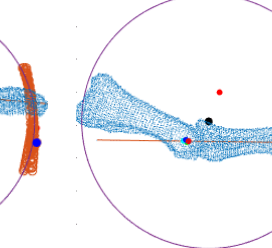
Joint (Finger)	MCP (Index finger)	MCP (Middle finger)	MCP (Ring finger)	MCP (Little finger)								
Position of joint CoRs												
												
M_DK	0.00	-1.22	-13.44	0.00	2.12	11.10	0.00	0.03	7.61	0.00	6.75	8.01
CT_DK	0.00	-3.62	-14.66	0.00	-0.95	13.84	0.00	-3.40	13.71	0.00	-6.35	13.52
Distance between CT_DK & M_DK		2.69		4.12			6.99			14.21		
Rotation angle		90.43		86.11			69.84			45.01		

Joint (Finger)	PIP (Index finger)	PIP (Middle finger)	PIP (Ring finger)	PIP (Little finger)								
Position of joint CoRs												
												
M_DK	0.00	-3.41	-8.09	0.00	-2.20	-12.18	0.00	-1.49	-7.05	0.00	9.95	-9.59
CT_DK	0.00	-3.52	-9.17	0.00	-1.82	-10.58	0.00	-2.48	-9.82	0.00	-3.02	-9.14
Distance between CT_DK & M_DK		1.08		1.64		2.94		12.98				
Rotation angle		115.34		105.23		118.13		55.37				

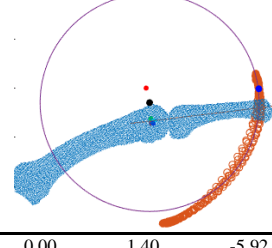
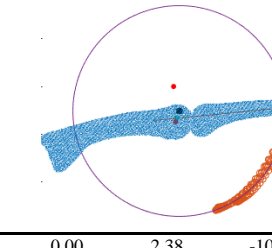
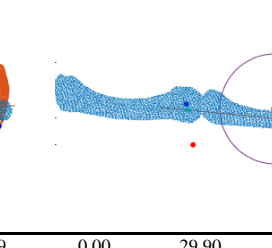
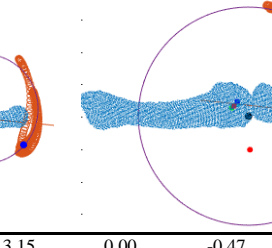
Joint (Finger)	DIP (Index finger)	DIP (Middle finger)	DIP (Ring finger)	DIP (Little finger)								
Position of joint CoRs												
												
M_DK	0.00	-9.78	-4.45	0.00	1.32	-5.80	0.00	1.53	-6.19	0.00	-4.47	-5.55
CT_DK	0.00	-0.96	-7.92	0.00	0.06	-7.96	0.00	1.24	-8.27	0.00	0.69	-7.51
Distance between CT_DK & M_DK		9.48		2.50		2.10		5.52				
Rotation angle		56.86		33.03		87.89		57.19				

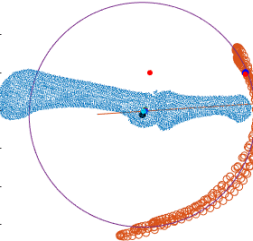
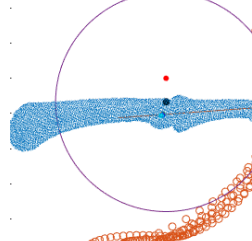
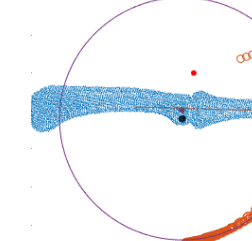
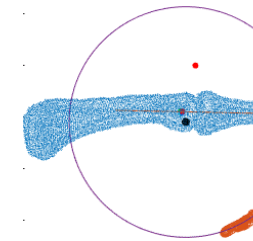
Participant 5

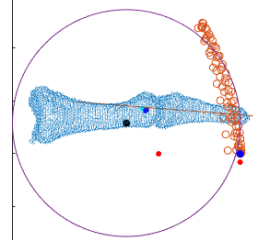
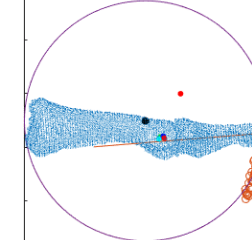
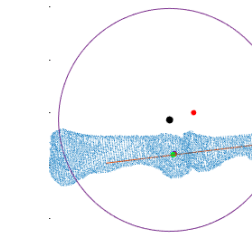
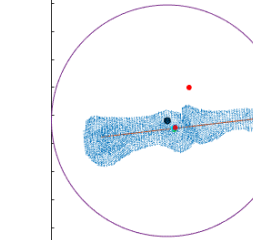
Joint (Finger)	MCP (Index finger)	MCP (Middle finger)	MCP (Ring finger)	MCP (Little finger)
Position of joint CoRs	 <p>Detailed description: This row contains four 3D circular plots representing the MCP joints of the index, middle, ring, and little fingers. Each plot shows a blue point cloud representing the bone model, a red circle representing the centerline of the distal bone, and a purple circle representing the fitted circle. A legend on the left side of the row defines the symbols: a blue square for 'Bone model', a red circle for 'CT-marker of proximal bone', a black circle for 'CT-marker of distal bone', a green circle for 'CT-based CoR by Bone Curvature', a blue circle for 'CT-based CoR by Reuleaux', a cyan circle for 'CT-based CoR by PCA', a red circle for 'CT-based CoR by Delonge-Kasa', an orange circle for 'Motion data', a black dot for 'Motion-based CoR by Delonge-Kasa', and a black line for 'Fitted circle'.</p>			
M_DK	0.00	-3.65	-12.21	0.00
CT_DK	0.00	-0.58	-13.23	0.00
Distance between CT_DK & M_DK	3.24	6.46	3.78	6.35
Rotation angle	77.68	63.48	93.94	82.04
Joint (Finger)	PIP (Index finger)	PIP (Middle finger)	PIP (Ring finger)	PIP (Little finger)
Position of joint CoRs	 <p>Detailed description: This row contains four 3D circular plots representing the PIP joints of the index, middle, ring, and little fingers. Each plot shows a blue point cloud representing the bone model, a red circle representing the centerline of the proximal bone, and a purple circle representing the fitted circle. A legend on the left side of the row defines the symbols: a blue square for 'Bone model', a red circle for 'CT-marker of proximal bone', a black circle for 'CT-marker of distal bone', a green circle for 'CT-based CoR by Bone Curvature', a blue circle for 'CT-based CoR by Reuleaux', a cyan circle for 'CT-based CoR by PCA', a red circle for 'CT-based CoR by Delonge-Kasa', an orange circle for 'Motion data', a black dot for 'Motion-based CoR by Delonge-Kasa', and a black line for 'Fitted circle'.</p>			
M_DK	0.00	-4.93	-6.55	0.00
CT_DK	0.00	0.21	-9.73	0.00
Distance between CT_DK & M_DK	6.04	10.46	1.90	1.78
Rotation angle	133.73	87.53	85.17	85.08

Joint (Finger)	DIP (Index finger)	DIP (Middle finger)	DIP (Ring finger)	DIP (Little finger)
Position of joint CoRs				
				
M_DK	0.00	-5.39	6.34	0.00
CT_DK	0.00	-2.36	7.91	0.00
Distance between CT_DK & M_DK	3.42	3.45	3.47	4.28
Rotation angle	67.58	92.56	55.56	72.08

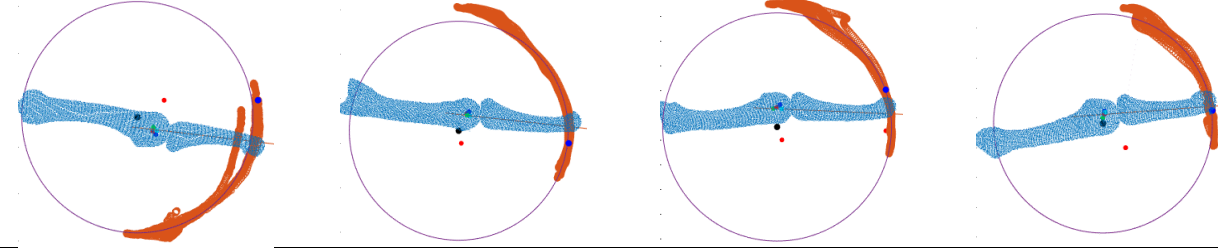
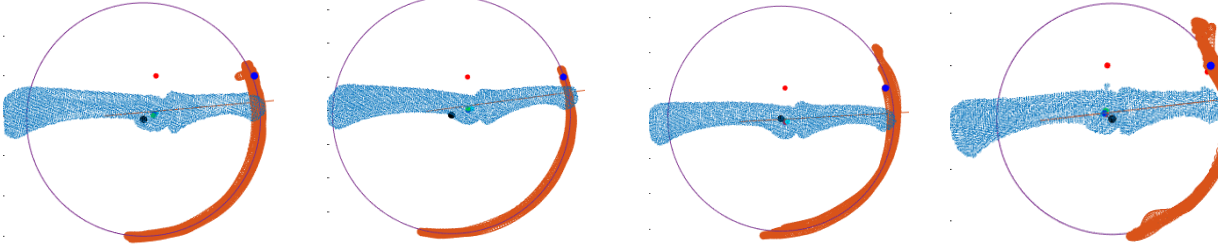
Participant 6

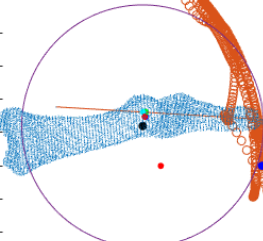
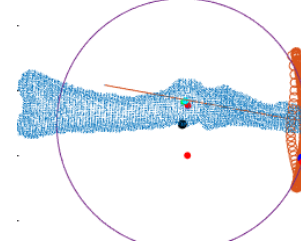
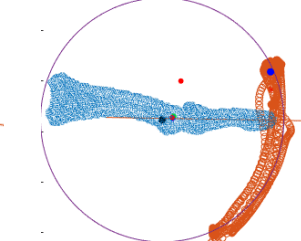
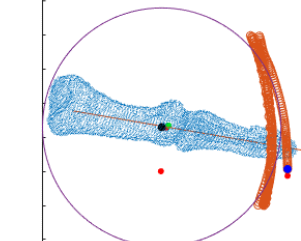
Joint (Finger)	MCP (Index finger)	MCP (Middle finger)	MCP (Ring finger)	MCP (Little finger)
Position of joint CoRs				
				
M_DK	0.00	1.40	-5.92	0.00
CT_DK	0.00	2.08	-14.30	0.00
Distance between CT_DK & M_DK	8.41	4.83	32.32	5.44
Rotation angle	106.95	90.92	41.22	99.61

Joint (Finger)	PIP (Index finger)	PIP (Middle finger)	PIP (Ring finger)	PIP (Little finger)								
Position of joint CoRs												
												
M_DK	0.00	-1.95	-11.09	0.00	0.01	-6.72	0.00	-3.01	-12.04	0.00	-1.86	-10.96
CT_DK	0.00	-1.20	-9.85	0.00	-1.06	-10.31	0.00	-3.04	-9.74	0.00	-2.51	-8.91
Distance between CT_DK & M_DK	1.45		3.74		2.30		2.15					
Rotation angle	134.26		142.44		120.57		110.12					

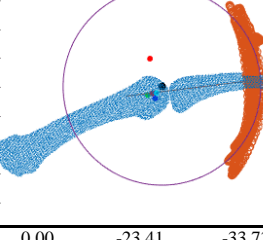
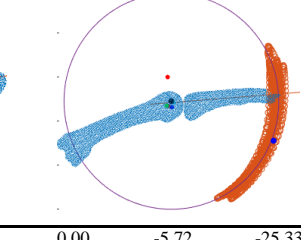
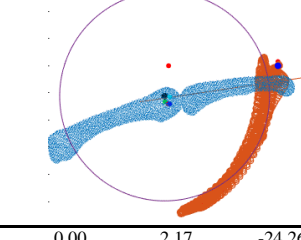
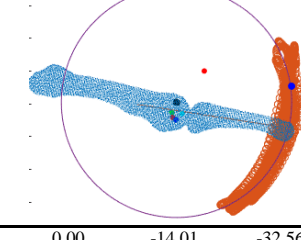
Joint (Finger)	DIP (Index finger)	DIP (Middle finger)	DIP (Ring finger)	DIP (Little finger)								
Position of joint CoRs												
												
M_DK	0.00	-6.08	5.80	0.00	-6.54	-5.09	0.00	-4.55	-1.37	0.00	-3.89	-5.92
CT_DK	0.00	-2.32	8.33	0.00	-3.04	-8.33	0.00	-3.61	-7.82	0.00	-2.47	-7.17
Distance between CT_DK & M_DK	4.53		4.77		6.52		1.89					
Rotation angle	75.81		65.48		55.35		66.68					

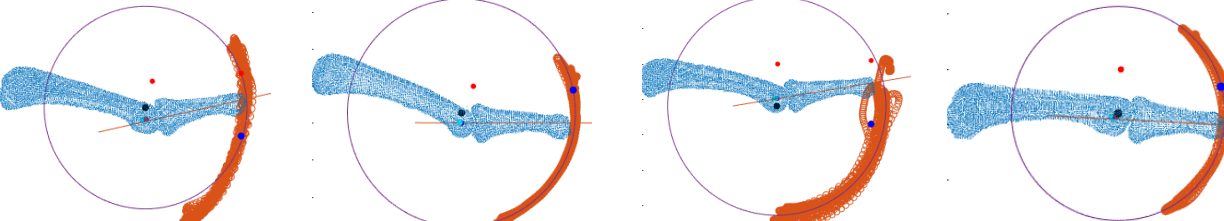
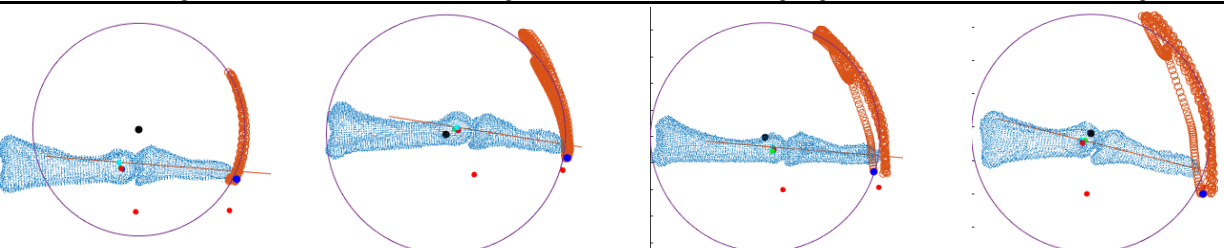
Participant 7

Joint (Finger)	MCP (Index finger)	MCP (Middle finger)	MCP (Ring finger)	MCP (Little finger)
Position of joint CoRs	 <p>Detailed description: This row contains four circular 3D plots representing the MCP joints of the index, middle, ring, and little fingers. Each plot shows a blue mesh representing the bone model and a red line representing the centerline of the distal bone. Small colored dots (red, green, blue) indicate specific markers or centers used in the analysis.</p>			
M_DK	0.00	-11.43	-7.26	0.00
CT_DK	0.00	-4.81	-13.28	0.00
Distance between CT_DK & M_DK	8.95	8.26	7.93	3.20
Rotation angle	106.68	130.22	105.49	91.65
Joint (Finger)	PIP (Index finger)	PIP (Middle finger)	PIP (Ring finger)	PIP (Little finger)
Position of joint CoRs	 <p>Detailed description: This row contains four circular 3D plots representing the PIP joints of the index, middle, ring, and little fingers. Similar to the MCP row, they show blue meshes and red centerlines for the distal bones, with colored markers indicating specific points of interest.</p>			
M_DK	0.00	-3.12	-10.89	0.00
CT_DK	0.00	-0.55	-9.47	0.00
Distance between CT_DK & M_DK	2.94	5.23	1.59	1.55
Rotation angle	127.12	125.78	140.46	133.05

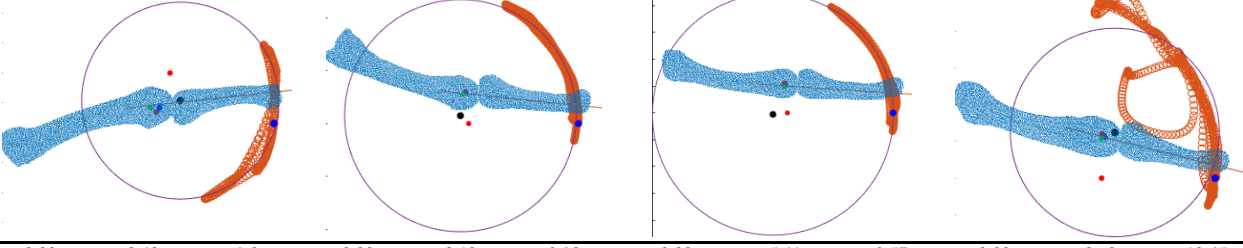
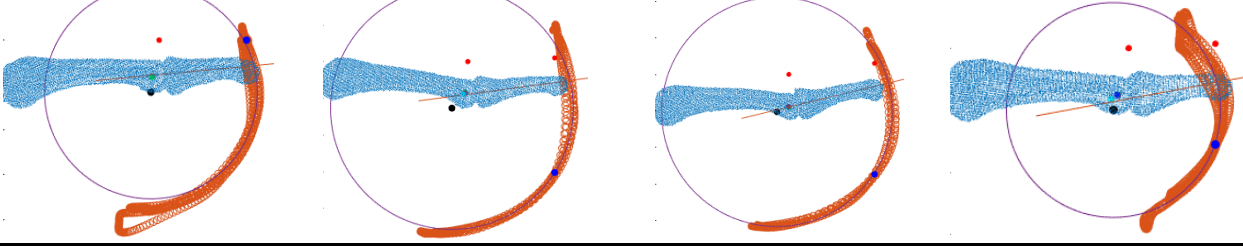
Joint (Finger)	DIP (Index finger)	DIP (Middle finger)	DIP (Ring finger)	DIP (Little finger)
Position of joint CoRs				
				
M_DK	0.00	-2.72	5.99	0.00
CT_DK	0.00	-2.43	7.38	0.00
Distance between CT_DK & M_DK	1.42	3.07	2.06	0.72
Rotation angle	99.38	69.53	109.97	90.99

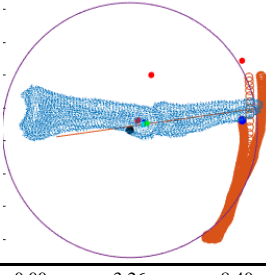
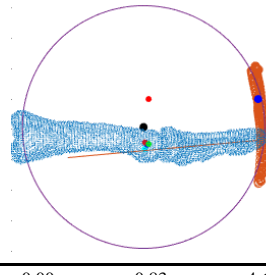
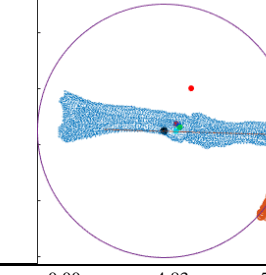
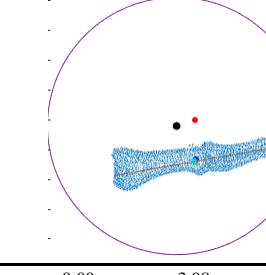
Participant 8

Joint (Finger)	MCP (Index finger)	MCP (Middle finger)	MCP (Ring finger)	MCP (Little finger)
Position of joint CoRs				
				
M_DK	0.00	-23.41	-33.73	0.00
CT_DK	0.00	-24.31	-34.50	0.00
Distance between CT_DK & M_DK	1.18	0.52	0.42	0.73
Rotation angle	94.43	93.61	109.10	93.10

Joint (Finger)	PIP (Index finger)	PIP (Middle finger)	PIP (Ring finger)	PIP (Little finger)
Position of joint CoRs				
M_DK	0.00	3.52	-25.95	0.00
CT_DK	0.00	3.58	-26.55	0.00
Distance between CT_DK & M_DK	0.60	0.51	0.44	0.19
Rotation angle	109.51	105.04	109.07	114.97
Joint (Finger)	DIP (Index finger)	DIP (Middle finger)	DIP (Ring finger)	DIP (Little finger)
Position of joint CoRs				
M_DK	0.00	0.50	13.53	0.00
CT_DK	0.00	-2.36	7.11	0.00
Distance between CT_DK & M_DK	7.03	2.43	2.95	1.90
Rotation angle	51.57	72.76	75.43	96.58

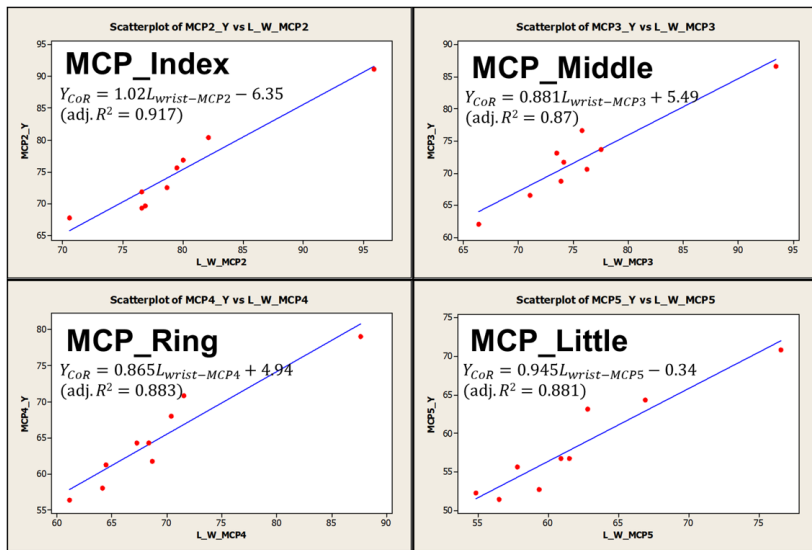
Participant 9

Joint (Finger)	MCP (Index finger)	MCP (Middle finger)	MCP (Ring finger)	MCP (Little finger)
Position of joint CoRs	 <p>Detailed description: This row contains four circular 3D plots showing the Multi-Center-of-Rotation (MCP) joints for the Index, Middle, Ring, and Little fingers. Each plot displays a blue point cloud representing motion data, a red line representing the centerline of the distal bone, and a purple circle representing the fitted circle. A legend on the left side of the row defines the symbols: a blue square for 'Bone model', a red dot for 'CT-marker of proximal bone', a black dot for 'CT-marker of distal bone', a green dot for 'CT-based CoR by Bone Curvature', a blue dot for 'CT-based CoR by Reuleaux', a cyan dot for 'CT-based CoR by PCA', a red dot for 'CT-based CoR by Delonge-Kasa', an orange circle for 'Motion data', a black dot for 'Motion-based CoR by Delonge-Kasa', and a purple circle for 'Fitted circle'.</p>			
M_DK	0.00	3.42	-9.26	0.00
CT_DK	0.00	-4.63	-13.14	0.00
Distance between CT_DK & M_DK	8.93	9.13	12.41	3.44
Rotation angle	92.52	90.52	82.51	114.65
Joint (Finger)	PIP (Index finger)	PIP (Middle finger)	PIP (Ring finger)	PIP (Little finger)
Position of joint CoRs	 <p>Detailed description: This row contains four circular 3D plots showing the Proximal Interphalangeal (PIP) joints for the Index, Middle, Ring, and Little fingers. Similar to the MCP row, they show blue motion data, red centerlines, and purple fitted circles. The legend on the left is identical to the one in the MCP row.</p>			
M_DK	0.00	-1.84	-11.61	0.00
CT_DK	0.00	-1.59	-8.00	0.00
Distance between CT_DK & M_DK	3.61	5.43	3.51	2.52
Rotation angle	129.01	137.25	144.42	128.27

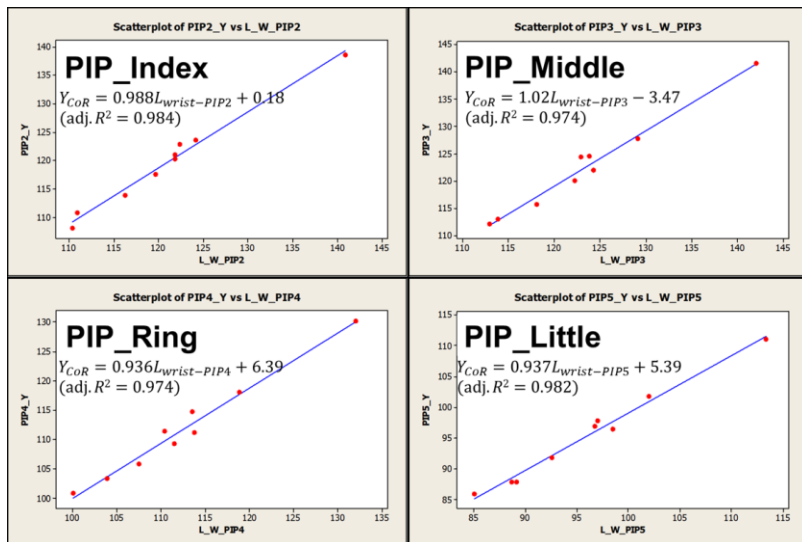
Joint (Finger)	DIP (Index finger)	DIP (Middle finger)	DIP (Ring finger)	DIP (Little finger)								
Position of joint CoRs												
M_DK	0.00	-3.26	-8.40	0.00	-0.83	-4.60	0.00	-4.83	-7.59	0.00	-3.08	-1.01
CT_DK	0.00	-2.04	-6.93	0.00	-0.60	-7.14	0.00	-2.66	-6.32	0.00	0.13	-6.61
Distance between CT_DK & M_DK		1.91		2.55		2.51		6.46				
Rotation angle		80.94		60.76		60.49		40.88				

Appendix G: Scatter Plot of Dependent Variables to Independent Variables

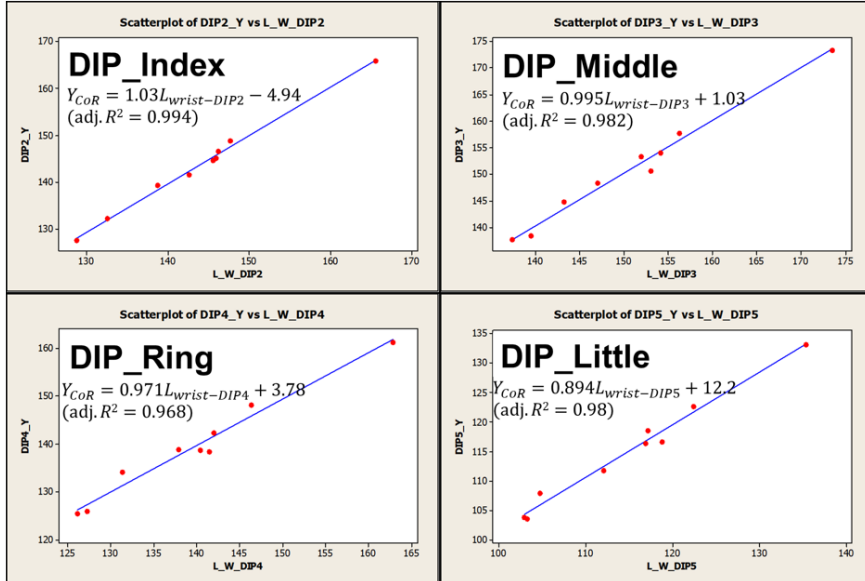
Scatter plot of y coordinate of joint CoR to perpendicular length from the landmark on the CMC joint to that on the MCP joint of each finger



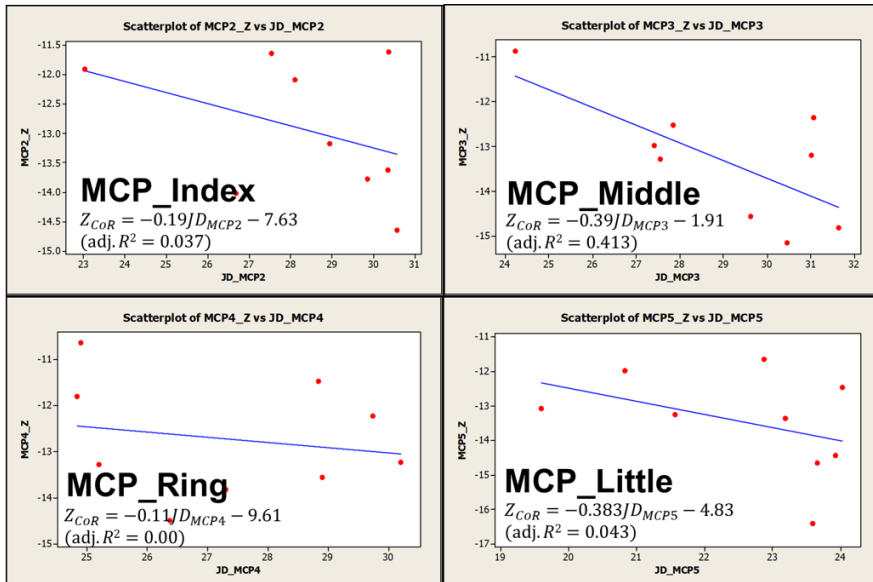
Scatter plot of y coordinate of joint CoR to perpendicular length from the landmark on the CMC joint to that on the PIP joint of each finger



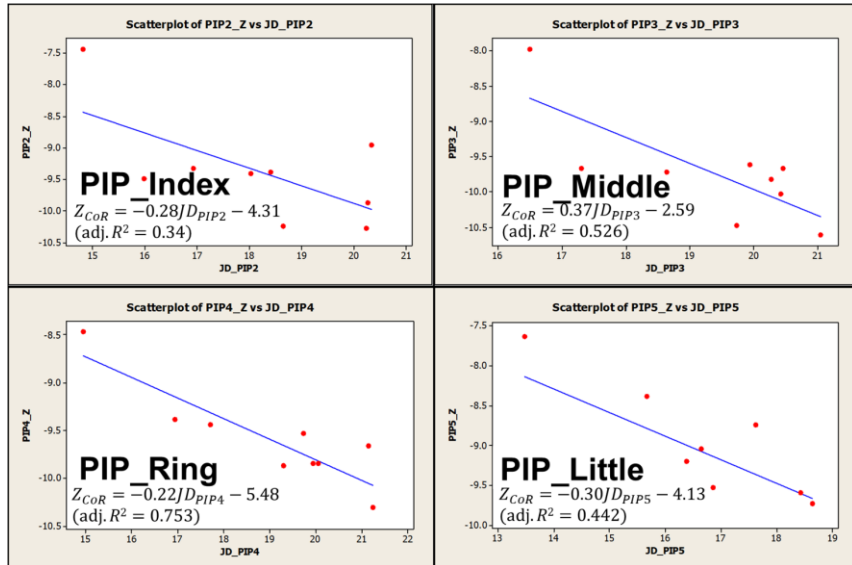
Scatter plot of y coordinate of joint CoR to perpendicular length from the landmark on the CMC joint to that on the DIP joint of each finger



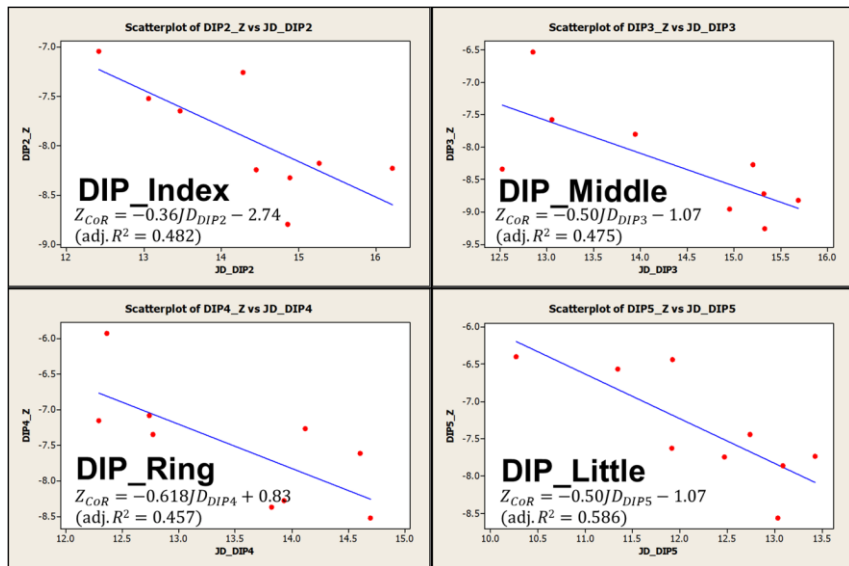
Scatter plot of z coordinate of joint CoR to MCP joint depth of each finger



Scatter plot of z coordinate of joint CoR to PIP joint depth of each finger



Scatter plot of z coordinate of joint CoR to DIP joint depth of each finger



ACKNOWLEDGEMENTS

The work presented here would not have been possible without the support of my family, my friends, and my mentors over the years. First and foremost, I would like to thank my advisor, Professor Heecheon You for his constant guidance throughout the whole period of my master studies. I would like to express my sincere appreciation to Dr. Xiaopeng Yang, who was my mentor in academic studies and always guide and supervise me. I am also grateful to my committee members, Professors Hyunbo Cho and Wonsup Lee, for providing valuable comments and suggestions. I wholeheartedly appreciate my colleagues in EDT lab, who always not hesitate to give me a hand when I have lost the way. I would also like to thank the faculty and staffs of the department of Industrial and Management Engineering, who have had a profound effect on my life through their generosity, intellect, friendships, and dedication to research. I would like to thank to POSCO Asia Fellowship, who recognize my qualification and financially support me in studying at POSTECH. To my close friends, Xiao Juan Jiang and Jia Chyi Wong, for patiently supporting me through all of the ups and downs we have encountered along the way. To my partner in crime, Elaheh Shakeri, who enlighten and encourage me to step out of my comfort zone and challenge the new life abroad. Lastly and most importantly, I am deeply grateful to my parents and brothers, Thomas Lim, Teoh Poh Lian, Alfred Lim and Lim Min Hong, for their love, support, and encouragement during these years.

CURRICULUM VITAE

LIM ZHI CHAN

Ergonomic Design Technology (EDT) Laboratory,
Department of Industrial and Management Engineering, POSTECH,
San 31 Hyojadong, Pohang, 790-784, South Korea

Education

M.S., Industrial and Management Engineering	August. 2018
Pohang University of Science and Technology (POSTECH), Pohang, South Korea	
B.S.(Hons), Mechatronics Engineering (Dual degree)	April. 2016
Asia Pacific University of Technology & Innovation at Kuala Lumpur, Bukit Jalil, Kuala Lumpur, Malaysia & Staffordshire University (Partnership university) at Stoke-on-Trent, Stoke-on-Trent, UK	

Publication

International Conference

1. Xiaopeng Yang, **Zhichan Lim**, Hayoung Jung, Wonsup Lee, Heecheon You (2018). ESTIMATION OF INSTANTANEOUS HAND JOINT CENTERS OF ROTATION USING 3D RECONSTRUCTED HAND SKELETON MOTION FROM CT SCANS. In *Proceedings of the Human Factors and Ergonomics*

Society (HFES) 62nd Annual Meeting. Philadelphia, Pennsylvania: The Human Factors and Ergonomics Society.

2. Hayoung Jung, Xiaopeng Yang, **Zhichan Lim**, Heecheon You (2017). Estimation of hand joint center of rotation using surface markers. In *Proceedings of the Human Factors and Ergonomics Society (HFES) 61st Annual Meeting*. Austin, TX: The Human Factors and Ergonomics Society.

Domestic Conference

1. **Zhichan Lim**, Xiaopeng Yang, Hayoung Jung, Heecheon You (2018). Estimation of Finger Joint Center of Rotation Using Finger Motion. In *Proceedings of the 2018 Spring Conference of the Ergonomics Society of Korea*.
2. Hayoung Jung, Minjae Kim, Younggeun Choi, Jihyung Lee, **Zhichan Lim**, Youngje Jung, Boyoung Park, Jihyun Oh, Jungbae Ko, Hoimin Choi, Dohyung Kim, Moonjin Kim, Heecheon You (2018). Ergonomic Evaluation of Premium Bus Accommodations. In *Proceedings of the 2018 Spring Conference of the Ergonomics Society of Korea*.
3. Minjae Kim, Hayoung Jung, Younggeun Choi, Jihyung Lee, **Zhichan Lim**, Youngje Jung, Boyoung Park, Jihyun Oh, Jungbae Ko, Hoimin Choi, Dohyun Kim, Moonjin Kim, Heecheon You (2018). Ergonomic Evaluation of Premium Bus Accommodations. In *Proceedings of the 2018 Spring Conference of the Ergonomics Society of Korea*.
4. **Zhichan Lim**, Xiaopeng Yang, Hayoung Jung, Heecheon You (2017). Development of Hand Link Model by Estimation of Joint Center of Rotation Using Surface Marker Motion. In *Proceedings of the 2017 Fall Conference of the Ergonomics Society of Korea*.

5. Hayoung Jung, Xiaopeng Yang, **Zhichan Lim**, Heecheon You (2017). Estimation of centers of rotation of finger joints using adjacent surface marker trajectory data. In *Proceedings of the 2017 Fall Conference of the Korean Institute of Industrial Engineers*.

6. **Zhichan Lim**, Hayoung Jung, Xiaopeng Yang, Heecheon You (2017). Estimation of Center of Rotation of PIP Joint Using Adjacent Surface Marker Motion. In *Proceedings of the 2017 Spring Conference of the Ergonomics Society of Korea*.

Honors and Awards

1. Award

Best Poster Award: Estimation of Center of Rotation of PIP Joint Using Adjacent Surface Marker Motion. In *Proceedings of the 2017 Spring Conference of the Ergonomics Society of Korea*.

2. Scholarship

POSCO Asia Fellowship 2016, period: 2016.9 ~ 2018.6

Research Projects

1. Research Assistant. Digital human modeling. 2016. 7 ~ 2018. 6.
2. Research Assistant. Development of swallowing signal diagnostic device. 2016. 9 ~ 2017. 9.
3. Research Assistant. Usability test of premium bus seat facilities. 2017. 4 ~ 2017. 12.